

2008

# CORROSION DAMAGE STUDIES THROUGH MICROSCOPY AND STRESS ANALYSIS

Ronak Patel

*Virginia Commonwealth University*

Follow this and additional works at: <http://scholarscompass.vcu.edu/etd>

 Part of the [Engineering Commons](#)

© The Author

---

Downloaded from

<http://scholarscompass.vcu.edu/etd/1620>

This Thesis is brought to you for free and open access by the Graduate School at VCU Scholars Compass. It has been accepted for inclusion in Theses and Dissertations by an authorized administrator of VCU Scholars Compass. For more information, please contact [libcompass@vcu.edu](mailto:libcompass@vcu.edu).

School of Engineering  
Virginia Commonwealth University

This is to certify that the thesis prepared by Ronak R. Patel entitled CORROSION DAMAGE STUDIES THROUGH MICROSCOPY AND STRESS ANALYSIS has been approved by his committee as satisfactory completion of the thesis requirement for the degree of Master of Science in Mechanical Engineering.

---

Ramana Pidaparti, Ph.D., Committee Chair, School of Engineering

---

Karla Mossi, Ph.D., School of Engineering

---

Manu Mital, Ph.D., School of Engineering

---

Mohamed Gad-el-Hak, Ph.D., Chair, Mechanical Engineering, School of Engineering

---

Rosalyn S. Hobson, Ph.D., Associate Dean of Graduate Studies, School of Engineering

---

Russell D. Jamison, Ph.D., Dean, School of Engineering

---

F. Douglas Boudinot, Ph.D., Dean, School of Graduates Studies

---

Date

© Ronak R. Patel 2008

All Rights Reserved

# **Corrosion Damage Studies Through Microscopy and Stress Analysis**

A thesis submitted in partial fulfillment of the requirements for the degree of Master of Science in Mechanical Engineering at Virginia Commonwealth University.

by

RONAK R. PATEL  
Bachelor of Engineering in Mechatronics Engineering  
S.P. University, Gujarat, India, Jan 2004

Director: RAMANA M. PIDAPARTI, PH.D  
DEPARTMENT OF MECHANICAL ENGINEERING

Virginia Commonwealth University  
Richmond, Virginia  
December, 2008



## **Acknowledgement**

First I would like to thank my advisor, Dr. Ramana Pidaparti, for his excellent advice, persistence, and patience over the last years. His guidance and support helped me immensely as I neared the completion of this thesis.

I would like to thank Dr. Karla Mossi and Dr. Manu Mital for their time and willingness to serve as members of my thesis advisory committee.

I would also like to thank the Engineering School of Virginia Commonwealth University, for giving me opportunity to pursue Masters Education in Mechanical Engineering. I would like to thank Dr. Kenneth J. Wynne for allowing me to use the AFM for my research. I would like to thank Kittisak Koombua for his continuous help and support during the research.

On the personal note, I would like to thank my parents and my brother for their constant love and support through many years of school.

This research work is supported by the U.S. National Science Foundation through a Grant DMR-0505039.

## Table of Contents

	Page
Acknowledgements .....	ii
List of Tables .....	v
List of Figures .....	vi
Nomenclature .....	ix
Abstract .....	x
<b>Chapter</b>	
1 Introduction .....	1
1.1 Motivation .....	1
1.2 Objective of Study .....	4
1.3 Outline .....	5
2 Introduction to Corrosion .....	6
2.1 Corrosion Principles .....	6
2.1.1 Factors affecting choice of engineering material .....	6
2.1.2 Corrosion Resistance .....	8
2.1.3 Electrochemical Aspect of corrosion .....	9
2.1.4 Environmental Aspect .....	13
2.1.5 Metallurgical Aspect.....	15
2.2 Types of Corrosion .....	18
2.3 Corrosion Detection Technique .....	23
2.3.1 Electrochemical technique of corrosion detection.....	25

2.3.2	Optical Microscopy .....	26
2.3.4	Atomic Force Microscopy .....	28
2.4	Effect of Corrosion on the Material life .....	30
3	Experiments .....	36
3.1	Sample Preparation.....	36
3.2	Experimental Protocols.....	38
3.3	Experimental Setup.....	39
3.4	Experimental Results.....	42
3.4.1	Corrosion Experimental Results.....	42
3.4.2	Optical Microscopy Results.....	47
3.4.3	Atomic Force Microscopy Results .....	58
4	Stress Analysis of Corrosion.....	71
4.1	Developing a Model from an Image.....	71
4.2	Finite Element Analysis for AA2024 and SS316.....	74
4.2.1	Corrosion Specimens under Bending Loading.....	77
4.2.2	Corrosion Specimens under Tension Loading.....	85
4.2.3	Corrosion Specimens under Shear.....	92
4.3	Comparison of maximum stresses in AA2024 and SS316 Specimen..	99
5	Conclusion .....	104
	References.....	110

## List of Tables

	Page
Table 2.1: Chemical composition of Al2024 and stainless steel type 316.....	8
Table 3.1: Experimental conditions for Al2024 and stainless steel type 316 .....	41
Table 3.2: Surface roughness from AFM for Al2024 and Stainless Steel type 316 .....	63
Table 3.3: Summary of the experimental and microscopy results for AA2024 specimen	69
Table 3.4: Summary of the experimental and microscopy results for SS316 specimen...	70
Table 4.1: Geometry of model and types of loadings for AA2024 and SS316 specimens	75
Table 4.2: Boundary conditions for different types of loading.....	76

## List of Figures

	Page
Figure 2.1: Factors affecting choice of an engineering material.....	7
Figure 2.2: Factors affecting corrosion resistance of a metal .....	9
Figure 2.3 Electrochemical nature of stainless steel in salt water.....	10
Figure 2.4: Electrochemical nature of aluminum alloy in salt water .....	12
Figure 2.5: Types of corrosion.....	19
Figure 2.6: Working principle of Electrochemical cell.....	26
Figure 2.7: Working Principle of Optical Microscope. ....	27
Figure 2.8: Working Principle of Atomic Force Microscope. ....	29
Figure 2.9: Corrosion fatigue model.....	31
Figure 2.10: Degree of deterioration that takes place on the metal during pit initiation and during growth.....	33
Figure 3.1: Experimental Protocol.....	39
Figure 3.2: Experimental Setup .....	40
Figure 3.3: Variation of current with respect to time for AA2024 specimen .....	43
Figure 3.4 Variation of current with time for SS316 specimen.....	45
Figure 3.5: Predicted corrosion rate for Al2024 and SS316 specimens from experimental results .....	46
Figure 3.6: Optical microscopy images of AA2024 specimen at different corrosion times. .....	49
Figure 3.7: Optical microscopy images of SS316 specimen at different corrosion times	54

Figure 3.8: AFM images of Al2024 at different corrosion time .....	59
Figure 3.9: AFM images of SS316 at different corrosion time .....	65
Figure 4.1: Developing a model form a height image of total corrosion time $t = 90$ minutes for Al2024 .....	72
Figure 4.2: Geometry of the model used Stress analysis .....	73
Figure 4.3: Mesh Convergence test.....	77
Figure 4.4: Von-Mises stress distribution on the model surface at different corrosion time for AL2024 under bending.....	79
Figure 4.5: Maximum von-Mises stress predicted from finite element analysis for corroded Al2024 sample at various corrosion time under bending.....	81
Figure 4.6: Von-Mises stress distribution on the model surface at different corrosion time for SS316 under bending.....	83
Figure 4.7: Maximum von-Mises stress predicted from finite element analysis for corroded SS316 sample at various corrosion time under bending .....	84
Figure 4.8: Von-Mises stress distribution on the model surface at different corrosion time for Al2024 under tension loading .....	87
Figure 4.9: Maximum von-Mises stress predicted from finite element analysis for corroded Al2024 sample at various corrosion time under tensile loading.....	88
Figure 4.10: Von-Mises stress distribution on the model surface at different corrosion time for SS316 under tensile loading.....	90
Figure 4.11 Maximum von-Mises stress predicted from finite element analysis for corroded SS316 sample at various corrosion times under tensile loading.....	92

Figure 4.12: Von-Mises stress distribution on the model surface at different corrosion time for AA2024 under shear loading.....	93
Figure 4.13: Maximum von-Mises stress predicted from finite element analysis for corroded Al2024 sample at various corrosion time under tensile loading.....	95
Figure 4.14: Von-Mises stress distribution on the model surface at different corrosion time for SS316 under shear loading.....	96
Figure 4.15: Maximum von-Mises stress predicted from finite element analysis for corroded SS316 sample at various corrosion times under shear loading.....	98
Figure 4.16: Maximum predicted stresses for AA2024 and SS316 specimens at different corrosion time for different types of loading. ....	100

## Nomenclature

I .....	Current (amp)
$i_{\text{corr}}$ .....	Current Density ( $\text{amp}/\text{cm}^2$ )
A .....	Area of the sample
CR .....	Corrosion Rate ( $\text{mm}/\text{year}$ )
EW .....	Equivalent Weight
$\rho$ .....	Density ( $\text{gm}/\text{cm}^3$ )
K .....	Constant ( $\text{mm}/\text{amp.cm.year}$ )
E .....	Modulus of Elasticity (MPa)
P .....	Pressure (MPa)
$\gamma$ .....	Poisson ratio (unit less)



# **Abstract**

## **CORROSION DAMAGE STUDIES THROUGH MICROSCOPY AND STRESS ANALYSIS**

By Ronak R. Patel

A thesis submitted in partial fulfillment of the requirements for the degree of Masters of Science at Virginia Commonwealth University.

Virginia Commonwealth University, 2008

Major Director: Ramana M. Pidaparti, Ph.D.  
Professor, Mechanical Engineering

Corrosion is the destructive result of chemical reaction between a metal or metal alloy and its environment. Airplanes, power generating plants, chemical process and manufacturing plants, concrete structure, and many others which widely uses aluminum alloy and stainless steel alloys are subjected to corrosion. The estimated cost of corrosion damage is in order of 3 to 5 percent of gross national product (GNP). Out of all forms of corrosion, pitting corrosion is most commonly observed in aluminum alloy 2024 and stainless steel type 316. There is a need to study the stress environment around the pits in order to predict the nucleation of the crack. The objective of this thesis is to investigate the

correlation between pits and stresses in AA2024 and SS316 alloys under different types of loading. Corrosion experiments were carried out on both alloys samples for a fixed time interval and were imaged on optical and AFM. The optical microscope provided the information on forms of corrosion expected on the surface while the AFM provided the pit profile on the surface. An analysis procedure was developed using CAD and finite element analysis to predict stresses resulting from corrosion pits under different types of loadings.

The average corrosion rate of AA2024 is six times higher than that of SS316 in 2 Molar NaCl corrosive environment. Based on the results from the optical microscope, AA2024 usually initiated with localized corrosion along with pitting and localized regions grows in size and soon uniform corrosion is observed. However, the stainless steel SS316 usually initiated with pitting corrosion and soon followed by film forming corrosion. Based on the analysis, it was observed that the stress distribution and levels on the corroded surface varied due to irregularities in the corrosion process. From the stress analysis result of AA2024 under bending, it was observed that there was 80% stress increase during first 30 min of corrosion and then the increase was about 6% from 30min to 60 min and then soon reaches a plateau. Similar results were obtained for both AA2024 and SS316 materials under different type of loadings. Initially, the stress increases sharply as time increases but the amount of stress increase demises as time progress and soon reaches a plateau. There was a sharp increase of Bending and shear loading are induces higher level of stresses compared to tension loading. From these stresses it is possible to estimate the initiation of crack, from which the life can be estimated for failure in the material.

# Chapter 1 Introduction

## 1.1 Motivation

Corrosion is the degradation of the metallic structure at its surface through chemical reaction of the metal with the species of the environment. The serious consequences of corrosion process have become a problem of worldwide significance. Practically every environment is corrosive to some extent. For examples air and moisture; fresh, salt and mine waters; rural, urban and industrial atmospheres; steam and other gases like chlorine, ammonia, hydrogen and fuel gases; mineral acids such as hydrochloric, sulfuric and nitric acid. The corrosion damage is not just limited to the appearance of the product but some time it can lead to catastrophic corrosion damage if ignored. For examples; sewer explosion in Mexico in 1992, loss of USAF F16 Fighter aircraft, Aloha aircraft incident in 1992 [1]. In 1995, the cost of corrosion for United States was almost \$300 billion per year [2]. This cost includes the plant downtime, loss of the product, loss of efficiency, contamination and over design by engineers. It was also found that 60% of the cost is unavoidable and remaining 40% of the cost is avoidable [2].

Corrosion control can be achieved by recognizing and understanding corrosion behavior of the material. Corrosion process is dependent on many parameters such as environment, temperature, metallurgical and chemical property of metals [3]. In this

particular thesis aluminum alloy 2024-T3 and stainless steel type 316 are studied for corrosion as these materials are widely used in aerospace, naval, civil and nuclear engineering due to low cost, low density and provide high resistance to corrosion. These materials are subjected to pitting corrosion and film forming corrosion due to presence of numerous constituent particles, which plays important role in corrosion pit and film formation. These film produce due corrosion are weak and can breakdown to form further some pits. Pitting form of corrosion is known to be one of the major damage mechanisms which affect the integrity of these materials and cause failure in some cases. To better understand the particle-induced pitting corrosion in these materials surface, optical microscopy, Scanning Electron Microscopy (SEM), Transmission Electron Microscope (TEM) and Atomic Force Microscopy (AFM) technique have being used.

The effects of corrosion on the life of the product have being studied over years but it's still based on the traditional theory. Ideally the life of the product is calculated on the bases of the crack initiation and crack propagation life [4-6]. Usually the crack propagation life is longer than the crack initiation life. Usually the product is replaced when it reaches maximum limit of crack size for failure but in some special cases where the safety and health of the people is concern the product is replaced before using crack propagation life. In these cases, corrosion fatigue crack initiation life plays a vital role to determine the life of the product. Corrosion fatigue generally starts with pitting and crack formation and ends with propagation of the crack initiated at the base of the pits. Thus, pitting directly activates the crack initiation. Corrosion will produce pits on the surface which can form crack from further corrosion or by fatigue. So effect of corrosion plays important role in

predicting crack initiation life. Corrosion pits generally initiate due to some chemical or physical heterogeneity at the surface such as inclusion, second phase particles, flaws, mechanical damage or dislocations. Many researchers have studied pitting corrosion for several decades and the details can be found in several books [1-3, 7-9]. The corrosion mechanisms depend on the material composition, electrolyte and other environmental conditions [7-9].

Many researchers are studying of corrosion based on electrochemical aspects, environmental effects and metallurgical aspects [10-14]. Several local probe technique based on electrochemical measurement at the metal surface have been applied to predict the spatial distribution of either potential or current and to quantify the corrosion rate. The electrochemical probe technique includes Scanning Reference Electrode Technique (SRET), Scanning Vibrating Electrode Technique (SVET), and Localized Impedance Spectroscopy (LEIS) [15-18]. In addition, various physical probe based on near field microscopy (SEM, AFM and STM) have been applied to quantitatively evaluate the local corrosion damage. Recently, Oltra and Vignal [15] have studied the effect of inclusion under straining of the surface preparation on the pitting sensitivity of stainless steel based on a combination of the local electrochemical measurement with finite element analysis. Currently there are no probing techniques which describe the stress environment around corrosion pits, which are responsible for stress corrosion cracking.

In order to predict the nucleation of cracks resulting from corrosion pits, there is a need to obtain the stress environment around the pits. Therefore, there is a need to investigate the pit induced stresses responsible for possible crack initiation using the AFM

images of the corroded specimens using finite element analysis. The analysis was performed using different types of loading to investigate stress distribution as a function of corrosion in order to obtain the correlation between them.

## **1.2 Thesis Objective**

The objective of this thesis is to investigate corrosion pit morphology through microscopy and to estimate the stress around the pits during corrosion growth process under different loading. To achieve this objective two different kinds of materials (aluminum alloy AA2024-T3 and stainless steel type 316) are considered. First the materials were corroded in the controlled environment (2 Molar NaCl solution) for specific time and then were imaged under by using optical and Atomic Force Microscopy techniques. This process is repeated again for further corrosion time.

The corrosion pit morphology is studied using Optical and Atomic Force Microscopy and results of both materials are compared to predict the forms of corrosion that can occur on the materials surface under this type of corrosive environment. To predict the stress acting on the surface due to corrosion, the AFM images of the corroded samples are converted to solid models for that particular time period using CAD and Rhinoceros software. The finite element analysis is performed on the model under different types of loading condition using ANSYS software.

The result of finite element analysis is used to predict the maximum stress in AA2024 and SS316 specimens at different corrosion time. The maximum stresses induced for different type of loading are compared for both materials.

### **1.3 Outline**

This thesis is organized as follows. Chapter 2 provides an introduction to corrosion in general. It expands on type of corrosions which describe what type of corrosion is expected to happen on a material at specific environmental condition. An overview of the corrosion detection techniques which were used during the research is also provided. The effect of corrosion on the fatigue life is also discussed.

Chapter 3 presents experimental approach for the research. The sample preparation and experimental setup have being described. The experimental protocols and troubleshooting have being described. This chapter concludes with the results from analysis, optical and atomic force microscopy.

Chapter 4 presents the stress analysis of the corrosion damage. It details the entire process how the model is made from a corroded AFM image using rhinoceros software. The finite element analysis is performed on these models under different loadings such as bending, tension and shear.

Chapter 5 will discuss the conclusion and Recommendations for future work.

## **Chapter 2 Introduction to Corrosion**

The corrosion principles and different aspects of corrosion are very important in understanding corrosion. Study of different types of corrosion is vitally important as it will help to predict the types of corrosion under different corrosive environment. There are different types of corrosion detection technique based on the types of corrosion. The accuracy of the corrosion detection depends upon the technique. This chapter will explain the corrosion principles and how corrosion affects the materials.

### **2.1 Corrosion Principles**

#### **2.1.1 Factors affecting choice of engineering material**

To view corrosion engineering in its proper perspective, it is necessary to remember that the choice of material depends upon many factors. Figure 2.1, shows some of the properties which determine the choice of a structural material. The corrosion resistance and cost of the material are the most important properties in most of the engineering application [4]. In some case like architectural applications, appearance is also a vital factor for choice of material. Fabricability, which includes the ease of forming, welding, and other mechanical operations must also be considered. In engineering applications, strength or mechanical behavior is most important factor and has to be considered even though the material is being selected for its corrosion resistance.



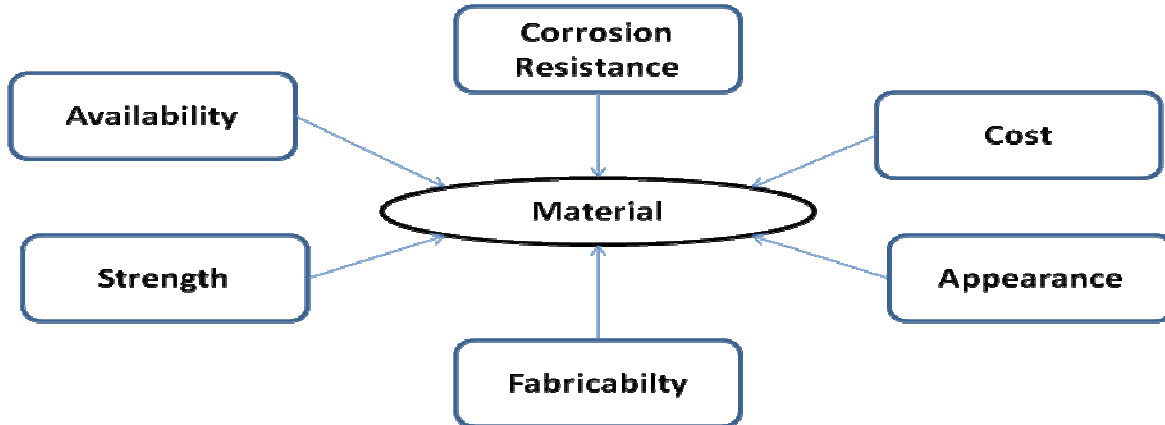


**Figure 2.1: Factors affecting choice of an engineering material [3]**

In this particular thesis, aluminum alloys AA2024 and stainless steel alloy SS316 are selected for corrosion study. The chemical compositions of these materials are defined in Table 2.1. AA2024 is mainly consisting of aluminum element with little traces of copper, magnesium and molybdenum metals. Adding of these elements in small amount will improve the microstructure, strength and corrosion resistance of the alloy. Similarly the stainless steel type 316 is majorly consisting of iron, chromium, nickel, magnesium and molybdenum metals. The chromium is added to steel to improve the corrosion resistance because when corroded, it forms a film on the surface which reduces further corrosion by isolating the atoms on the surface from corrosion environment. Small amount of carbon is added to the steel to improve the surface hardness of the steel. Nickel, magnesium and molybdenum improve the strength of the steel.

**Table 2.1: Chemical composition of AA2024 and stainless steel type SS316 [19]**

<b>AA2024</b>	
<b>Elements</b>	<b>Weight %</b>
Al	93.5
Cu	4.4
Mn	0.6
Mg	1.5

<b>Stainless steel type 316</b>	
<b>Elements</b>	<b>Weight %</b>
Fe	62.045-72.0
Cr	16.0-18.0
Ni	10.0-14.0
Mo	2.0-3.0
Mn	2
Si	1
C	0.08
P	0.045
S	0.03

### 2.1.2 Corrosion Resistance

Corrosion resistance or chemical resistance depends upon many factors. Its complete and comprehensive study requires knowledge of several fields of scientific knowledge as indicated Fig.2.2. Thermodynamics and electrochemistry are of great importance for understanding and controlling corrosion.

Thermodynamic studies and calculations can determine whether the corrosion is theoretically possible and can also predict the direction of spontaneous reactions [2]. Electrochemistry studies can help to understand how exactly the corrosion process takes

place between the material and environment. Metallurgical factors frequently have a pronounced influence on corrosion resistance. In many cases, the metallurgical structure of alloy can be controlled to reduce the corrosive attack [3]. Physical chemistry can be useful to study the mechanism of corrosion reactions, surface condition of metals and other basic properties [8].

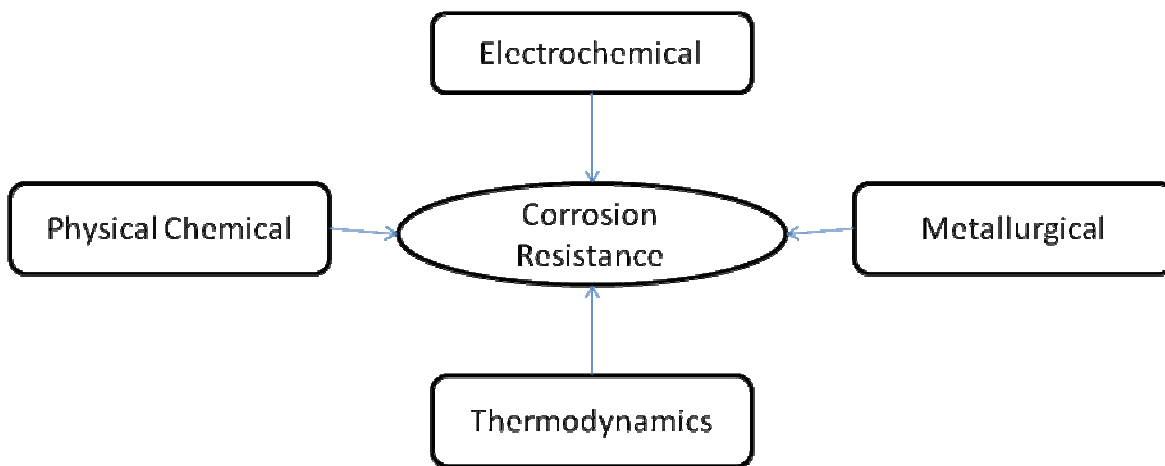


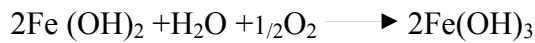
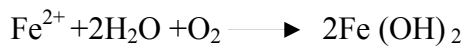
**Figure 2.2: Factors affecting corrosion resistance of a metal [3]**

### **2.1.3 Electrochemical Aspect of corrosion**

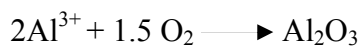
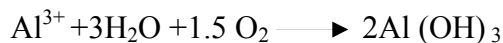
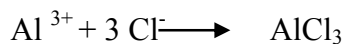
Corrosion is thermodynamically possible for most environmental conditions. Thus it is primary importance to know how fast corrosion occurs. Most of the alloys corrode slowly in many environments [7]. As new technology demands higher operating conditions for aircraft, automobiles, and energy generation, and manufacturing applications, corrosion rates are forced to a higher level.



Some ions of iron and chromium will react with the water and atmospheric air to form chromium oxide and ferric salt (ferric oxide). However, first the iron will form ferrous hydroxides but this component is unstable in oxygenated solution and so it will further oxidize to form ferric salt. The chromium oxide forms a passive film on the surface which reduces the rate of the further corrosion by providing the passivity to the stainless steel.



The electrochemical nature of corrosion in aluminum alloy AA2024 in salt water is shown in Fig 2.4. Aluminum alloy AA2024 is majorly consist of aluminum metal. When AA2024 is corroded in salt water in presence of oxygen, the aluminum ions are formed on the surface. There is a presence of chloride ions in the water which react with these ions and can form aluminum chloride ( $\text{AlCl}_3$ ). Aluminum ions can also react with water in presence of oxygen can oxidize to form aluminum hydroxides or it can react with oxygen and form aluminum oxide



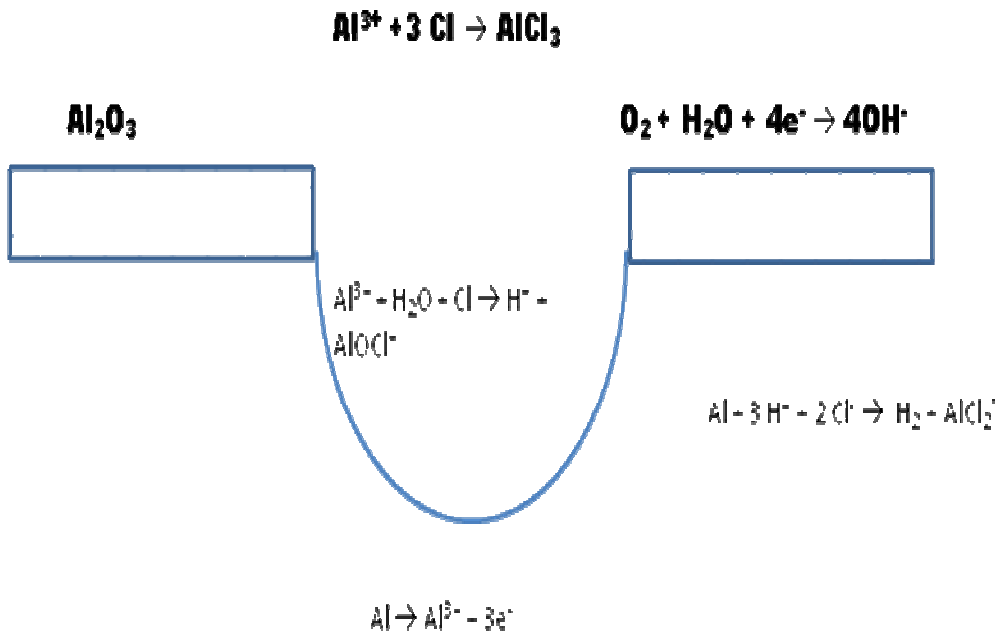


**Figure 2.4: Electrochemical nature of aluminum alloy in salt water.**

Chloride imposes severe localized corrosion damage to AA2024 at the defect sites on the surface like pitting and oxides film formation. The interaction of the chloride and alloy surface is crucial as the chloride influences the oxide film composition and structure which is crucial in corrosion invitation process as ions at the oxides films play a deterministic role in passive film stability.

The rate of electrochemical reaction is limited by various physical and chemical factors [3]. Hence, an electrochemical reaction is said to be polarized or retarded by environmental factors. Polarization can be divided into two different types, activation polarization and concentration polarization. Activation polarization refers to an electrochemical process which is controlled by the reaction sequence at the metal-

electrolyte interface [3]. Basically it covers entire process how the metal react with hydrogen ions to create the metal ion and hydrogen molecule, then these molecules combine to form a bubble of hydrogen gas when a metal is reacted with water. Concentration polarization refers to electrochemical reactions which are controlled by the diffusion in the electrolyte [3]. The number of hydrogen ions in the solution is quite small, and reduction rate is controlled by the diffusion of hydrogen ions to the metal surface. In most of the cases the reduction rate is controlled by the process occurring within bulk solution rather than at the metal surface [2]. Activation polarization is usually the controlling factor during corrosion in highly concentrated acids.

Passivity is also important factor in study of corrosion. In many metals like iron, nickel, chromium, titanium, and cobalt, corrosion rate decreases above some critical potential [3]. This corrosion resistance above the critical potential needs a high driving force for further corrosion, is defined as passivity [2]. Passivity is caused by formation of a thin, protective, hydrated oxide, corrosion-product surface film that acts as a barrier to the anodic dissolution reaction. Passivity does have some disadvantage like the passive film is thin and often fragile; its breakdown can result in unpredictable localized forms of corrosion, including pitting, corrosion in crevices and embrittlement by stress corrosion cracking [3]. Chromium is a key alloy element forming resistant passive oxide films on the surface. However, chromium cannot be used alone because of its brittleness.

#### **2.1.4. Environmental Aspect**

Environment plays an important factor in the corrosion process. There are many factors in which controlled the environment like oxidizers, velocity of oxidizers, change in

temperature and change in corrosive concentration [3]. If any one of the variables in environment is changed then the rate of the corrosion changes, which can be predictable. If two or more variables of the environment are changed simultaneously then a complex behavior may be observed and prediction can be difficult.

The effect of oxidizer in the corrosion process is very complex. Knowledge of basic characteristics of a metal or alloy is essential to understand the rate of the corrosion. For normal metal like copper and Monel which don not passivate, when the oxidizers are increased then the corrosion rate also increases but too some extent followed by a rapid decrease [7]. Then the corrosion rate is independent of oxidizer concentration, is a characteristic of both active-passive metal. For passive metals like stainless steel which have tendency to produce a passive film to resist corrosion, initially when oxidizer is increased then rate of corrosion increase but after production of the passive film there is a sudden decrease in corrosion rates [7]. However, if the oxidizer is increased to overcome its critical potential then the corrosion rate increases again followed by a rapid decrease due to transpassive effect [2].

The effect of velocity of the oxidizer also plays a vital role in determining the corrosion rate. For corrosion processes which are controlled by activation, polarization, agitation and velocity have no effect on the corrosion rate. If the corrosion process is under cathodic diffusion control, then agitation increases the corrosion rate, this effect is generally occurs when an oxidizer is present in very small amounts, as is the case for dissolved oxygen in acid or water [4,7]. But if the process in under diffusion control and metal is readily passivated, then the rate of corrosion increases initially followed by a rapid



decrease and then effect of velocity no longer affect the rate of corrosion. If the material is exposed to extremely high corrosive environment, mechanical damage or removal of these passive films can occur, resulting in an accelerated attack in corrosion rate [2].

As the temperature increase the rate of almost all chemical reactions also increases. In a corrosion process, temperature is important parameter but it is also dependent on the material properties [2-3, 11]. For example; in metals like Nickel and Monel, the rate of corrosion increases rapidly or exponential and in stainless steel there is a negligible effect of temperature initially followed by a rapid rise in corrosion rate with increase in temperature.

The effect of corrosive concentration on the corrosion process is simple and predictable. If the concentration of the corrosive concentration increases then the hydrogen ions which are active species in the acid concentration also increases and thus accelerating the rate of corrosion [1-3, 11]. However, as the acid concentration is increased further, a corrosion rate reaches a maximum and then decreases. This is mainly due to the fact that a very high concentration of acids ionization is reduced.

#### **2.1.5. Metallurgical Aspect**

Metals and alloys are crystalline solids. That is, atoms of metal are arranged in a regular, repeating array. The three most common crystalline arrangements of metal are; body-centered cubic, face-centered cubic and hexagonal close packed lattice structure [1-3, 20]. Metallic properties may differ from those of other ceramics and chemical salts. They are ductile and are good conductor of electricity and heat. These properties results from the non-directional bonding of the metals – each atom is bonded to many of its neighbors.

When a metal solidifies during casting the atoms, which are randomly distributed in the liquid state, arrange themselves in a crystalline array. However, this ordering usually begins at many points in the liquid, and as these blocks of crystals or grains meet, there is a mismatch at their boundary. When the metal solidified and cooled there will be numerous region of mismatch between each grain. These regions are called grain boundaries. In most of the stable configuration of the metal is its particular crystal lattice, grain boundaries are high-energy areas and are more chemically active [3, 20]. Hence, the grain boundaries are less resistant to corrosion compared to grain itself.

Alloys are mixture of two or more metals or elements. There are two kinds of alloys- homogenous and heterogeneous. Homogenous alloys are solid solution that its components are completely soluble in one another, and the material has only one phase. Stainless steel is an example of homogeneous or solid-solution alloy, where the iron, nickel, chromium, and carbon are dissolved completely and the alloy has a uniform composition [1-3, 7-9]. The heterogeneous alloys are the mixture of two or more separate phases. The components of these alloys are not completely soluble therefore the composition and structure of these alloy are not uniform throughout the material [20]. Both types of alloys have certain advantages and disadvantages. Solid solution alloy are generally more ductile and have lower strength than the heterogeneous alloy. Homogenous alloy are more corrosion resistant than the alloys with two or more phases [5].

Very pure metal is more corrosive resistant than the any alloys. The formation of alloys is usually results in some impurities like; oxides and other inclusions, mill scale, orientation of grain, dislocation of array, differences in composition of the microstructure,

precipitated stresses, scratches, and nicks. These impurities can result in high energy areas and become more chemical active than other regions.

Aluminum alloy AA2024 has a complex microstructure due addition of alloying element and to the presence of impurities. The precipitation sequence of AA2024 alloy consists in the formation of GBP (Guinier-Preston-Bagaryatsky) zones at room temperature, which can be classified as a short-range ordering of the Cu and Mg solute atoms. After artificial ageing, these zones are dissolved and replaced by semi-coherent  $S''$  ( $Al_2CuMg$ ) precipitates. Finally, after long exposure times, stable S ( $Al_2CuMg$ ) phase are formed [20]. In AA2024, the alloying elements Mn and Cu are generally added to control grain structure and corrosion resistance. Copper (Cu) is added to improve mechanical resistance of the Al matrix. However, Copper together with other elements, also precipitates as bigger intermetallics (IMs), which attain high surface densities. The electrochemical activity associated with these intermetallics is different from the matrix, and gives rise to localized corrosion phenomena. Moreover, in their vicinity, the passive layer can be weaker and Cu depleted zones can be formed leading to localized attack of the matrix. For AA2024 alloy, it is generally accepted that Al-Cu-Mg (S-phase) intermetallics are initially anodic and become cathodic to the matrix due to selective corrosion of their noble constituent, namely Al and Mg, leaving nobler Cu-rich remnants that provoke the corrosion of the adjacent matrix [20]. Overall, AA2024 have heterogeneous composition and undergo heterogeneous composition that can occur in form of the pitting corrosion.

Stainless steel type 316 (SS316) alloy have duplex microstructure as there is presence of lot of elements in small concentration. The chromium and nickel are the

principal alloying elements in stainless steel, other element may be added for the specific purpose and therefore consideration must be given to the effort of these other alloying elements on the microstructure. The chromium and molybdenum promotes the formation of delta ferrite structure (BCC crystal structure) at the high temperature whereas the nickel and nitrogen promote the formation of austenite structure (FCC crystal structure) in the steel. The resulting microstructure is a favorable combination of the two phases and is called duplex microstructure [20]. There should be balance in composition of chromium and nickel, and other element like carbon, manganese and copper achieve the balance in formation of ferrite-austenite microstructure. The ferritic structure provides high immunity to chloride stress corrosion cracking (SCC) and the austenite structure provides high ductility to the steel. Molybdenum strengthens the passive film and improves the corrosion resistance. Carbides tend to precipitate at the disperse austenite-ferrite interfaces, preventing sensitization to the intergranular corrosion by grain boundary precipitation. However, the SS316 is still vulnerable to localized corrosion like pitting and film forming corrosion. The break-down of the passive film can form more pits on the surface.

## **2.2 Types of corrosion**

Figure 2.5 shows the different types of corrosion that can occur depending on the metals and corrosive environment. They are basically divided into two categories; uniform and localized form of corrosion. In uniform corrosion is the one in which the corrosion reaction starts at the surface and proceed uniformly. This type of corrosion is commonly observed in pure metals which are metallurgical and compositionally uniform. Atmospheric corrosion is probably the most common example of uniform corrosion at a

visual apparent rate. Uniform corrosion represents the greatest destruction of metal on a tonnage basis [21]. However uniform corrosion is preferred from a technical viewpoint because it is predictable and life of the product can be easily estimated by performing simple tests.

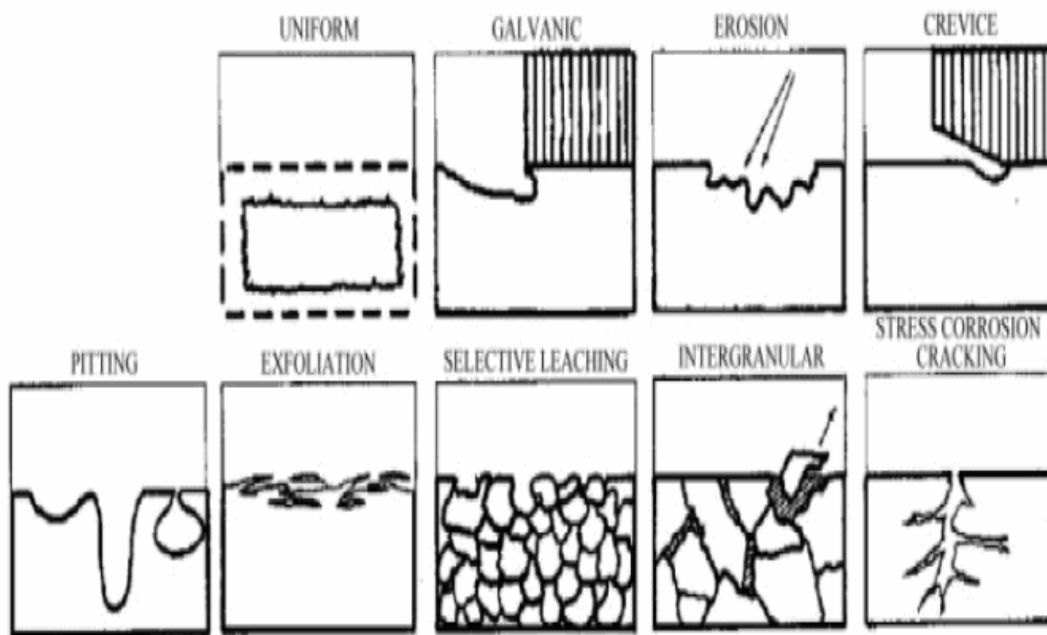


**Figure 2.5: Types of Corrosion [22]**

In localized corrosion there is an intense attack at localized sites on the surface of a component while the rest of the surface is corroding at much lower rate. Localized corrosion can further classified as pitting corrosion, galvanic corrosion, crevice corrosion, selective corrosion, erosion corrosion, intergranular corrosion and stress corrosion cracking (SCC).

Pitting is a form of extremely localized attack that results in holes or cavity in the materials. These holes can be small or large in diameter depending on the corrosive environment, but in most of the cases they are relatively small. Pits are sometime isolated or so close together that they look like rough surface. Pitting is particularly most vicious form of corrosion because it is localized and intense form of corrosion, and failures often occur with extreme suddenness [21-33]. However, the damage on the basis of weight loss is less compared to other types of corrosions [8]. It is often difficult to detect pits because of their small size and because the pits are often covered with corrosion products. Pitting corrosion is highly unpredictable because the location of pit and no of pits on the surface can vary for identical corrosion condition [25]. The stainless steels and nickel alloys with chromium are susceptible to pitting by local breakdown of the film at isolated sites.

Galvanic corrosion occurs when two dissimilar metals are immersed in a conductive solution in presence of some potential difference and there is a flow of electron between the metals. The metal which is less corrosive resistant becomes anode and metal with more corrosive resistance become cathode. The corrosion of the less corrosive resistance is usually increased and attack on more resistant material is decreased. This type of corrosion needs some electrolyte and electric current for the corrosion process, so it can be easily predictable. For example, loss of USAF F16 Fighter aircraft where the graphite grease used as a lubricant in a fuel valve due to its cost over molybdenum disulphide. Unfortunately, graphite grease is well known to cause galvanically induced corrosion in a bimetallic couple. Since the fuel valve was controlled by the electric power supply, the necessary current and electrolyte induced galvanic corrosion which results in

failure of the fuel valve. So it results in shut off of fuel line to aircraft engine in mid-flight [8].

Crevice corrosion is an intense localized form of corrosion usually associated with a stagnant solution on the micro environmental level [1-3]. This type of corrosion frequently occurs within the crevice and other shielded areas on the metal surface exposed to corrosives or with another material. This type of attack is usually associated with small volumes of stagnant solution caused by holes, gaskets surface, lap joints, surface deposits, and crevice under bolt and rivets heads [3]. Since this is localized form of corrosion it is very hard to predict this type of corrosion. For example, the aloha aircraft incident in 1988 where there was a continuous buildup of corrosion product between the lap joints, which leads to “pillowing,” by faying surfaces [11].

Selective leaching or selective corrosion is the removal of one element from a solid alloy by corrosion process [13]. The most common example is the selective removal of zinc in brass alloy whereby produced a weakened porous copper structure is produced. The selective removal of zinc can be in a uniform manner or localized scale. Similar process occurs in other alloy systems in which aluminum, iron, cobalt, chromium, and other elements are removed [3]. This type of corrosion is usually detected easily as the colored corrosion product form the surface. This type of corrosion is most commonly found in structural and architectural application. However this type of corrosion can't be ignored since removal of one of the element may result in drastic change in mechanical properties and its behavior.

Erosion corrosion is the cumulative damage induced by electrochemical corrosion reactions and mechanical effects from relative motion between the electrolyte and the corroding surface [21]. Metal is removed from the surface as dissolved ions, or it forms solid corrosion products which are mechanically swept from the surface. Erosion corrosion is found in the systems such as piping, valves, pumps, nozzles, heat exchangers, turbine and mills [3]. Erosion corrosion is characterized in appearance by grooves, gullies, waves, rounded holes, and valleys and usually exhibits a directional pattern. This is the most dangerous type of corrosion as it involves the corrosion along with high mechanical wear and tear. Many materials like aluminum, stainless steel and lead alloys are designed to develop a surface film of some sort to be more corrosive resistant [8]. Due to erosion corrosion this films are removed from the surfaces and impingement of corrosion pits are formed, which are subject to more corrosion and also act as stress raiser when the load is applied on them. The corrosion damage on the weight basis by this form is corrosion is high because of the most of the product is subjected to some kind of relative motion [8].

Stress corrosion cracking is the brittle failure at a relatively low constant tensile stress of an alloy exposed to a corrosive environment. Pure metal are comparatively resistant to stress corrosion cracking. In order to produce stress corrosion cracking three conditions must be present simultaneously; a critical corrosive environment, an alloy and some component of tensile stress [2]. The environment plays a vital factor as it is most acute corrosive environment which transforms the ductile alloy to brittle alloy. For examples; hot aqueous chloride solution readily crack stainless steel, brass in ammonia solution, carbon steel in nitrates.



Localized attack at and adjacent to grain boundaries, with relatively little corrosion on the grains, is intergranular corrosion [3]. This type of the corrosion is mostly observed at the reactive impurities which may segregates at the grain boundaries. As a result, the grain boundaries or adjacent region are often less corrosion resistant and preferential corrosion at the grain boundary may be severe enough to drop the grain out of the surface. The alloy might disintegrate and/or loses its strength. This type of corrosion is most expected to happen during manufacturing process at elevated temperature [2].

### **2.3 Corrosion Detection Technique**

Corrosion detection is usually the observation of the damage done by the corrosion on the material at any given time. There are many different kinds of technique to detect corrosion based on; surface morphology, chemical identification and composition, electrochemical polarization, and nondestructive material evaluation [7].

Nondestructive material evaluation (NDE) methods are primitive methods used for detection of corrosion. It includes dye penetrant testing, magnetic particle techniques, and conventional ultrasonic and industrial x-ray technique. These types of testing have a resolution in order of 0.1 mm [34]. These tests can detect the crack but detection and quantification of early stages of damage require high resolution. NDE are still in use for maintenance purpose, if the product is not subject to potential hazards or safety of the people.

Surface morphology or imaging technique is also commonly used to inspect or predict the corrosion. It includes optical, scanning electron, atomic force and scanning tunneling microscopy. These techniques will provide the details of the surface affected by

the corrosion like number of pits, pit size and their locations and roughness [9, 34]. Type of corrosion can also be predicted from the imaging technique due to high resolution.

Chemical identification and composition technique identify the elements which are present in the material and it also show it's atomic and weight percentage respectively. Energy dispersive x-ray spectroscopy, x-ray diffraction and auger electron spectroscopy are the example of chemical identification technique. These techniques will help to determine which element is most reactive to the environment and what kind of corrosion product is form on the surface. It can also determine the weight loss of overall material and element by corrosion [34].

Electrochemical technique is used in labs or for research in order to study the corrosion process in an artificial environment using an electrochemical cell. This technique is used whenever there is an electrochemical cell. The current in the electrochemical cell is studied by supplying the voltage to the cell. Based on the current, the corrosion rate is studied. This technique help in studies like sensitivity to low corrosion rate and well-established theoretical understanding of corrosion.

In this thesis the corrosion study is performed on the bases of electrochemical and imaging techniques. Electrochemical technique will help to provide the corrosion rate and the potential-current relationship will details how the corrosion process is proceeding. Imaging technique will determine what forms of corrosion are expected on the material and along with the surface characteristic like number of pit's, size and their locations. These surface details can be of further use to determine the maximum stress developed

during corrosion process. These stresses might be useful to predict the remaining life of the product after corrosion damage.

### **2.3.1 Electrochemical technique of corrosion detection**

In this method electrochemical cell is used to corrode the specimen in an aqueous solution by applying voltage to the cell. The electrochemical cell consists of electrolyte and three electrodes; working, reference and auxiliary electrodes as shown in Fig. 2.6. Sample which had to corrode has to be working electrode. Reference electrode was used to measure the working electrode potential. A reference electrode should have a constant electrochemical potential as long as no current flow through it [35]. Auxiliary electrode is a conductor that completes the cell circuitry. In this cell, the auxiliary electrode used was graphite. The electrolyte create environment for corrosion by providing ions. Ideally the electrode which is supposed to be corroded is kept as anode and potential voltage is supplied to cell in order to initiates the corrosion process.

Potential provides an indication of the tendency of metals to corrode, but it does not provide information on the rate of corrosion reaction. The rate of corrosion is proportional to the rate of electron transferred between the electrode and electrolyte. The rate of electron transfer is represented as current (I). The amount of current (I) per unit surface area (A) is the current density (i).

$$i_{\text{corr}} = I_{\text{corr}} / A$$

Based on Faraday's law the corrosion rate (CR) or can be calculated as

$$CR = I_{\text{corr}} \cdot K.EW / (\rho \cdot A)$$

Where  $K$  is constant and is equal to  $3272 \text{ mm}/(\text{amp.cm.year})$  for AA2024. The corrosion rate constant ( $K$ ) will change depending upon type of metal [35].

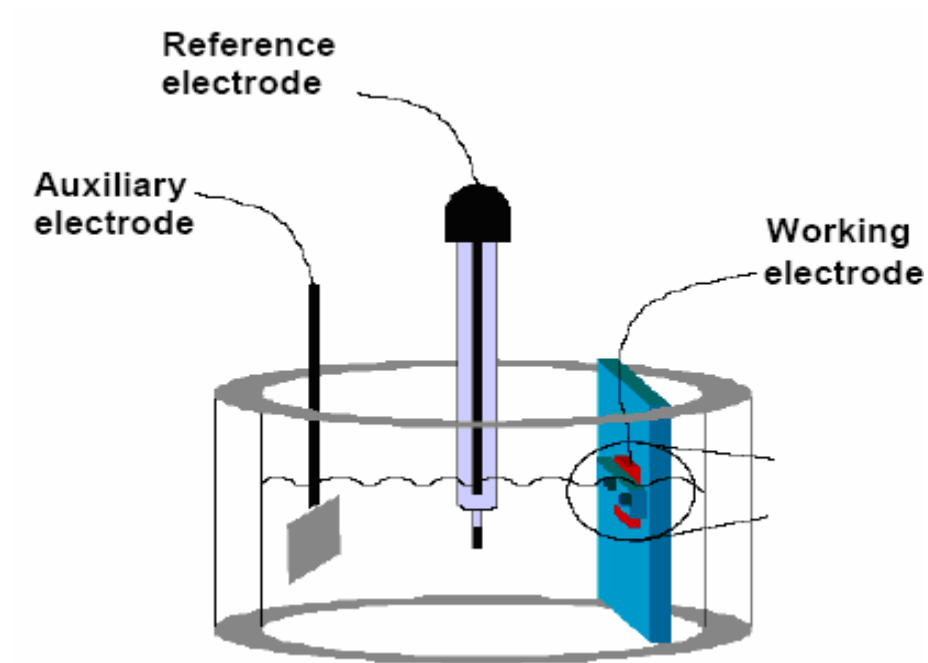


**Figure 2.6: Working principle of Electrochemical cell [35]**

### 2.3.2 Optical Microscopy

Reflective or inverted optical microscope is used for examining metals and other materials that cannot easily be made thin enough to be optically transparent. In this microscope the objective and the ocular are below the stage and the illumination is above the stage for transmitted light [20]. This is a primitive method used for the imaging, since its resolution is varies from millimeter to few hundred microns.

Working principle of reflective microscope is shown in Fig. 2.7; the image is formed by the light reflected from the surface of the specimen [20]. First, the light is emitted from the source to the half-silvered mirror which deflects the light to the sample through objective lens. This light is reflected back from the surface of the sample through the deflector's mirror, which passes the light to the eyepiece and image is appeared on the bases of variation of reflectivity on the surface. If the surface is smooth then it will provide little or no contrast compared to the uneven surface whose reflectivity varies from one location to other.

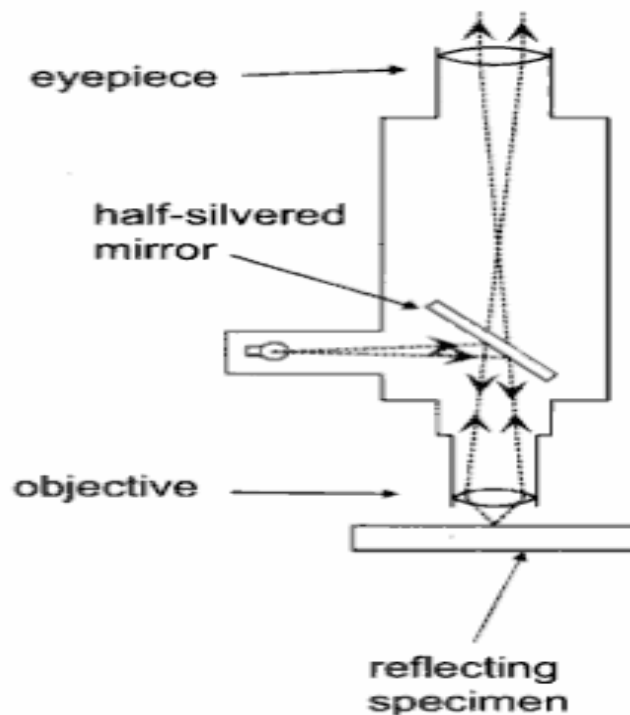


**Figure 2.7: Working Principle of Optical Microscope [20]**

### **2.3.4 Atomic Force Microscopy**

The atomic force microscopy (AFM) was invented in 1986 by Binnig and Quate recognized the need of microscopy technique that could examine insulating surface using a force mechanism [36, 37]. Using an ultra small probe tip at the end of the cantilever, the atomic force microscopy can achieve extremely high resolutions. Now, with the capability to micromachine such as levers, commercial instruments are available which uses lasers to detect the deflection. AFM is heavily relied tool for researcher and can be used to image conducting, insulating, and biological specimens [38-41].

The fundamental AFM design as shown in Fig. 2.8 consists of a micromachined cantilever that is brought into contact with a sample surface while the tip-sample force is monitored during scanning. The force is measured by reflecting a laser beam off the backside of the cantilever and monitored the beam's reflected position with a photodetector. As the cantilever bends due to the induced tip-sample forces, the laser moves on photodetector. [36, 37] There are two basic methods used to scan the sample surface: contact mode and tapping mode. In contact mode, the tip is always in contact with the sample and the feedback circuit maintains a constant tip-sample force as the sample is scanned. In this manner, the reflected laser beam is in a fixed position on the photodetector to reduce the errors. In tapping mode, the cantilever is vibrated at its resonance frequency while scanning. When the tip approaches the sample, it only touches the surface during the downward cycle of its oscillation. A feedback loop is used to control the tip-sample forces by maintaining a constant oscillation amplitude as surface is scanned [42].

## Atomic force microscopy

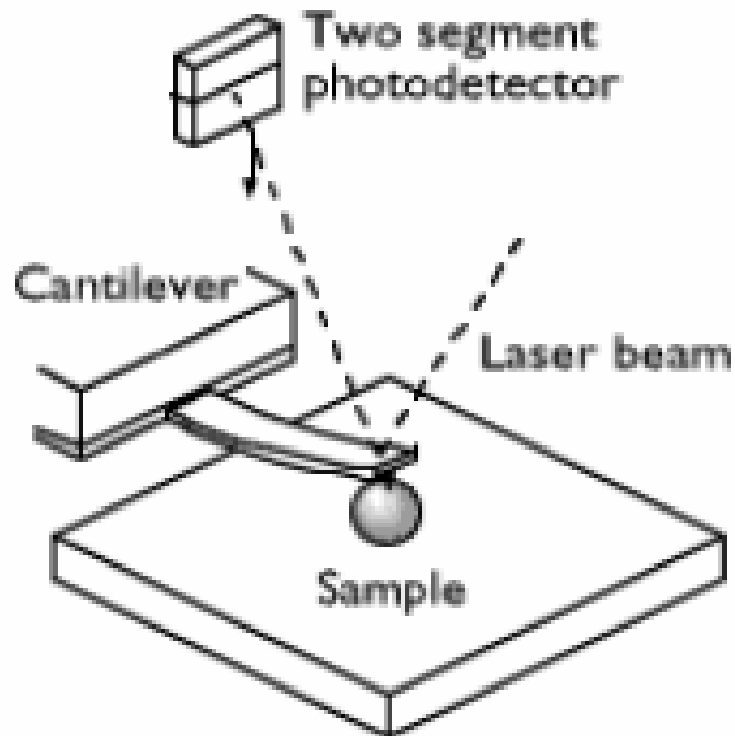


**Fig 2.8: Working Principle of Atomic Force Microscope [36]**

AFM have ability to provide height, phase and amplitude data's on one single scan. The height data is good measure of the height of the surface feature but does not show the distinct edges. The height data can be achieved by monitoring the vertical position of the probe tip is and noting changes in the length of the z-axis on the xyz-scanning probe. Phase data provide the information on differing elasticity on the sample surface. When probe tips engage with the sample surface, the phase of the offset of the oscillating cantilever changes

by some angle with respect to the phase offset of the input drive signal. As regions of differing elasticity are encountered on the sample surface, the damping experience by the probe tip will differ and results in the phase change between two signals. These differences are plotted as the so-called “phase image”. Amplitude data tends to show the edges of the surface features. There is sudden increase or decrease in the amplitude at the edges of the surface features which are continuously monitored by the photodiode detectors.

#### **2.4 Effect of Corrosion on the Material life**

For long time, the effect of corrosion was neglected in predicting the life cycle of the product. The life of the product was predicted on the basis of fatigue alone and effect of environment was neglected. It was assumed that the crack is initiated by the fatigue from large inclusion, flaws, mechanical damage or dislocations [4]. However, many researchers have proposed that effect of corrosion is also important in predicting the life of the product. The corrosion often results in pits, film forming and removal of the material from the surface. The presence of corrosion pits can significantly shorten the fatigue life crack initiation life and decrease the threshold stress intensity of an alloy by as much as 50% [28]. These imperfections usually act as a source of nucleation of the crack. Nucleation of crack can further form a crack either from fatigue or by further corrosion, this phenomena is called corrosion fatigue model [19, 43].



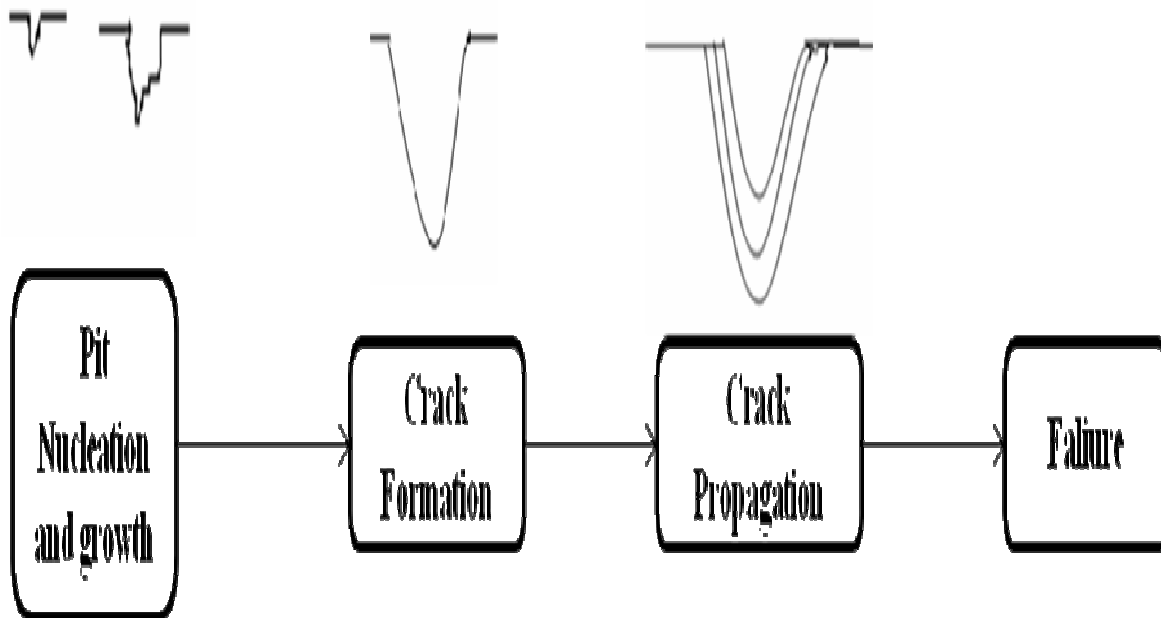


**Figure 2.9: Corrosion fatigue model.**

The corrosion fatigue model shown in Fig. 2.9 include the effect of both corrosion and fatigue in the predicting the life of the product [28]. The corrosion fatigue life usually starts from the nucleation of the pits and its growth. The pits almost anyway initiate at some chemical or physical heterogeneity at the surface, such as inclusion, second-phase particles, flaws, mechanical damage, or dislocation. For this particular model the pits are assumed to be initiated from the corrosion. These pits grow in a corrosive environment and form crack. This crack then propagates till the complete failure of the product. The dominating factor for crack propagation is fatigue, as the corrosion process is slow and it takes long time compared to fatigue to propagate the crack to its failure. The crack

initiation is due to combination of both fatigue and corrosion. The life of crack initiation is very important in some cases where safety and health of the people is concerned; the product had to be replaced as soon as the first crack is detected.

Pit nucleation and growth consist of three stages; Pit initiation, metastable pit stage and stable pit. Pit initiation is the first step of pitting in which the pits are formed on the surface due to corrosion or by the breakdown of the passive film on the alloy surface. The initiation of the pits can take place at random places depending upon the microstructure of the alloy. These initial pits require suitable environment to grow into stable pits. The stage where the pits may repassivate in case of unsuitable environment is known as metastable stage. If the proper conditions are satisfied, these initial pits grow into stable pits. These stable pits then grow and lead to deterioration of the whole metal as shown in Fig. 2.10. Stable pit growth, in which the pit propagates effectively indefinitely, is preceded by a metastable state. The metastable state of growth occurs while the pit is still very small, and its continued propagation to reach stable state is not guaranteed. Many metastable pits which do not achieve stability are not in themselves necessarily structurally damaging, although they affect surface finish on a microscopic scale. When the stable pits reach the detectable size then it is called crack.

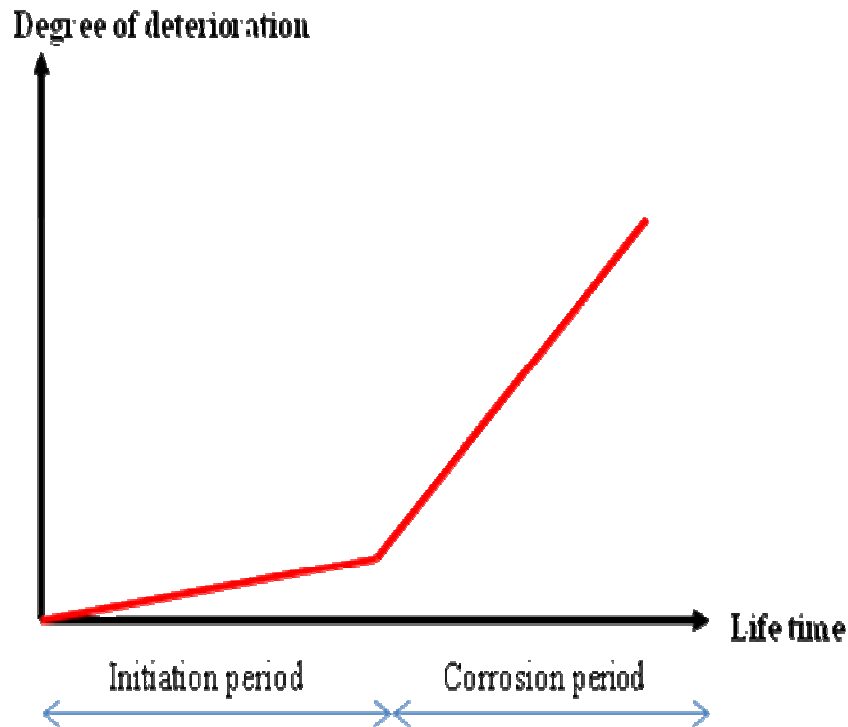


**Figure 2.10: Degree of deterioration that takes place on the metal during pit initiation and during growth.**

Wang et.al. [28], have proposed a analytical corrosion fatigue model where, the effect of both corrosion as well as fatigue was taken in study. According to him, the total life of the product of the life can be summation of crack initiation life and crack propagation life. The crack initiation life is assumed on the parallel bases of fatigue and corrosion effect. However, their model assumed that the crack is nucleated in the largest corrosion pits and other pits are ignored. Their model suggested that the pit size is varied as the cube root of the time or corrosion cycle. Ishihara et al.[24], have proposed similar corrosion fatigue model which suggests that the pits size is varied as function to time under

in an unstressed environment. However, their model assumed that the crack nucleation will be due to corrosion and effect of fatigue crack nucleation was neglected.

In a series of papers, Harlow and Wei [30-32] have developed a probabilistic model for the probabilistic model for the prediction of corrosion and corrosion fatigue life. Their model was based on the growth of a single dominant flaw from the pit to a small surface crack and then into a through crack. However, their model fail to include the fatigue crack nucleation, the nucleation of the crack was assumed due to corrosion. Rokhlin, Kim and Zoofan [33] have developed a fracture mechanics model for fatigue crack initiation and propagation from a single artificial and actual pits based on the two different stress intensity factors. However, their model fails to consider the effect of pit nucleation and growth. Zamber and Hillberry [44] developed a probabilistic approach for predicting fatigue life based entirely on crack propagation, the crack initiation life was assumed small compared with the total life and was neglected. This approach might lead to significant errors if both the applied cyclic loads and pitting corrosion levels are low.

Duquesnay, Underhill and Britt [45] have showed that the most important factor determining the corrosion fatigue life was the corrosion pit depth. Ishihara et al.[46], reported that the growth rate of corrosion pits increased with an increase in the stress amplitude. M. Jakubosi [43] developed a corrosion fatigue crack growth, where the crack growth rate is assumed to be proportional to current flowing through the electrolyte within the crack during a load cycle. This approach predicts the total corrosive fatigue crack growth rate in a corrosive environment rather than the environmental component of the total rate.

The most important factor which effect the life of the component is stress induced on the surface, stress concentration factor, pit depth [28]. However, there are no researches which determine the maximum stress developed on the corroded surface and how the stress distribution changes as corrosion take place. This thesis is trying to develop a local method which can predict the maximum stress developed on the corroded surface using Finite Element Analysis. This method will help to show how the stress distribution on the surface changes as corrosion occurs on the surface. Using this method, it's easy to predict the damage done on the surface stresses due to corrosion and this result can be used to calculate remaining life of the product.

## Chapter 3 EXPERIMENTS

Corrosion damage experiments were conducted in a controlled environment for specific amount of time. After the specimen is corroded for the specific time, the surface morphology was examined using AFM and optical microscope. The details about the corrosion experiments and the AFM results are presented in this chapter.

### 3.1 Sample Preparation

Two materials, aluminum alloy AA2024 and stainless steel 316(SS316) are considered in conducting corrosion damage experiments. Metal specimens of AA2024 and SS316, are first cut into samples of 3cmx 3cm. Initially, these samples are first inspected visually and optical microscopically for any imperfections on the surface, and if sample have imperfection then it is not taken for the study. Surface imperfections can act as source of initiation of corrosion due low corrosion resistance and it may create an artifact in the corrosion process. After selection of the sample with no imperfection on the surface, these samples are grinded and polished according to the material.

Aluminum alloy AA2024 samples are grinded on the grinding machine which uses emery papers as the rotor. To ensure the grinding is done in a smooth manner the sample are grinded with different grids of emery papers from rough to smooth. For AA2024 sample were grinded with 200, 500, 800 and 1200 grid emery papers. Initially, the sample was grinded with 200 grid emery papers at 60 rpm for about 2 minutes. Water is used as

coolant to remove the waste material. This process is repeated for other grid papers 500 and 800. When the sample is grinded with 1200 grid emery paper, the revolution on the emery paper is increased to 120 rpm and grinded for 4 minutes, this is to ensure that no sharp edges are left on the surface while grinding. After the grinding is completed, the samples were washed with fresh water and then dipped in the ethanol solution for complete removal of the waste from the grinded surface. Then the sample is polished using the polishing plates with 6 $\mu$ m and 1  $\mu$ m diamond spray. The rotation of the polishing plates is kept at 120 rpm and polished for 4 minutes on both plates. After polishing, the samples are washed with fresh water and are taken for further cleaning.

After the samples are polished, then the samples are cleaned using the ultrasonic cleaning machine. The samples were initially dipped in a diluted acetone solution, thereby to 70% ethanol solution and finally to distilled water for 15 minutes in each solutions. After completing the cleaning process, the samples were removed from the ultrasonic cleaning machine and were allowed to dry under air. Once the sample is completely dried, an area of 1mm x 1mm is selected for corrosion study and rest of area on the sample was coated with a paint. The coating of sample ensures that there is no corrosion on the sample surface except the selected region for the corrosion studies.

The preparation methods of stainless steel type 316 (SS316) samples are same as the AA2024 except using different grid emery papers (150, 400, 600, 800 and 1200) for grinding.

### 3.2. Experimental Protocols

Initially, different samples were considered for different times in a 5 molar NaCl corrosive environment but the results from optical imaging were random. Corrosion varied from one sample to another under identical corrosive environment. This effect may be due to change in metallurgical properties of the samples identical material. As we know that the corrosive resistant is dependent on many factors, so this resistance varies in same material. To avoid the randomness in the result, same sample was used for further corrosion. The goal of this study is to systematically study the corrosion with respect to time.

The elimination of different sample for different corrosion time helped to eliminate randomness in the optical imaging but there was a severe corrosion during 15minutes of corrosion process. This effect was due highly corrosive environment formed by the 5 molar NaCl electrolyte solutions when voltage was applied to the electrochemical cell. So it was difficult to predict the effect of corrosion with respect to time. To avoid rapid corrosion in the material, the corrosive environment was diluted to 2 molar NaCl solution in the electrochemical cell. A reference or set point is required to compare the images when comparing the images. So the sample is scanned with Optical and Atomic Force Microscopes before the corrosion to set a reference point.

The experimental protocol was defined to perform the experiment on both AA2024 and stainless steel type 316 samples. As shown in Fig.3.1, the sample is corroded in electrochemical cell. Then the sample is cleaned with distilled water in an ultrasonic cleaning machine for 15 min and then air dried. The corroded sample is imaged using



Optical Microscope and then followed by Atomic Force Microscope (AFM) for surface morphology during the corrosion process.

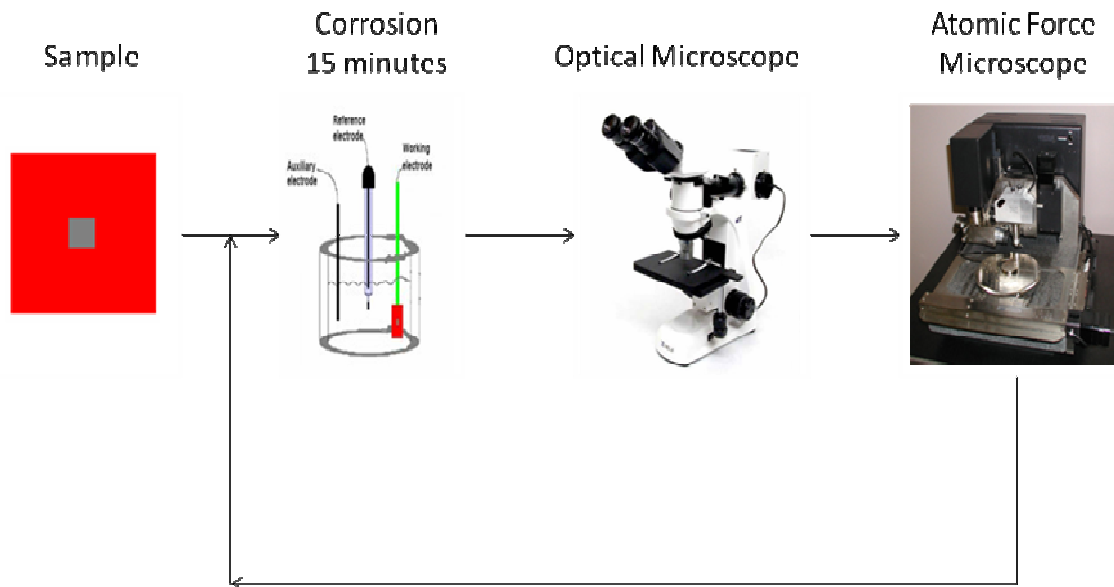


**Figure 3.1: Experimental Protocol**

After the sample is imaged using both microscopes, the sample is washed in distilled water in an ultrasonic cleaning machine for 15 minutes interval. A fresh 2 Molar NaCl electrolyte solution is made for the electrochemical cell. Sample is used again in electrochemical cell for further corrosion for 15 minutes. The same procedure is repeated again until total corrosion period is 2 hours.

### 3.3 Experimental setup

The experimental set up for performing the corrosion experiments using the corrosion cell is shown in Fig. 3.2. There are three different electrodes, First is working electrode which is connected to cathode (negative) of the power supply, other one is

auxiliary electrode which is connected to the anode (positive) of the power supply and third one is a reference electrode which is connected to the ground. The electrolyte solution used for the corrosion process is 2 molar NaCl. The corroded sample is connected to the working electrode and the auxiliary electrode is kept as graphite as it is good conductor of electricity. The reference electrode helps to complete electric circuit and maintain constant potential voltage in the corrosion cell. A sensor is connected to the cathode to monitor the flow of current during the experiment. The reason for connecting working electrode to cathode is that the sensor can only be connected to the cathode of the electric circuits. A resistor of  $10^6$  Ohms is connected between the anode and the power supply to avoid the voltage fluctuation in the electrochemical cell.

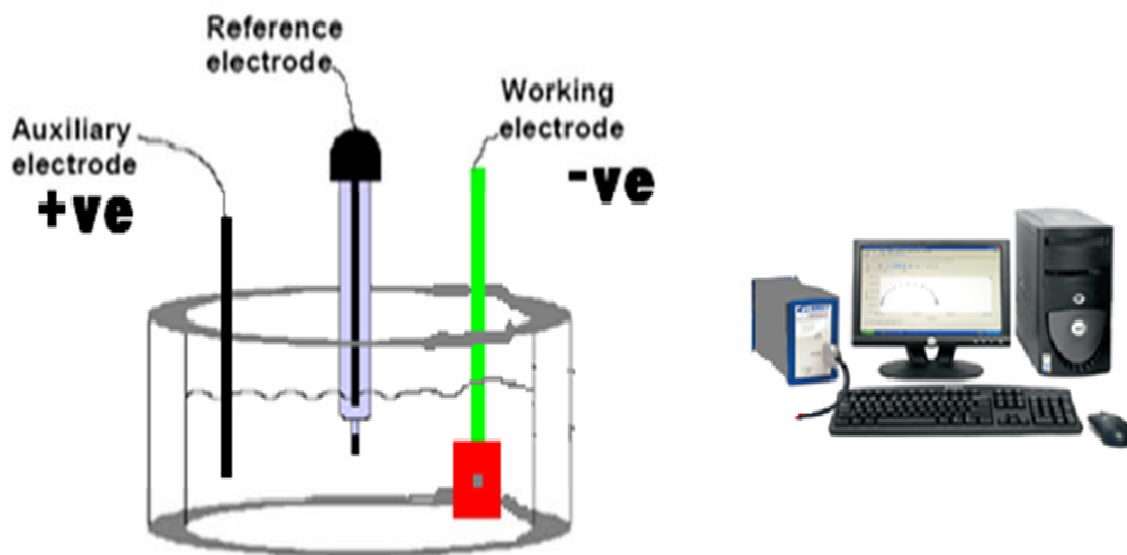


**Figure 3.2: Experimental Setup [14]**

A Gamry instrument is used for the powering, controlling and monitoring the corrosion process. A potentiostatic DC corrosion program was selected to supply a constant potential voltage to the electrochemical cell. For AA2024 experiment, the initial and final voltage was applied to -0.63V. In order to enable corrosion on the specimen the specimen should be anodic to emit electron and forms metal ions on the surface of the specimen. So a negative voltage on the cathode where the specimen is connected make sure that the specimen is anodic compared to the graphite electrode. Similarly for stainless steel 316, the initial and final voltage was applied to -0.45V. Other experimental conditions for both AA2024 and SS316 are described in table 3.1

**Table 3.1: Corrosion experimental conditions for Al2024 and SS316**

<b>Conditions</b>	<b>AA2024</b>	<b>SS316</b>
Initial voltage(V)	-0.63	-0.45
Final voltage (V)	-0.63	-0.45
Sample period (sec)	10	10
Limit I (mA/cm <sup>2</sup> )	2500	2500
Sample area (cm <sup>2</sup> )	2	2
Density (gm/cm <sup>3</sup> )	2.7	7.9
Equivalent wt.	10.28	19.78

Initially, different potentials were applied on samples of both materials and these samples were imaged under optical microscope to study the effect of the potential on the corrosion behavior of both materials. If the potential was higher than selected potential

then corrosion process is expedited but the goal of the thesis is to systemically study how the corrosion is growing with respect to time on both materials. When the potential was lower than the selected potential then reverse current flow through the sample, which restrict the corrosion process.

During the experiment the voltage and current is constantly monitored and recorded after every 10 seconds. The corrosion rate is controlled by the current flowing through the electrochemical cell. The experiment is designed to limit the current to few micro amperes to ensure that the corrosion process is slow and steady.

### **3.4 Experimental results**

The result obtained from corrosion electrochemical experiments, optical microscopy and atomic force microscopy are obtained to characterize the localized corrosion. The electrochemical experiment provides the current which can help to determine the corrosion rate with time. The optical microscopy image is performed at 5x zoom at the surface of the specimen, so area of 1mm x 1mm was perfectly visible under microscope. This provides the details how the corrosion is progressing with respect to time. Finally, AFM provide the details how the corrosion surface morphology changes at nano/submicron level with respect to different corrosion time.

#### **3.4.1 Corrosion experiment results**

Results of current are obtained at 10 seconds intervals the electrochemical cell for the AA2024 specimen under 2 Molar NaCl solution at constant voltage of -0.63 V are presented in Fig. 3.3. The sample is corroded in interval of every 15 minutes till the total corrosion time reaches 1 hour and after that it is corroded for 30 minutes interval. The

applied voltage to the electrochemical cell is held constant and continuously monitored by the Gamry instrument. Initially, when the corrosion begins the value of current is close to zero and then current increases as time increases. When the corrosion process is initiated, the corrosion resistance for aluminum alloy is high, so it doesn't allow the atoms on the surface to form ions. As time of corrosion increases, the atoms on the surface had gathered enough energy to form ions and there by more ions are formed on the surface. This effect will tend to increase the current as the corrosion time progresses.

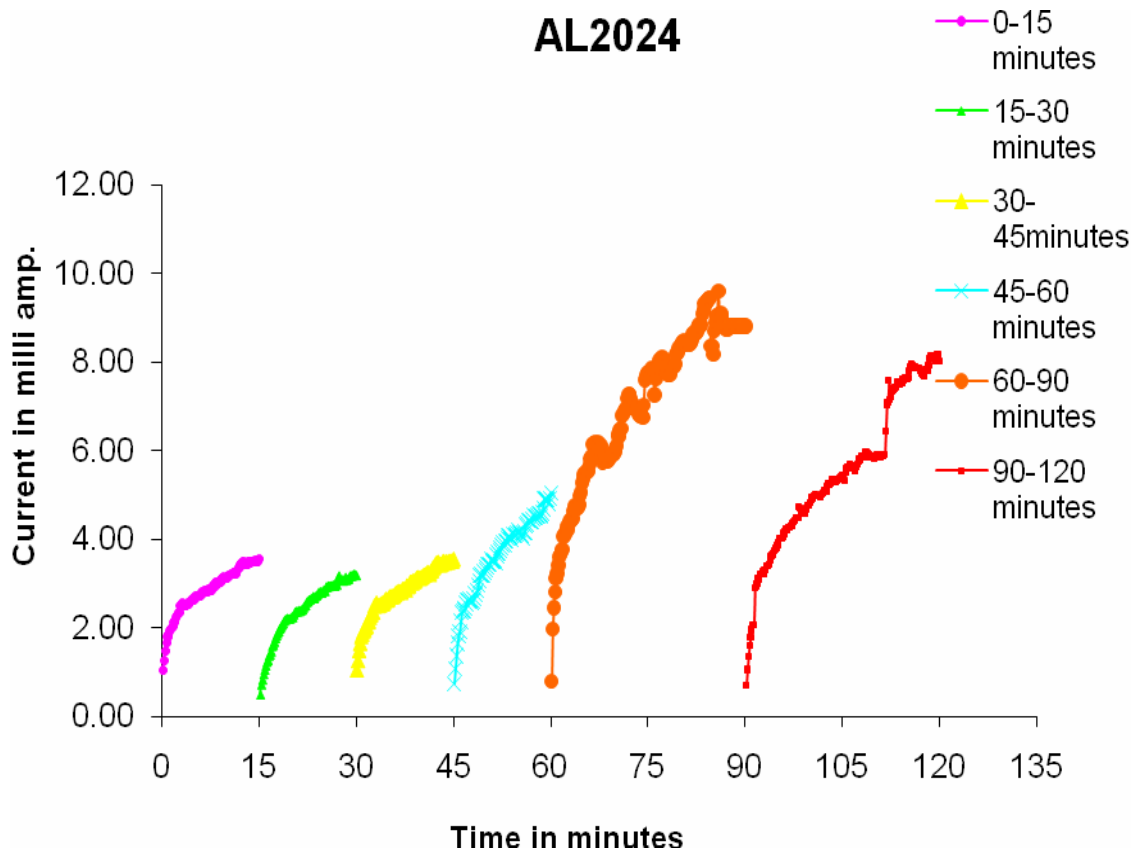


**Figure 3.3: Variation of current with respect to time for AA2024 specimen**

The first three intervals where the total corrosion time reaches to 45 minutes, the corrosion resistance of AA2024 is high which restricted the maximum current flowing through the cell to less than 4 mA. So it can be predicted that AA2024 initially offer high resistance to corrosion process when it is initiated in this particular environment. In time interval of 45-60 minutes, the increase in current is little higher than the first three intervals which can due to reduce of resistance on the surface affected by corrosion. The maximum current flowing through cell is observed in the time interval of 60-90 minutes, so it can be predicted that maximum corrosion took place during this period. As the total time reaches to 2 hours, there is little decrease in the maximum current which can due to saturation in availability of number of atoms to form ions.

On the bases of current result it can be predicted that AA2024 have a high corrosive resistance when the corrosion process is initiated. As the process continues, there is decrease in resistance due to corrosion but after a period of time it reaches to saturation where there are little chances for further corrosion. It was seen that when the sample was corroded again then its initial current value was close to zero. So if the corrosive environment is not uniform then the aluminum alloy offer more resistance to corrosion.

The sample of stainless steel alloy type 316 (SS316) is corroded in 2 Molar NaCl solution at a constant voltage of -0.45 V. The result of current obtained at 10 seconds interval for SS316 specimen is presented in Fig 3.4. Corrosion process is initiated similar to that of AA2024, but the maximum value of corrosion is less than 1 mA. In the second interval 15-30 minutes, SS316 specimen offer high corrosive resistance which restricted the maximum value of current less than 0.5 mA. The effect of high corrosive resistance is

further observed till the corrosion time reaches 60 minutes. During the time intervals of 60-90 minutes and 90-120 minutes, there is a sudden change in current flowing through the electrochemical cell. Stainless steel has a tendency to restrict further corrosion by forming film on the surface. Atoms on the surface need more energy to form ions if the film is formed on the surface. However, the breakdown of such a film will result in the pitting corrosion on the surface.

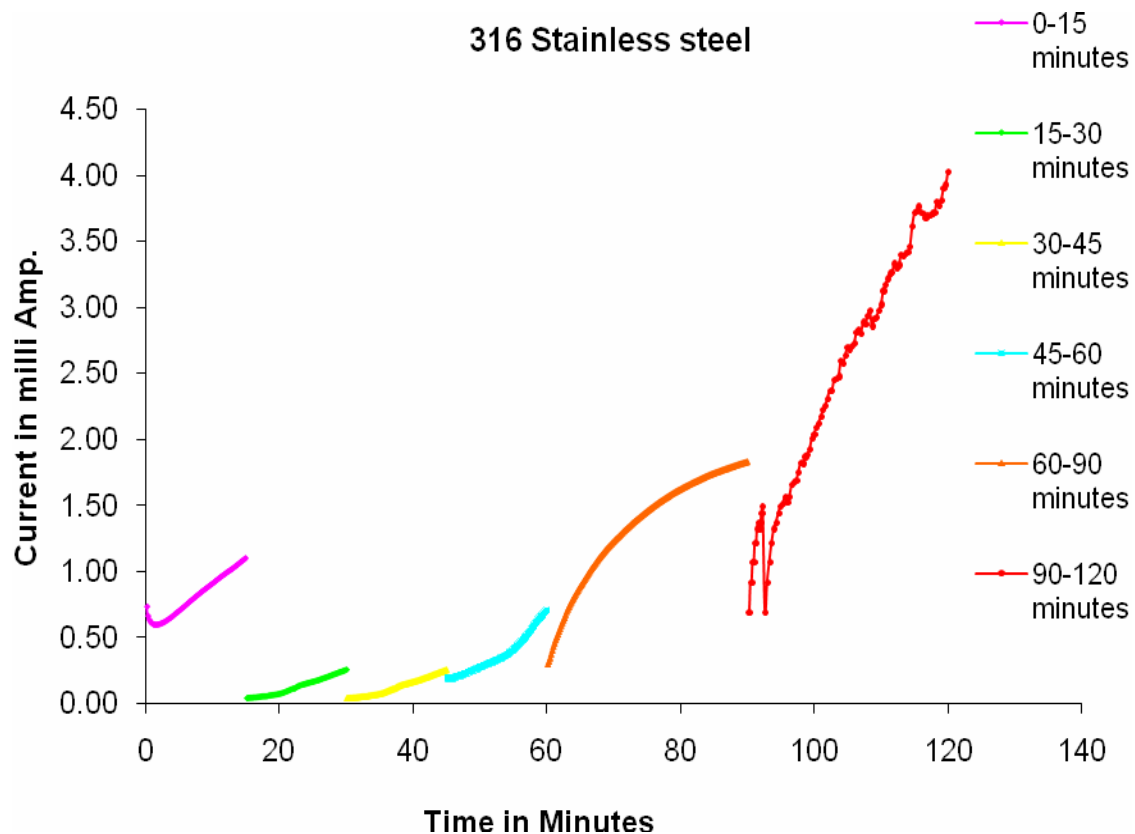


**Figure 3.4: Variation of current with time for Stainless steel type 316 (SS316) specimens**

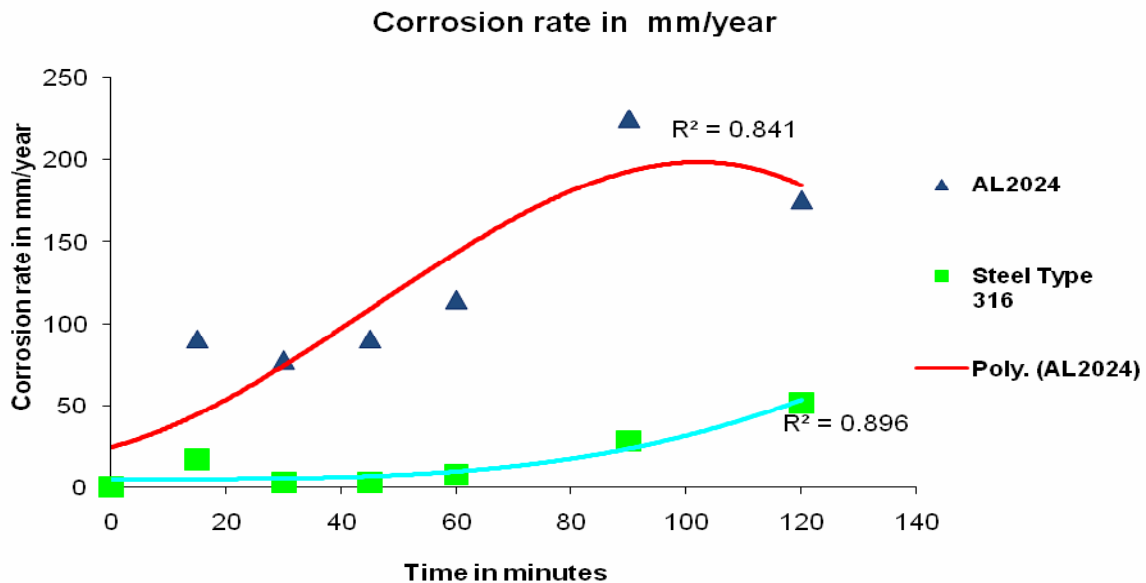
The stainless steel offers more corrosive resistance than that of AA2024 in this particular environment. At any given time, the current flowing through the cell in case of 316 steel is less than that of current flowing through the cell when AA2024 is corroded.

Figure 3.5 shows the rate of corrosion was calculated in material removed from the surface (in mm/year) from the average flow of current during each time interval using Faraday laws.

$$CR = I_{\text{corr}} * K * EW / (\rho * A)$$

Where K is constant and is equal to 3272 mm/(amp.cm.year)

Area, density and equivalent weight for each specimen are taken from table 3.1. Average current is taken for each time interval and the corrosion rate is predicted for that time interval.



**Figure 3.5: Predicted corrosion rate for AA2024 and SS316 specimen from experimental results**



As seen from the results that the average flow of current in AA2024 is higher than the SS316 therefore the corrosion rate of AA2024 is higher than SS316 according to Faraday law. The average corrosion rate for AA2024 is almost 7 times higher than that of the SS316 specimens. The corrosion rate increases sharply initially for both AA2024 and SS316 specimen when corroded but it offer passivity due to which the corrosion rate have decreased. The increase corrosion rate is limited in AA2024 and it is decreased in SS316 due to passivity. The corrosion rate in AA2024 increases sharply after 60 minutes of total corrosion time and there was a decrease in corrosion rate due to saturation of the corroded regions on the surface. There was a sharp increase in corrosion rate in SS316 after 60 minutes but the saturation of corrosion was still unachieved. Polynomial trend is used for predicting the corrosion rate in both specimens using R-squared value. Third-order polynomial is used to predict the trend in corrosion rate in AA2024 and SS316. According to this trend, the corrosion rate for AA2024 specimen gradually increases till 90 minutes and then there is a decrease due to saturation in corrosion. However, the increase in corrosion rate for SS316 is very small during first 60 minutes of corrosion but after 60 minutes the corrosion rate seemed to be increasing sharply after that but the saturation in corrosion is still unachieved.

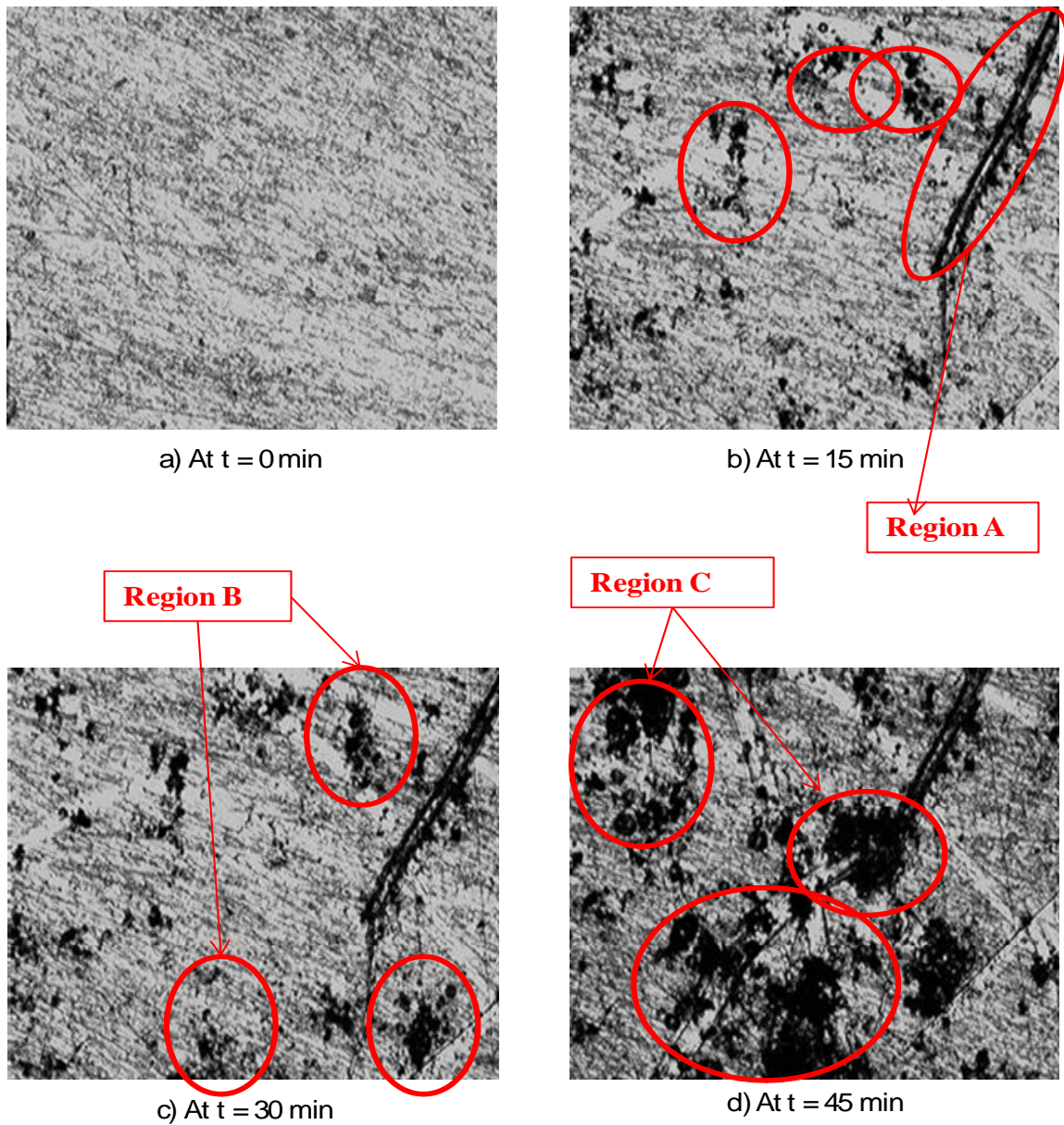
### **3.4.2 Optical Microscopy results**

Figure 3.6 shows the optical microscopy result of the AA2024 sample at different corrosion time when corroded in 2 Molar NaCl solution at -0.63 V. As seen from Fig 3.6(a), at time  $t = 0$  minutes there is very little or no corrosion product form on the surface

of the sample. When the sample is first corroded for 15 minutes (Fig. 3.6(b)), some localized effects of corrosion are seen along with some general corrosion. Uniform corrosion had taken place in sample but some severe corrosion is seen on the highlighted region. Some pitting effect is seen on the highlighted region A of the sample since there is a difference in the phase due to reflection of the light. Rest of the sample is subjected to the uniform or general corrosion where the corrosion products are formed on the surface of sample.

When the sample is corroded for another 15 minutes (Fig 3.6(c) for  $t = 30$  minutes) the corrosion seems to grow further. Mostly uniform corrosion is observed at this particular time. The regions which were previously corroded at  $t = 15$  minutes are corroded further and they grow in size and some regions on the sample are randomly corroded (Region B). So the corroded region acts like a source of corrosion initiation. This is due to the complex microstructure of AA2024, in which the Al-Cu-Mg (S-phase) intermetallics are initially anodic and become cathodic to the matrix due to selective corrosion of their noble constituent, namely Al and Mg, leaving nobler Cu-rich remnants that provoke the corrosion of the adjacent matrix. At total time  $t = 45$  minutes (Fig 3.6(d)), more uniform corrosion is seen on the surface of the sample. Previously corroded region seems to expand and few other region with severe uniform corrosion also seen (Region C). Few white spots and long groove kind of pits are appeared in the highlighted region C. The Previous corroded region seems to have a very low corrosive resistance than the rest of the sample because there was an intense growth in corrosion product when further corroded. However, corrosion rate at this particular time is seen higher than 15 and 30 minutes. Al 2024 seems

to have a decrease in corrosion resistance as the corrosion process forms some product or pits on the surface of the sample.



**Figure 3.6: Optical microscopy images of AA2024 specimen at different corrosion times.**

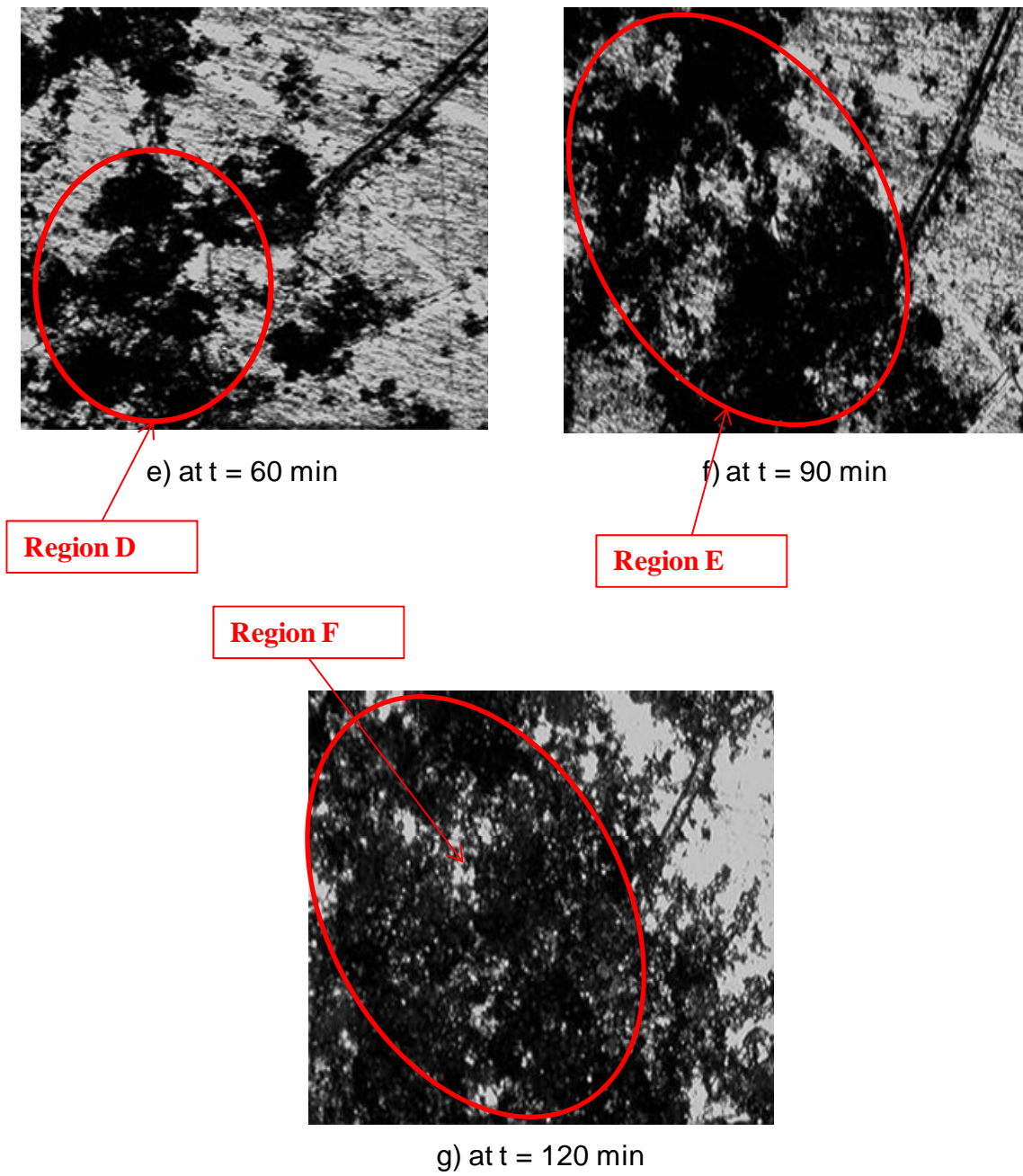


**Figure 3.6(cont.):** Optical microscopy images of AA2024 specimen at different corrosion times.

At total corrosion time  $t = 60$  minutes (Fig 3.6(e)), the previously corroded region expanded in size and more uniform corrosion regions are also seen. However, the intensity of the corrosion seems to be higher than before corrosion. The highlighted region D had a severe corrosion during corrosion time interval (45-60 minutes), in which there were huge deposits of oxides and few pits are also visible on this region. The rate of corrosion is expected to be higher than before as there is a huge reduction in corrosion resistance. Mostly the dark regions indicate that there is corrosion on the surface with corrosion products such as rust or film. There are some white spots on the surface, which may be due to some pits or un-corroded regions. There will be a height difference between the corroded region and un-corroded spots due to the accumulation of the corrosion products. These un-corroded spots are also considered as pits as long as corrosion products are present on the surface.

When the AA2024 sample is corroded further to  $t = 90$  minutes (Fig 3.6(f)), the corrosion region seems to grow further in size. At this time most of the sample area is covered with the corroded region. There has been growth in the previously corroded region (Region D to Region E) as the corrosion time was increased. Accumulation of the corrosion product on the surface is seen to be increased (Region E). A combination of uniform corrosion and pitting corrosion over the entire surface is observed. At time  $t = 120$  minutes, the previously corroded region (Region E) seemed to be expanded and accumulation of the corrosion product on the surface is increased (Region F). The intensity of the dark region seemed to be increased as the regions appeared darker than before. Appearance of more white spots on the dark regions has also increased compared to the 90-minute sample. However, the expansion of the dark regions or corroded regions has decreased compared to earlier

corrosion. So it can be suggested that there will be little expansion of the corrosion on the surface but there are chances that more accumulation of the corrosion product on the corroded region.

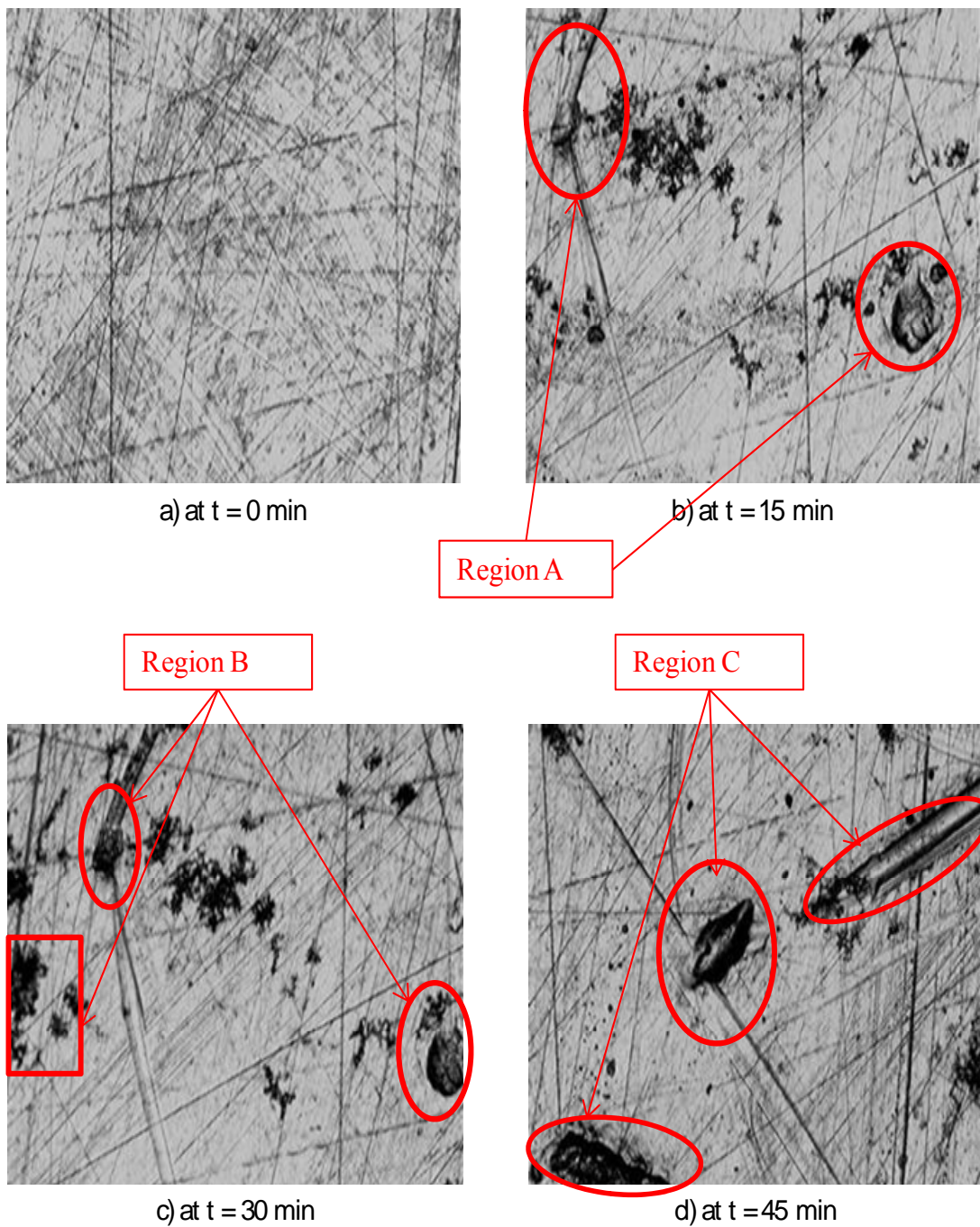
For particular environment considered, corrosion of AA2024 sample seemed to have combination of both uniform and pitting corrosion. Initially, the corrosion begins uniformly over entire surface but there is some localized intense corrosion. The regions which are previously corroded are subjected to more corrosion if the total corrosion time is further increased. This corrosion can be seen on the surface either by increase in surface area of the corrosion or more accumulation of the corrosion product on the corroded regions or combination of both. In this particular case combination accumulation and increase in surface area of corrosion is clearly seen. However, initially as the corrosion process begins, the increase in surface area of corrosion seemed to be dominated but as time was increased further the accumulation of corrosion product seemed to be more dominating. AA2024 have formed pits as the corrosion process began and more pits had observed with further increased in time. From the images (Fig 3.6), the rate of corrosion increases as the total corrosion time increases. Similarly there is a decrease in corrosion resistance with increase in total corrosion time.

Figure 3.7 shows the optical microscopy results of SS316 specimen at different corrosion time, when corroded in 2 Molar NaCl solution at -0.45V. The resolution of microscope is kept same 5X optical zoom as in case of AA2024 sample. At  $t = 0$  minutes (Fig 3.7(a)) there is little or no corrosion on the surface of the SS316 sample. However, few scratches seem to appear on the surface after grinding and polishing. As SS316

specimen is corroded for first 15 minutes (Fig. 3.7(b)), some pits and some localized corroded regions are observed on the surface. There is a phase difference in the reflection of the light which suggests that there are pits formed on the corroded region. Two pits are observed on the highlighted region A. However, the pits are covered with black region which indicate that pit does have little accumulation of corrosion product. Pit formation on the stainless steel started instantly as soon as corrosion process is initiated.

As the corrosion time is further increased by 15 minutes (Fig 3.7(c) for  $t = 30$  min), there is a very little progress in corrosion. When the previously corroded regions with pits (Region A) have corroded further, there was increase in deposition of the oxide within them and there was a new localized region which had oxide deposits on it (Region B). The regions which are already corroded offers high resistance to growth of the corrosion region in size. It appears that SS316 offers high corrosive resistance when corroded which decreases the rate of further corrosion. At time  $t = 45$  min (Fig. 3.7(d)), it appears that there is an expansion of the existence pit and new pits are formed (Region C). The new pit formed may be due to removal of the accumulated corrosion product in electrolyte solution. However, there is change in intensity of the dark regions in the pits which suggests that there is increase in accumulation of the corrosion products within the pit. There is very small or no increase in surface area of the corroded regions so there a very little change in corrosive resistance. So the change in rate of corrosion is also very small.





**Figure 3.7: Optical microscopy images of SS316 specimen at different corrosion times.**



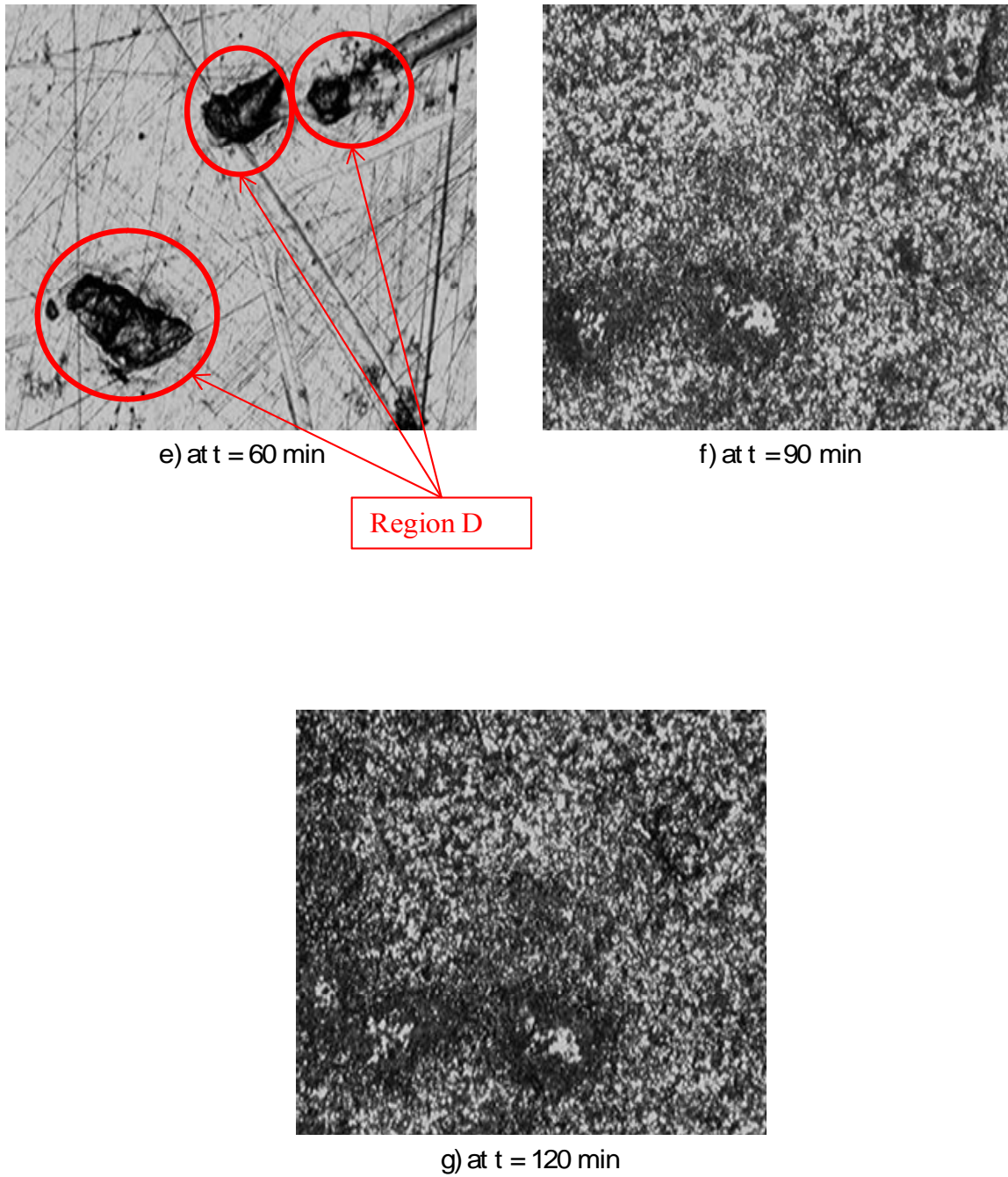


**Figure 3.7(cont.): Optical microscopy images of SS316 specimen at different corrosion times.**

At time  $t = 60$  minutes (Fig 3.7(e)), there was an expansion in size of the existence pit and new pit is formed (Region D). New pit is formed on the previously corroded region (Region C) due to removal of the oxides from the surface in the electrolyte solution. The pits seemed to be expanded but the change in size is very small. These frequent removals of the corrosion product in the electrolyte solution suggest that the corrosion product accumulated on the surface is very weak structurally and chemically. Stainless steel has a tendency to form a film but the film is strong both structurally and chemically. This film breakdown when subjected to load or due to erosion. The atoms on the surface of the stainless steel sample continue to offers resistance to further corrosion so, there is a very small change in the rate of corrosion.

When sample is corroded further to time  $t = 90$  minutes (Fig 3.7(f)), a severe combination of both film forming (uniform) corrosion and pitting corrosion is observed. An ideal uniform corrosion is observed with a further increase in the corrosion time. The accumulation of the corrosion products is seen over entire surface area. The big pits which visible earlier at  $t = 60$  minutes are covered with the corrosion product which suggests that there is a huge amount of accumulation of corrosion product on the sample surface. Due to presence of chromium element it promotes the formation of delta ferrite structure (BCC crystal structure) in SS316. These delta ferrite structures provide high corrosion resistance to SS316 but chromium oxidizes and forms a film on the surface. There are some white spots in the dark regions due to difference in the height in the region. These white spots indicate either there is a pit or some non-corroded regions. The rate of corrosion is increased as there is an increase in the dark corrosion region on the sample surface.

When corrosion time is increased further to  $t = 120$  minutes (Fig 3.7(g)), the intensity and density of the dark region on the sample surface had increased. There is an increase in the uniform corrosion, as some of the white spots in the dark region are corroded and covered with corrosion products. The intensity of the dark region also increased, which suggests that there is an increase in the accumulation of corrosion product. This effect may be film formation as the deposited corrosion product did not dissolve in the electrolyte solution. More uniform corrosion is observed as the film formation process takes place. The rate of corrosion seems to be a little less than that of  $t = 90$  min. As predicted from the literature review that, the film formation on the stainless steel increases the corrosive resistance which restricts further corrosion. There is a small reduction in the corrosion rate due to incomplete formation of the film.

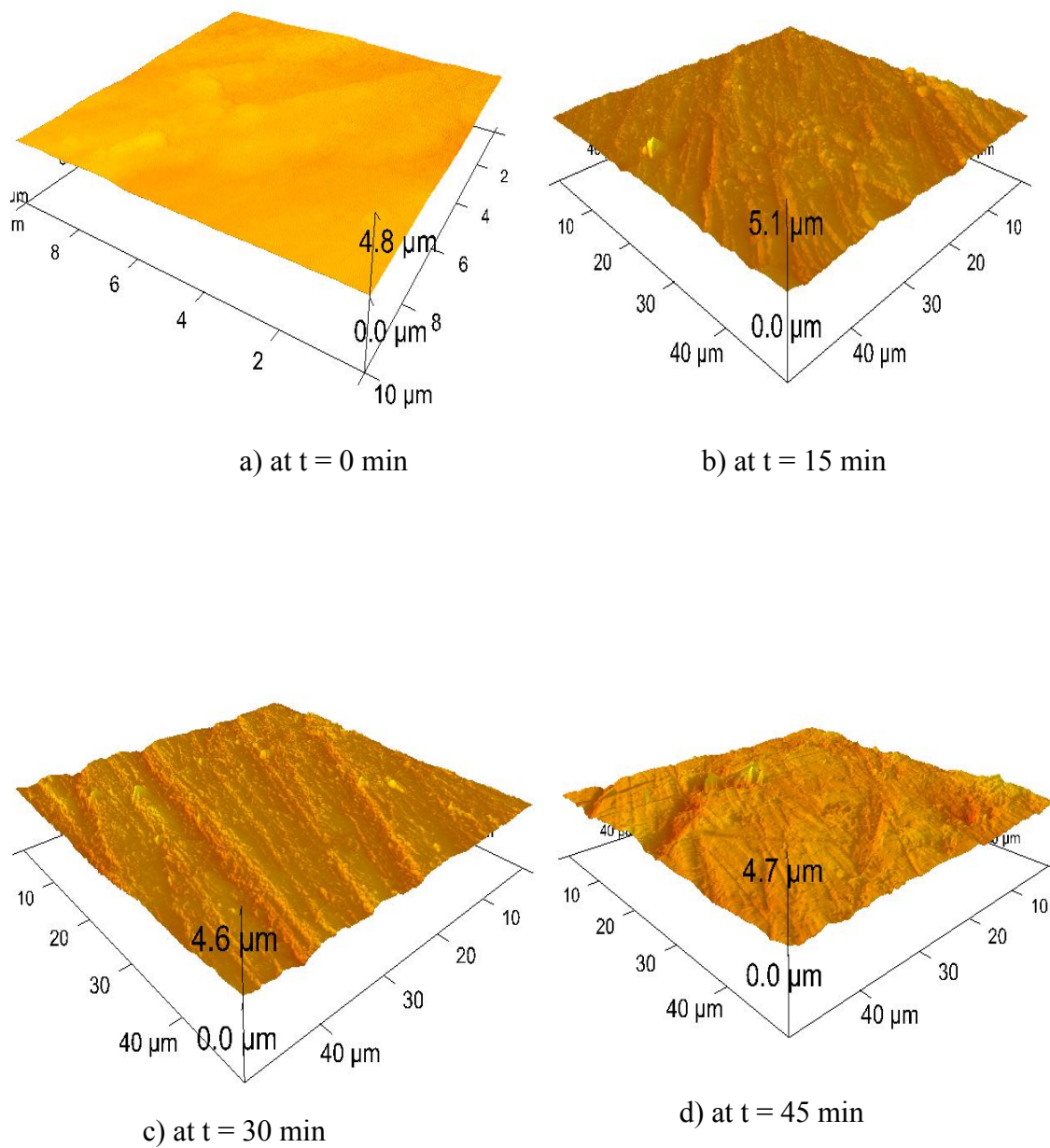
The SS316 sample usually initiates corrosion by pitting and film forming (general) corrosion in the particular environment considered. SS316 has a duplex microstructure which increases the corrosion resistance of the steel and localized forms of corrosion are expected followed by film forming corrosion. The corrosion product deposited on the surface during the initial corrosion is usually weak structurally and chemically, so it can be easily removed from the surface and forms more pits. The corrosion resistance of SS316 seems to be higher than AA2024 material. After the corrosion takes place, the corroded region offers higher resistance to further corrosion. Initially the corrosion rate is a little higher followed by a sudden decrease. After a certain corrosion time, atoms on the surface of the sample seem to have gained sufficient amount of energy to react with the electrolyte solution and form a uniform film over the entire surface. The corrosion rate is

drastically increased after 60 minutes, while forming the film by depositing the corrosion product on the surface. After corroding the sample for 120 minutes, a uniform film is deposited on the entire surface of the sample. This deposited film on the sample surface will further provide the passivity for further corrosion by increasing the corrosion resistance of the atom on the surface. Film formed on the surface of the sample is strong chemically but weak structurally. So a little loading on the surface will result in breakdown of film and formation of more pits on the surface. The corrosion of SS316 is extremely dangerous as it initiates with pitting corrosion and film forming, this film can breakdown and forms more pits. These pits can act as stress raisers when loading is applied on it and can drastically reduce the product life. In some cases, pitting corrosion can also result in sudden failure of the product.

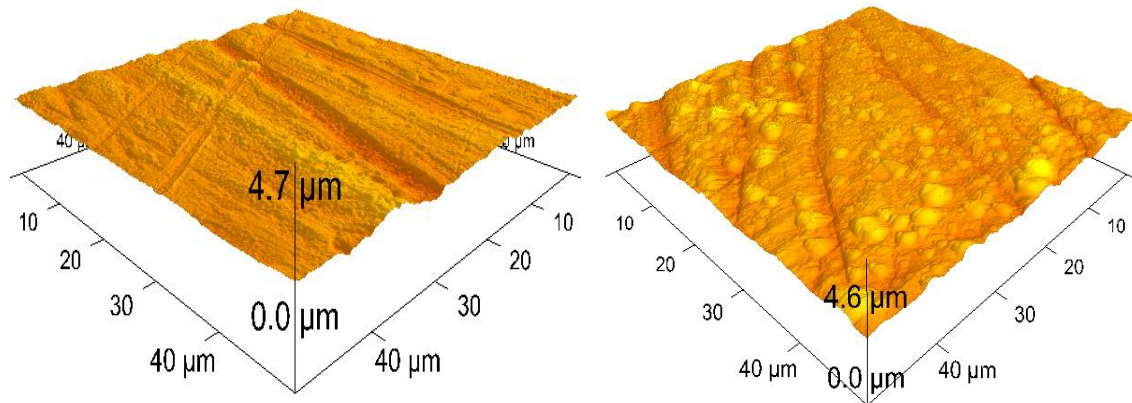
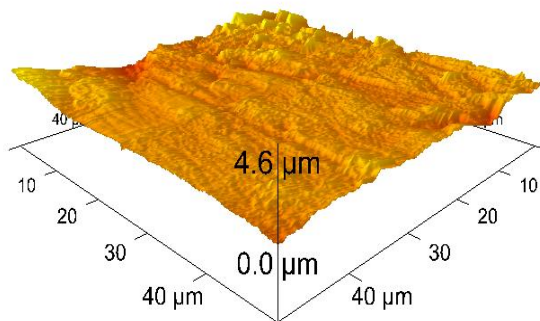
### **3.4.3 Atomic Force Microscopy result**

After the sample is scanned under optical microscope, the sample is then taken to AFM for micro-scanning of the surface features. The heights of the AFM results are used to predict the surface topography of the sample due to corrosion. 3-D images are constructed in the offline nanoscope software (v710) using the height images. The scanning size of the sample is kept at  $50\ \mu\text{m} \times 50\ \mu\text{m}$  for all corrosion time.

Figure 3.8 shows the atomic force microscopy results for AA2024 in a 2Molar NaCl solution at  $-0.63\text{V}$  with respect to different corrosion time. At time  $t = 0\ \text{min}$  there is very small or almost no corrosion at all. The sample surface has very small features visible due to grinding and polishing. At total corrosion time  $t = 15\ \text{minutes}$  (Fig 3.8(b)), some regions of the surface seemed to be corroded uniformly. It seemed that there is some



**Figure 3.8: AFM images of Al2024 at different corrosion time**

e) at  $t = 60$  minf) at  $t = 90$  ming) at  $t = 120$  min**Figure 3.8 (cont.): AFM images of Al<sub>2024</sub> at different corrosion time**

accumulation of the corrosion product on the sample surface. These deposition corrosion products on the surface raise the height of the region on the surface which is corroded. So regions which are not corroded are at lower height than that of the corroded regions. There is a wavy pattern in corrosion, as the corroded and un-corroded region seemed to gather together and wavy pattern is formed due to height difference between them.

At time  $t = 30$  minutes (Fig. 3.8(c)), the wavy pattern seemed to be growing as time is increased. This indicates that the regions which are corroded offers less corrosion resistance to further corrosion compared to the un-corroded regions, so the deposition of the corrosion product on the corroded region increases. The regions which are not corroded are at lower height and deep groove are appeared on the surface. These grooves are often considered as pits as they will act as stress raiser when loading is applied on the surface. A uniform form of corrosion is observed as the sample is corroded evenly on the surface leaving some micro-regions but the deposition of the corrosion surface is varied in nanometers.

When the sample is further corroded for 15 minutes (Fig. 3.8(d) at  $t=45$ min), the deposition of the corrosion product on the surface seemed dominant. The average surface roughness of the specimen was doubled when compared to the roughness prior to corrosion. The deposition of the corrosion product might have isolated the atoms on the surface to form further ions, which have raised their corrosion resistance in this region. The un-corroded region with less corrosion resistance got corroded by depositing the corrosion products on the sample surface. There are few pits appeared on the surface due unevenly deposition of the corrosion surface. At total corrosion time  $t = 60$  minutes, uniform form of

corrosion is observed due to deposition of the corrosion products on the sample surface. At this particular time, sample surface at this scanning size ( $50\ \mu\text{m} \times 50\ \mu\text{m}$ ) looks corroded but there is a variation in amount of the corrosion product deposition. Due to this variation there is a height difference between the regions on the surface. It is clearly seen that there is a uniform corrosion on the surface but the corrosion resistance varies from point to point.

At total corrosion time  $t = 90$  minutes (Fig 3.8(f)), the accumulation of the corrosion product and the average surface roughness continue to increase. There are bumpy kinds of structure formed on the surface due to increased corrosion. The deposition on the corrosion product on the corroded surface seemed to be increased, but is not uniform. There is some excess deposition at some places, where the bumps are formed and within the grooves which result in narrowing the grooves. When the total corrosion is further increased to  $t = 120$  minutes, the deposition of the corrosion product continues and sample surface roughness have increased by 23.9%. The rate of deposition of the corrosion product at this particular time seemed to be random and decreasing, as the sample surface is corroded unevenly and few peaks and valley kind of structure are clearly visible on the surface. The sample surface looks roughest at this particular time.

The AFM imaging of AA2024 provided the details of the surface at micron level. Initially, when the process begins the accumulation of the corrosion product at micron level on the surface was unevenly even though the uniform corrosion process was seen in optical imaging. There were some peaks and valleys formed due to this uneven deposition. There was a further growth in this deposition on corroded regions as time was further



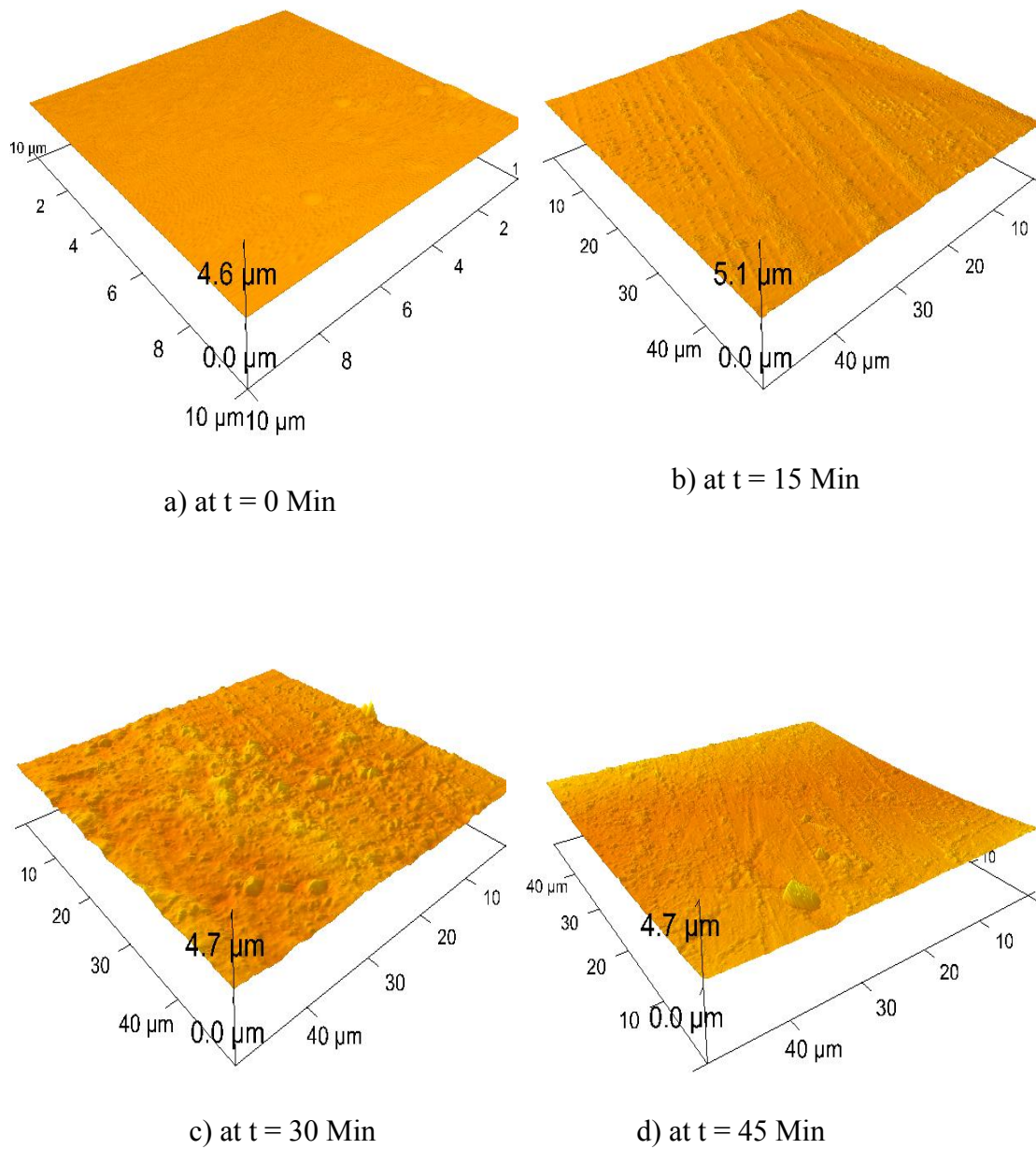
increased. But after some time of corrosion process, a complete surface was seemed to be corroded and deposition of the corrosion product was seen in all region of the surface. Even the pits which were formed during the corrosion process did have some deposition of the corrosion product within them. Overall a uniform form of corrosion process is observed but the deposition of the corrosion product was not uniform on entire surface. The surface roughness of the sample had increased sharply when the AA2024 specimen was initially corroded. On further corrosion the increase in surface roughness seemed to demising due to saturation of the number irregularity on the surface. There was an increase in surface roughness due to accumulation of the oxides on the surface.

**Table 3.2: Surface roughness obtained from AFM for AA2024 and SS316 specimen**

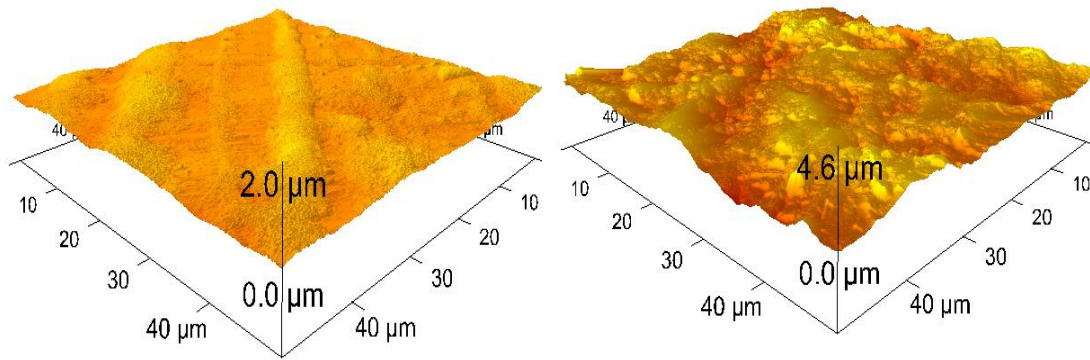
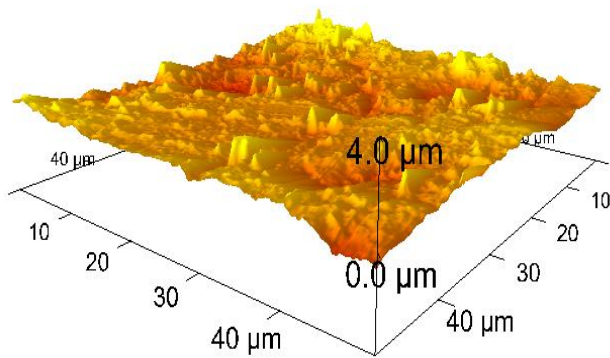
Corrosion time Minutes	AA2024			316 steel		
	R <sub>q</sub> nm	R <sub>a</sub> nm	R <sub>max</sub> nm	R <sub>q</sub> nm	R <sub>a</sub> nm	R <sub>max</sub> nm
0 min	74.4	60.5	501	24.9	19.5	252
15 min	117	89	1582	69.8	37.4	457
30 min	134	102	1743	130	56.2.	534
45 min	139	105	1936	149.2	101	1222
60 min	170	127	2014	162	135	1386
90 min	176	134	1961	319	243	2393
120min	235	166	2476	334	270	3174

Figure 3.9 shows the atomic force microscopy results for stainless steel SS316 specimen in a 2Molar NaCl solution at -0.45V with respect to different corrosion time. Table 3.2 shows the surface roughness of the SS316 specimen at different time. At  $t = 0$  minutes (Fig 3.11(a)), the average surface roughness of the sample is 19.5 nm, so the surface is considered almost smooth with no sudden bump or pits. As the total corrosion time is increased by 15 minutes (Fig 3.11(b), at  $t = 15$  minutes), the surface seemed to be corroded and corrosion product seemed to be deposited in a straight lines. The average roughness of the sample is increased to 37.4 nm and the maximum size of the peak on the surface is 457 nm. The deposition of the corrosion product is localized to the regions which have low corrosion resistance and few bumps are visible due to this accumulation. The atoms on the sample surface showed more resistance to form ions than that of the AA2024 sample, so the corrosion resistance of SS316 specimen is higher than AA2024 sample.

At total corrosion time  $t = 30$  minutes (Fig 3.9(c)), a uniform form of corrosion is observed. The most of the regions on the surface is covered with the deposition of the corrosion product but the amount of deposition is not uniform over entire surface. Due to variation in the accumulation there is a height difference within the surface which increased the average roughness of the sample to 56.2 nm. The increase in average roughness is not that high since most of the surface is corroded and there are few regions on the sample at high height than the others. Some small pits and grooves are also observed.



**Figure 3.9: AFM images of SS316 at different corrosion time**

e) at  $t = 60$  Mine) at  $t = 90$  Mine) at  $t = 120$  Min**Figure 3.9 (cont.): AFM images of SS316 at different corrosion time**

When the total corrosion time is further increased by 15 minutes (Fig 3.9(d), at  $t = 45$  minutes), a big pit is observed and some regions within the pit are corroded. As discussed in the optical microscope results that the oxides or corrosion products formed on the surface were weak and were removed from the surface when corroded again. So a big pit with minor axis little more than  $50 \mu\text{m}$  is observed on the surface. Some regions within the pit are covered with the deposition of the corrosion products and which is not uniform throughout the pit. The average surface roughness is increased to  $101 \text{ nm}$  because of the variation in height in a pit and due to accumulation of the corrosion product on it. The average surface roughness is increased but the rate of corrosion seemed to be less as there is no huge accumulation of the corrosion product on the surface. Pitting corrosion with some accumulation of the corrosion product is observed till now. At time  $t = 60$  minutes (Fig 3.9(e)), further uniform form of corrosion is observed but the deposition of the corrosion product is not uniform. The entire pit structure is covered with the corrosion product and few bumps are formed on the surface. The rate of corrosion seemed higher at this particular time as the accumulations of the oxides have increased. The average surface roughness of the sample has also increased to  $135 \text{ nm}$ .

When the corrosion is further increased by 30 minutes (Fig 3.9(f), at  $t = 90$  minutes), uniform film form of corrosion is observed. A sudden thick film has formed on the surface of the sample due to accumulation of the corrosion products. Stainless steel contains chromium which reacts with the oxygen and form a film on the surface which provides passivity to the steel. This film of the chromium oxide isolates the atoms of the surface from the atmosphere and thereby increasing the corrosion resistance of the steel. A

uniform corrosion is observed but the deposition of the oxides on the surface is not uniform. The average surface roughness is increased to 243 nm which almost 100 nm more than that of 60 minutes of corrosion time, which indicates that the rate of corrosion is increased drastically. At total time  $t = 120$  minutes, uniform form of corrosion is observed further and film on the surface grows thick. The deposition of the oxides was uneven because the corrosion took place where the corrosion resistance was low. There is an increase in average surface roughness but the amount of increase is around 30 nm which suggests that there is a decrease in the corrosion rate from this point onwards.

Initially, when the stainless steel 316 sample is corroded few regions were corroded by depositing the corrosion product on it. When the corrosion process initiated, the rate of corrosion is low for 45 minutes as there was no sudden increase in the average surface roughness. The pitting form of corrosion was observed due depletion of the corrosion product from the surface. On further corrosion, the accumulation of the corrosion product was observed on the pits and there are chances that pits might grow with further corrosion if the corrosion products formed are weak. The chromium oxide film is suspected to be formed on the sample surface uniformly which increased the average surface roughness by 100 nm. After forming a film on the surface of the sample, there was a little decrease in further corrosion. So it can be stated that the rate of corrosion increased when the film was developing on the sample surface and there was little decrease in rate of corrosion after that. Overall stainless steel 316 is suspected to have a combination of both pitting and film forming form of corrosion in this type of the corrosion environment. The breakdown of this oxide film can further result in generation of more pits on the sample surface.

**Table 3.3: Summary of the experimental and microscopy results for AA2024 specimen**

AA2024			
Time	Experimenta l	Optical Microscopy	AFM
t = 15 minute s	Rate of corrosion increases sharply	Few localized regions are corroded and one long pit was observed	The surface roughness increases sharply by 47.1% and wavy profile is observed with few long groove kind pits.
t = 30 minute s	Passivity observed, rate of corrosion decreases by 14.2%	Growth of previously corroded regions but due to passivity the growth is limited	Growth of wavy pattern and pit enlargement is observed. The surface roughness have increased by 14.6%
t = 45 minute s	Rate of corrosion increases gradually by 16.52%	Further growth of corroded regions are observed and new pit kind of groove are observed	Depositions of oxides on the surface increases and some pits are covered with corrosion product. Three pits are observed at this particular time and there is negligible increase in surface roughness
t = 60 minute s	Further raise in corrosion rate by 26.62%	Huge accumulation of corrosion deposits were observed along with little growth in corroded region and the pits enlarges due to corrosion	Few pits are covered with oxides and the rest of pits are expanded in size. Wavy kind of profile is observed and the surface roughness is increased by 21% due to accumulation of oxides
t = 90 minute s	Sharp rise in corrosion rate by 96.44%	The corroded region got united due to further growth in corrosion and uniform of corrosion was observed	Few bumps are observed on the surface and pits are narrowed due to oxide depositions. However, the increase in surface roughness was negligible.
t = 120 minute s	Rate of corrosion decreases by 22.08% due to saturation in corrosion	There is a little growth in corrosion region but the corrosion deposits on the corroded region increases	Random deposition of oxide is observed over entire area due to few pits and bumps are observed and the surface roughness has increased by 23.9%.

**Table 3.4: Summary of the experimental and microscopy results for SS316 specimen**

SS316			
Time	Experimental	Optical Microscopy	AFM
t = 15 minutes	Rate of corrosion increases sharply	Two big pits and few localized corroded regions are observed	Depositions of oxides are observed in some localized regions. The surface roughness is increased due to corrosion
t = 30 minutes	High passivity observed, rate of corrosion decreases by 84.2%	Few oxide deposition are observed in pits and some localized regions	Few bumps and pits are observed. The surface roughness has increased by 50.3%.
t = 45 minutes	Passivity continues but there was a negligible increase in rate of corrosion	Growth of pits are observed and new pit is formed due to erosion of the oxides in a electrolyte solution	A big pit is observed due to removal of oxides due to erosion corrosion. The surface roughness is increased by 79.7%.
t = 60 minutes	There was a sharp rise in corrosion rate of 175% after passivity.	Few pits are growing and again a new pit was observed from erosion corrosion. Corrosion oxide deposits are observed within these pits	Depositions of oxides are observed within that pit and temporary wavy profile is achieved. The surface roughness is increased by 33.7%.
t = 90 minutes	The corrosion rate continues to increase sharply by 257%.	A film forming corrosion is observed. All pits are covered with the oxides layer	Huge depositions of oxides are observed due to film forming and the surface roughness is drastically increased by 80%.
t = 120 minutes	The corrosion rate continue to increase but the amount of increase seemed demising	The film on the surface seemed to get thick due to corrosion	The corrosion oxides seemed to be thickening due to further corrosion. However, the amount in increase in surface roughness seemed to be demising.



## **Chapter 4 STRESS ANALYSIS OF CORROSION**

The AFM images of corrosion pit profile are used to obtain the image-based finite element model. A methodology is developed to predict the stresses on the corroded surface. Different types of loading are applied on the models of different corrosion times to study the effect of induced stress with respect to time. These are described in this chapter.

### **4.1 Developing a model from an image**

A model is required to perform the stress analysis of the sample at any given corrosion time. Since most of the corrosion results are images of the corroded surface, so a technique is required to convert these images to solid models. A NURB modeling software, Rhinoceros is used to make this solid model as it can create the surface on the basis of the height field. The optical microscope images are good in predicting the forms of corrosion on the sample surface but there is no scale available on it. Atomic Force Microscope height field images were used for stress analysis, as the detail provide by them are in micrometers and with little or less noise. However, the height field images do contain the scale information of the height and scanning size which should removed from the image. So the image should be cropped and only the height field of the sample surface is kept and rests of the regions should be deleted.

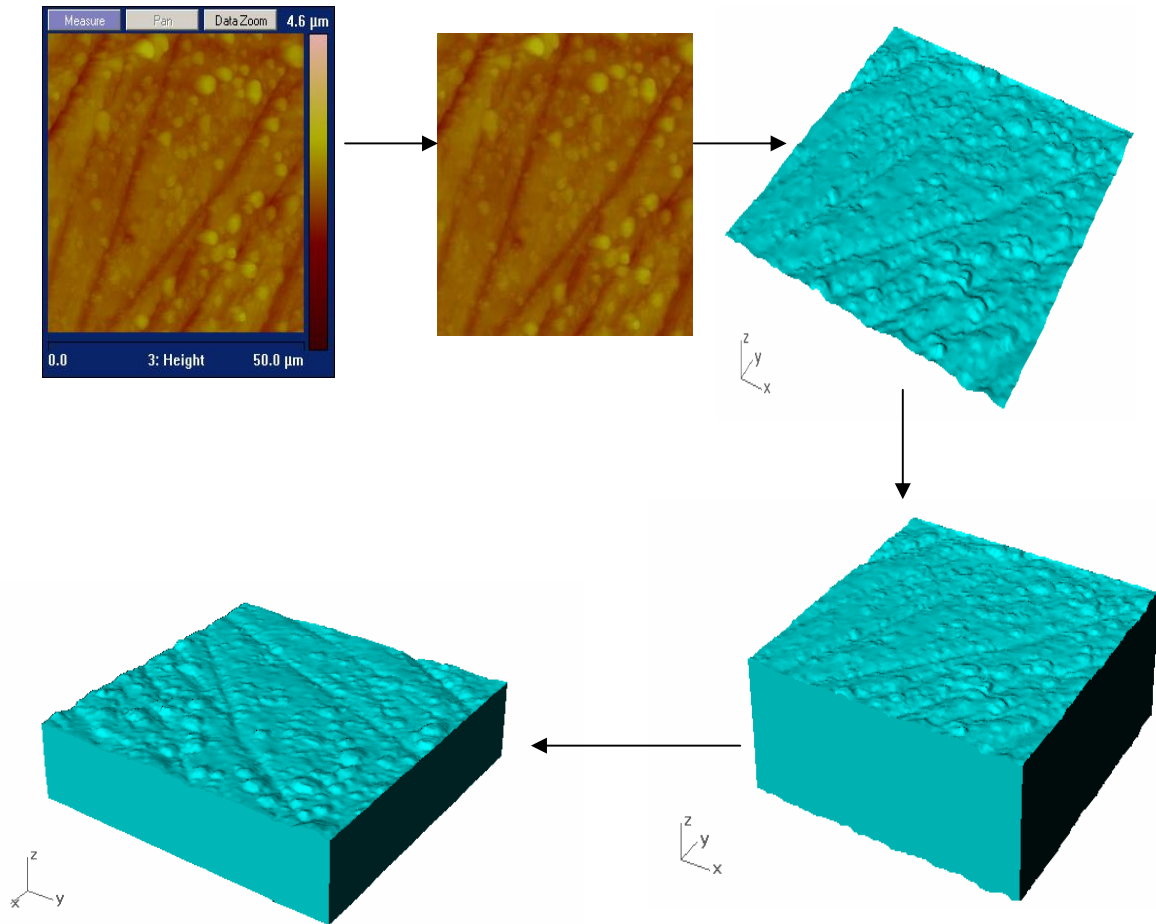


**Fig 4.1: Developing a model form a height image of total corrosion time  $t = 90$  minutes for Al2024**

Figure 4.1 shows the process, how the model is developed from the AFM height field image for total corrosion time  $t = 90$  minutes. Firstly, the height field image is cropped such that just the sample surface is visible and rest of the information like sample and height size is deleted. Then the surface is created on the bases of their height field in Rhinoceros software by importing the cropped bitmap image. The size of the surface is

kept same as that of seen on the AFM height image. For this particular image, the scanning size is  $50\ \mu\text{m} \times 50\ \mu\text{m}$  and the maximum height is kept at  $4.6\ \mu\text{m}$ . which is obtained from AFM. The number of sample point while creating a surface from the image is kept same as that of the scanning resolution which is  $256 \times 256$ . The resolution, height and size are kept same as that of AFM images to reduce the errors in forming the surface. This surface formed is extracted to  $20\ \mu\text{m}$  to form a solid and this solid is trimmed such that its final dimension is  $50\ \mu\text{m} \times 50\ \mu\text{m} \times 10\ \mu\text{m}$  as shown in Fig 4.2.

Same technique is applied to prepare model form the images of different corrosion time for AA2024 and stainless steel 316. The solid model is exported to ANSYS software in IGES format for Finite Element stress Analysis.

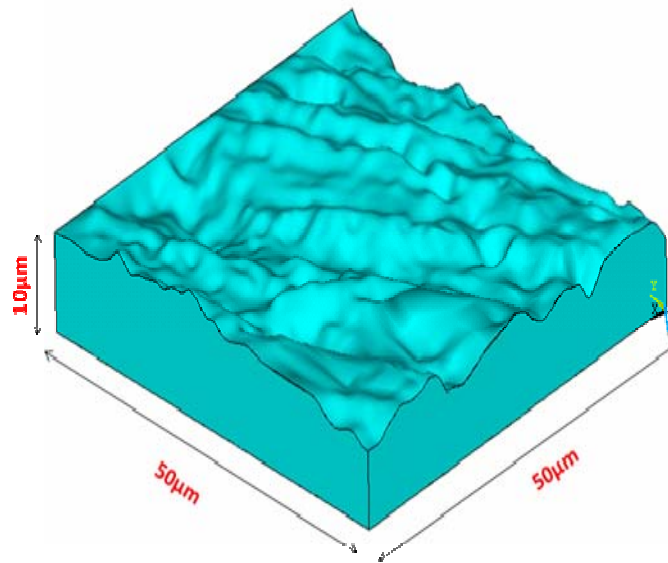


**Figure 4.2: Geometry of the model used Stress analysis**

## 4.2 Finite Element Analysis for AA2024 and SS316 Specimens

The Models developed in Rhinoceros software of AA2024 and SS316 at different corrosion time are analyzed for maximum stress using ANSYS software. There is no local experimental technique to find out how the stress varies on the surface after the specimen is corroded. The purpose of this thesis is to find how the generated stress change as the surface is corroded and to find maximum stress out of it. As it is known that maximum stress varies when the load or type of loading is changed. The effect of the loading on the maximum stress is also studied by changing the type of loading. In this particular thesis, study of the three different types of loadings; bending, tension and shear are studied. Table 4.1 shows different types of loading, geometry and amount of pressure applied to the models.

The Model is imported in the ANSYS software to perform the finite element stress analysis on it. A dimension check is performed to make sure that the model is in right dimension as it was in AFM image and if not than the model is scaled accordingly. The tetrahedral element was used to perform stress analysis on the model. Initially, hexahedral element was used as its accuracy is higher than that of tetrahedral element but meshing failed as the model surface became rough, so a tetrahedral element was used for all models of AA2024 and SS316 specimen for different corrosion time. Structural properties like Modulus of Elasticity and Poisons Ratio are specified for the all the models of AA2024 and SS316 specimen ( $E = 72 \text{ GPa}$  and  $\gamma = 0.3$  for AA2024 and  $E = 204 \text{ GPa}$  and  $\gamma = 0.3$  for

SS316 specimen). Linear isotropic structural analysis is performed by applying the boundary conditions on the model.

**Table 4.1: Geometry of model and types of loadings for AA2024 and SS316 specimens**

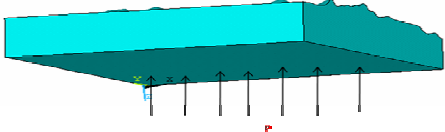
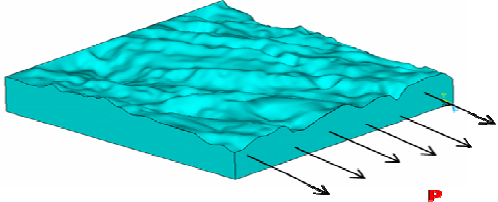
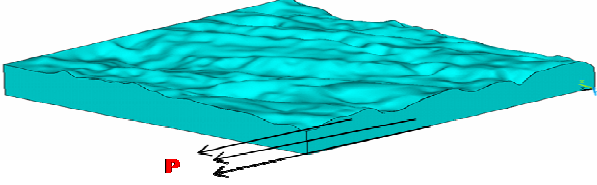
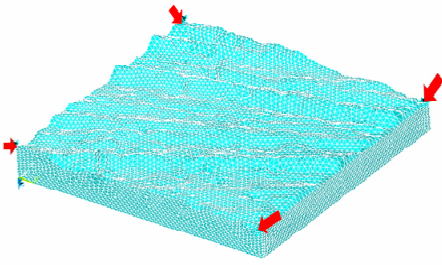
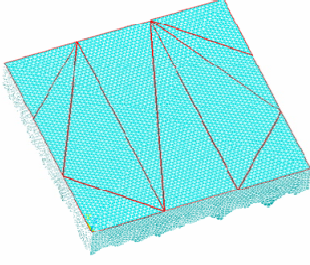
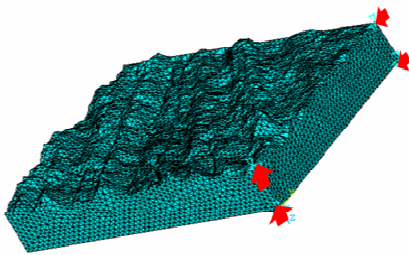
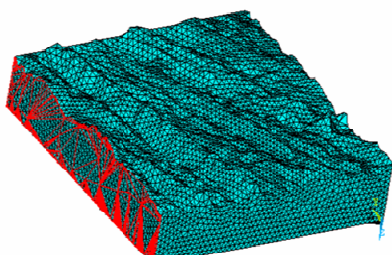
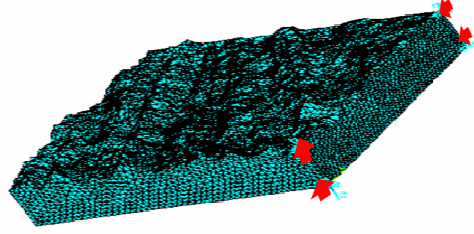
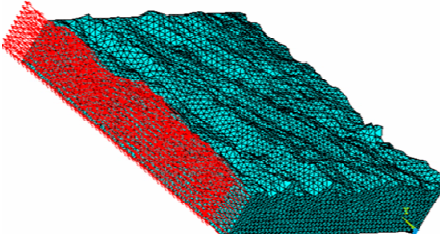
Loading case	Type of loading required	Loads applied
Bending		<b>P = 1MPa</b>
Tension		<b>P = 1MPa</b>
Shear		<b>P = 1MPa</b>

Table 4.2 shows the boundary condition for different types of loading. Under bending loading, the fixed displacement is applied to the top four corner of the surface and a uniform pressure of 1 MPa is applied to bottom surface of the model. For tension loading, four corner of face on the model in  $-X$  direction are applied fixed displacement and a uniform pressure of 1 MPa is applied to the face in  $+X$  direction. For the shear loading, four corners of the face on the model in  $-X$  direction are applied fixed displacement and a uniform pressure of 1 MPa is applied to the face in  $-Y$  direction. The

finite element stress analysis is performed on the model after applying the appropriate boundary conditions for a particular type of loading.

**Table 4.2: Boundary conditions for different types of loading**

<b>Types of Loadings</b>	<b>Fixed displacements</b>	<b>Loading pressure of 1 MPa</b>
<b>Bending</b>	 <p data-bbox="418 907 915 974"><b>Fixed displacement is applied on the four corner of the top surface</b></p>	 <p data-bbox="959 907 1317 974"><b>A Unit uniform pressure is applied on the back surface</b></p>
<b>Tension</b>	 <p data-bbox="410 1285 911 1352"><b>Fixed displacement applied on the four corner of the face in -X direction</b></p>	 <p data-bbox="950 1285 1352 1352"><b>A unit uniform pressure is applied on the side face in +X direction</b></p>
<b>Shear</b>	 <p data-bbox="410 1642 911 1709"><b>Fixed displacement applied on the four corner of the face in -X direction</b></p>	 <p data-bbox="959 1642 1365 1709"><b>A unit pressure is applied on the side face in +Y direction</b></p>

The mesh convergence test was performed on model of different materials at different corrosion time to optimize the maximum induced stress. For example, a convergence test was performed on the model of AA2024 at time  $t = 45$  minutes under bending is shown in Fig. 4.3. As the numbers of mesh elements are increased the maximum stress induced also increases and soon reaches a plateau. When this maximum induced stress reaches plateau indicates the number of mesh elements have being optimized and any further increase in number of elements have negligible effect of the maximum induced stress. In most of the models, the solution had optimized when the numbers of elements are in range of 350000-450000.

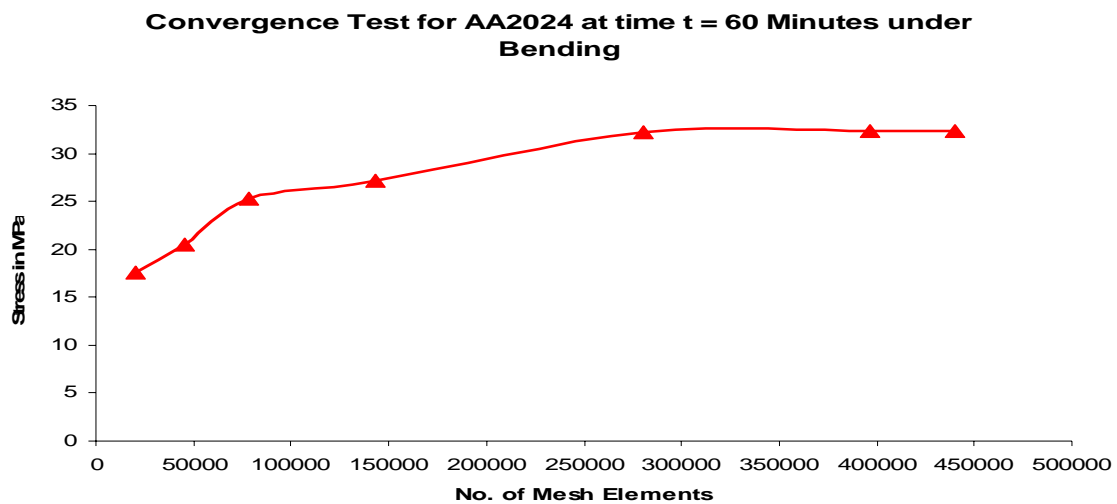


**Figure 4.3: Mesh Convergence test**

#### **4.2.1 Corrosion Specimens under Bending Loading**

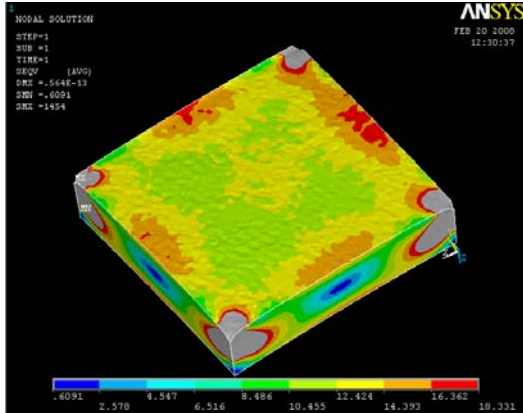
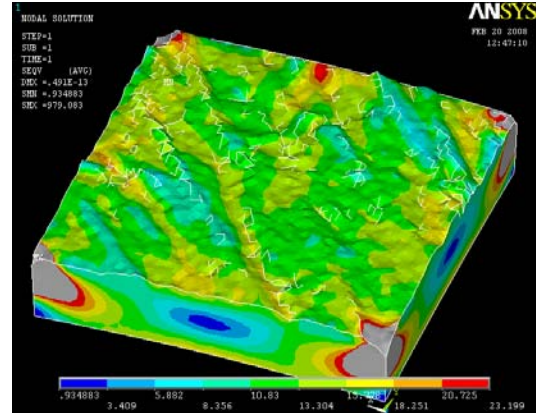
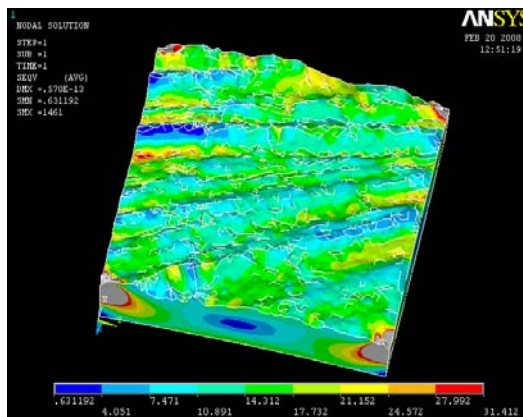
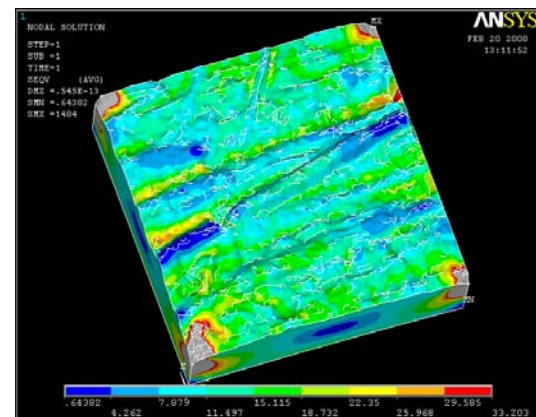
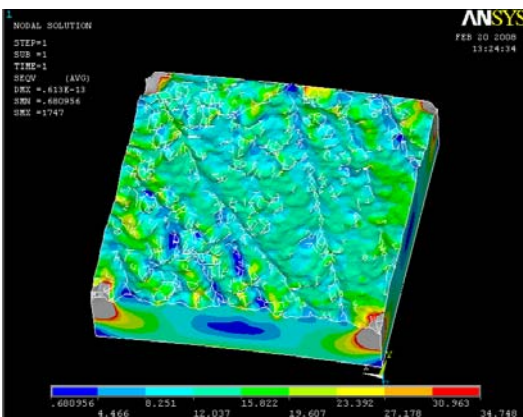
The model of the AA2024 and SS316 specimens for different corrosion time are analyzed under bending for the induced stress distributions.

### **AA2024 Specimen under Bending Loading**

Figure 4.4 shows the von-Mises stress distributions on the model surface obtained from the finite element analysis of the corroded AA2024 sample at different times under bending. Initially when the sample is not corroded at  $t = 0$  minutes (Fig 4.3(a)), the induced stress distribution under loading seems uniform over entire surface. The regions near the corners which were assigned fixed displacement are neglected from the study as those regions show more induced stress due to fixed displacement. The induced stress level is varied from region to region in surface model, the maximum stress level is observed at the side. However, the middle region of the model surface is at a little higher stress level than that of regions on their side. The maximum induced von-Mises stress is at 16.9 MPa.

Figure 4.4(b) shows the induced von-Mises stress distribution from the finite element analysis for the sample corroded for  $t = 15$  minutes. The maximum von-Mises stress is at 22.5 MPa and it is induced at the pit located on the side of the model surface. The surface which are at higher height like bumps formed due to accumulation of the oxides have induced low stress region on them. While the long pit like structure have induced high stress on them. The induced stress changes as the height is varied on those bumps and pits. At corrosion time = 30 minutes (Fig. 4.4(c)), there is an increase in the induced maximum stress as the roughness of the sample is increased. The bumps and valley have grown in size and shape due to accumulation of the oxides on the sample surface. The stress distribution is not uniform due to this surface roughness and maximum stress of 30.43 MPa is observed at high pit depth.



a) at time  $t = 0$  minutesb) at time  $t = 15$  minutesc) at time  $t = 30$  minutesd) at time  $t = 60$  minutese) at time  $t = 90$  minutes

**Figure 4.4: Von-Mises stress distribution on the model surface at different corrosion time for AL2024 under bending**

For corrosion time  $t = 60$  minutes and  $t = 90$  minutes (Fig 4.4(d) and Fig 4.4(e)), similar stress distribution is observed as that of  $t = 30$  minutes. But the surface roughness has increased during these times and so is their maximum induced stress. However, the increases in induced maximum stress have decreased as the time is increased.

Figure 4.5 shows the correlation of maximum von-Mises stress as a function of corrosion time. It can be seen that as the corrosion time increases the pit stresses increases and reach a plateau. Initially, the stress increase faster due to sharp pits and then become flat due to sharp pits become blunt. There is a stress increase of 80% within first 30 minutes and the increase is about 6% when the sample is corroded from 30 to 60 minutes. After 60 minutes of total corrosion time, there is negligible increased of 2 % in maximum stress when corroded further. This suggests that further growth of oxide layers don't affect increase the maximum stress. However, the strength of the oxide layers are less than that of the sample and it might result in failure under these loading. The failure of oxide layer is not considered in this particular analysis. The failure of these oxide layers may result in formation of more pits or enlargement of the pit which further increases the maximum stress on the sample surface. The pit stress level of 30 MPa obtained from this study are reasonable to initiate the crack, since the fracture toughness of AA2024 alloys are in range of  $26-37 \text{ Mpa.m}^{0.5}$ .

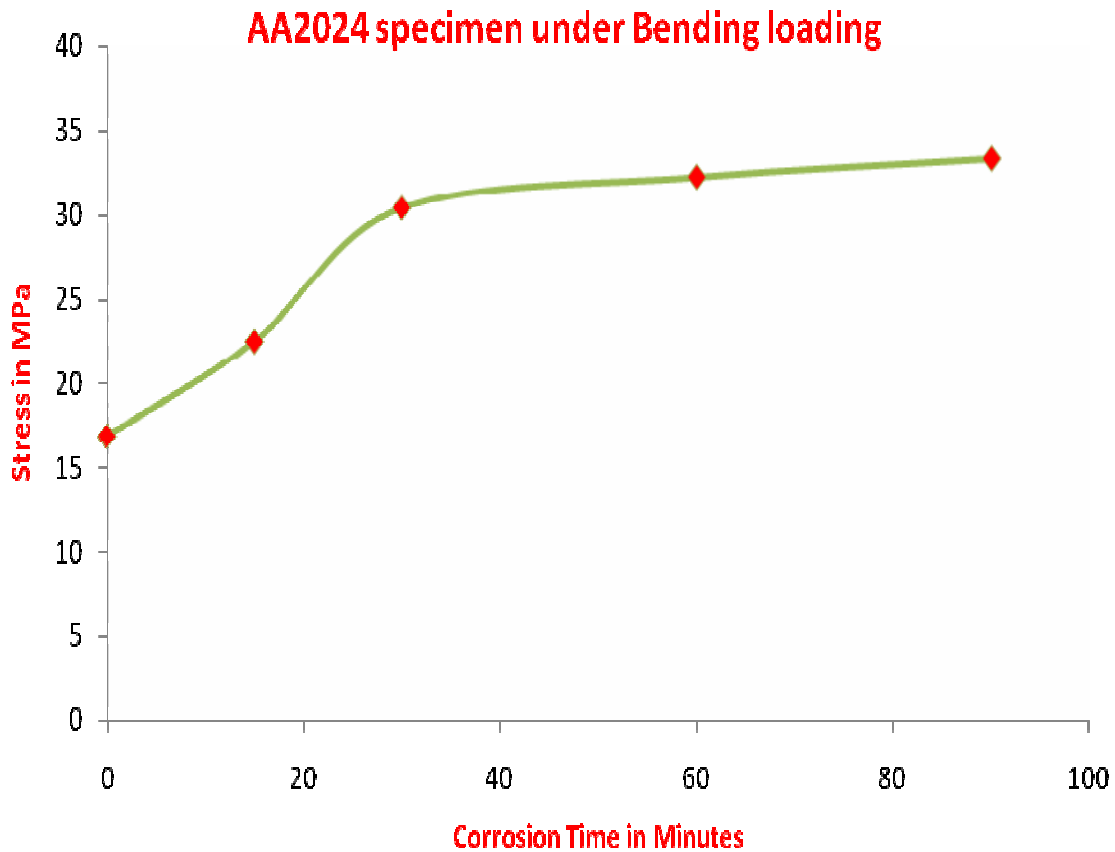


**Figure 4.5: Maximum von-Mises stress predicted from finite element analysis for corroded Al2024 sample at various corrosion time under bending**

### **SS316 Specimen under Bending Loading**

Figure 4.6 shows the von-Mises stress distributions on the models surface obtain from the finite element analysis of the corroded SS316 sample at different times under bending loading. The stresses induced on the corners are ignored from the studies since those corners were applied fixed displacement. At time  $t = 0$  min (Fig 4.6(a)), the sample surface does have some imperfections on it but a uniform stress distribution is induced on

the surface. Higher stress levels are observed on the side of the model and lower stress level are observed in the middle portion of the model. The stresses on the imperfections are higher than their neighboring regions. When the SS316 was corroded for first 15 minutes (Fig. 4.6(b)), the surface seemed to have few pits and deposition of oxides on few regions. The stress distribution seemed to be uniform in the regions where there is no pits and deposition of the oxides. The regions with deposition are at low stress level than that of the non-corroded regions and pits are at high stress levels. The maximum stress is observed on the pit which located towards the side of the model.

As the corrosion time is further increased, there was a little increase in formation of pits and depositions of the oxides on the surface. Non-uniform stress distribution is observed on the surface due to surface roughness. It is clearly seen that the induced stress is dependent upon the height and location of the irregularity on the surface. The maximum stresses are observed on the pits on the end of the surface. The film forming process is observed at  $t = 90$  minutes (Fig 4.6(e)), there is a massive deposition of the oxides on the surface but the deposition is not uniform. Due to this lot of bumps and pit regions are formed on the surface. So a non-uniform stress distribution is induced on the surface and very low is induced on the surface where there is high deposition of the oxide. Maximum stress is observed on the maximum pit height.

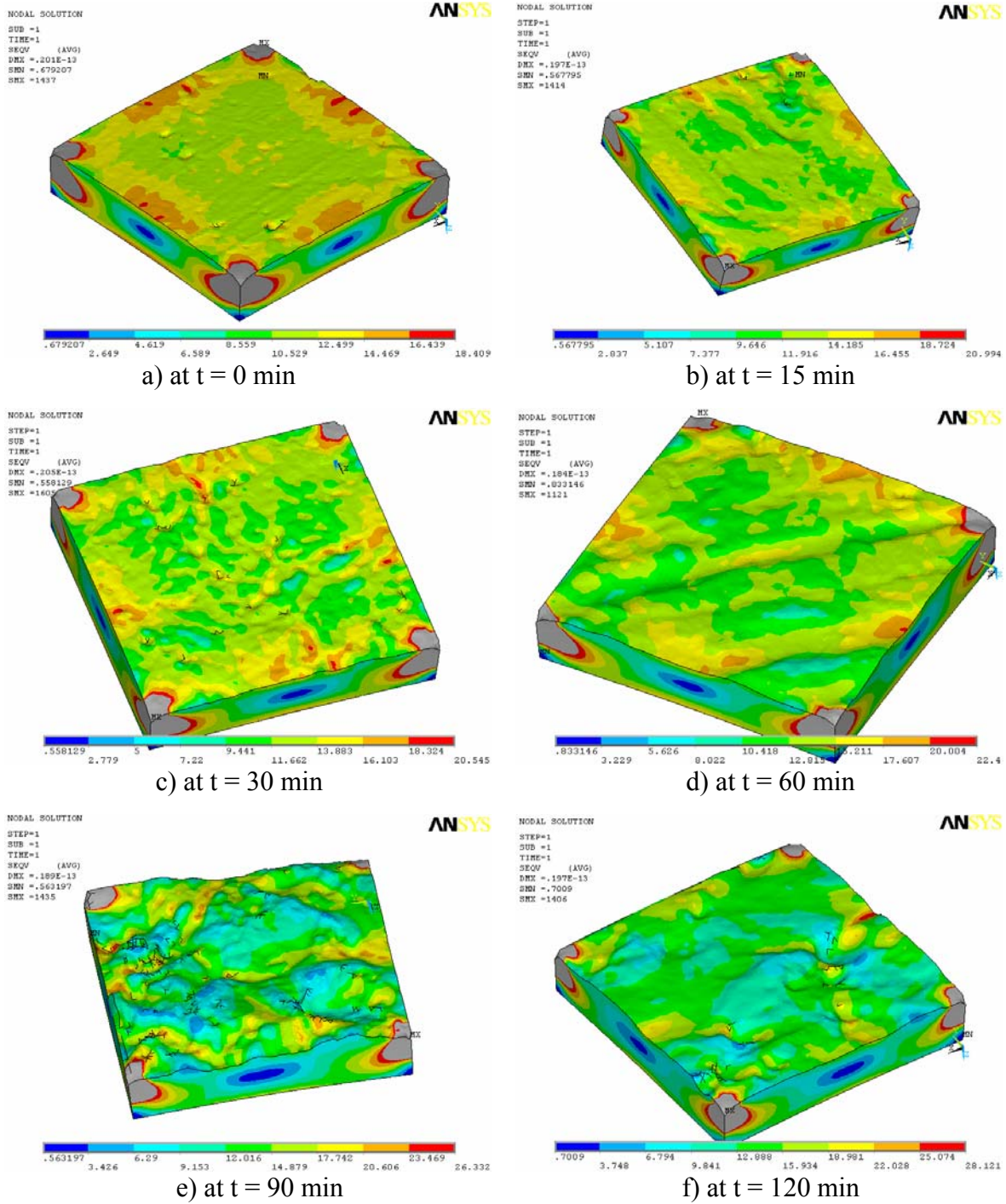


**Figure 4.6: Von-Mises stress distribution on the model surface at different corrosion time for SS316 under bending**

A uniform stress distribution is observed when the sample is not corroded. A non-uniform stress distribution is observed as the stainless steel corrodes further. Pitting and film forming forms of corrosion is observed and this has changed the induced stress distribution on the surface. The maximum stresses are observed on the pits on the surface and low stresses are observed on the regions with high deposition of oxides. So it can be suggested that height of the imperfection also plays a vital factor in inducing stresses when load is applied. However, the location of pit is also an important factor in determining the maximum stress induced on the surface.

### SS316 Specimen under bending

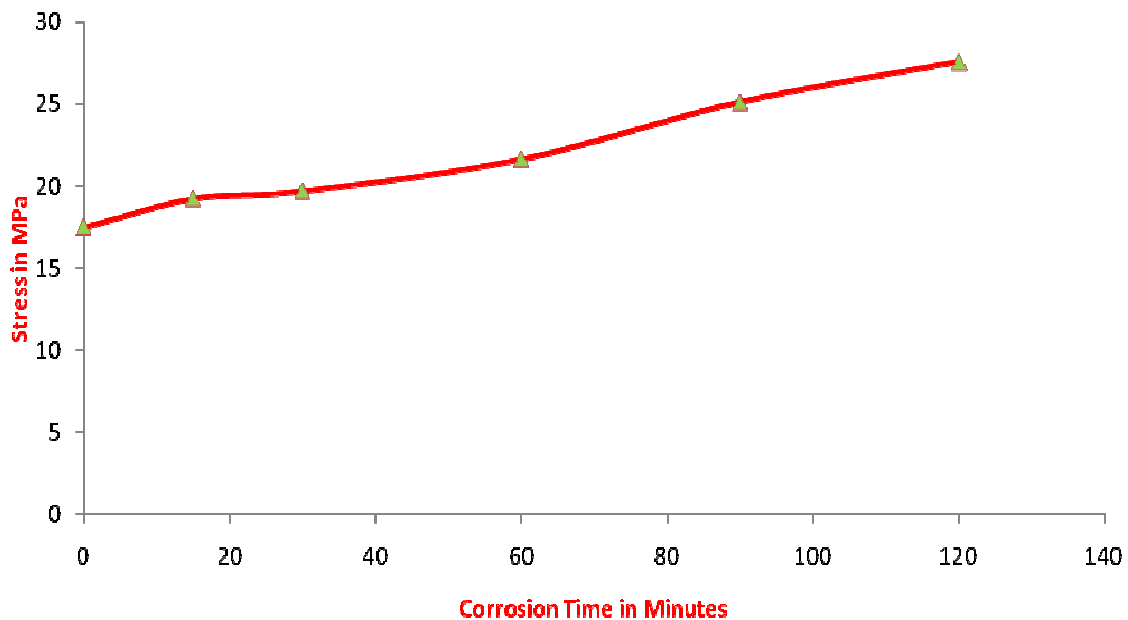


**Figure 4.7: Maximum von-Mises stress predicted from finite element analysis for corroded SS316 sample at various corrosion time under bending**

Figure 4.7 shows the maximum von-Mises stress predicted for SS316 at different corrosion time under bending loading. Initially, when the sample is not corroded the maximum stress is at 17.81 MPa when 1MPa bending pressure is applied. When the sample is corroded for first 30 minutes there was an increase of 12.72% in maximum stress. This increase in maximum stress was due to formation of the pits on the surface formed during corrosion. At time  $t = 60$  minutes there was a increase of 23.78% increase in maximum stress. The depositions of oxides have increased during this period which increased the relative height of the pit with their neighboring regions. When the corrosion time is further increased to 90 minutes there was an increase of 16.10% in maximum stress. When the film forming process is continued further there was increase of 9.75% in maximum stress. The increase in maximum stress seemed to be demising as time increases and soon the maximum stress will reach to maximum limit and there will be little or no increase in maximum stress. It is clearly seen that the maximum stress increases as pitting and film forming corrosion increases.

#### **4.2.2 Corrosion Specimens under Tension Loading**

The model of the AA2024 and SS316 specimens for different corrosion time are analyzed under bending for the induced stress distributions.

##### **AA2024 Specimen under Tension Loading**

Figure 4.8 shows the von-Mises stress distribution on the model surface obtains from the finite element analysis of the corroded AA2024 sample at different times under tension loading. As seen from Fig 4.8(a), when the sample is not corroded the induced stress distribution on the surface seems to be uniform. The maximum stress induced is 1.04

MPa and in the regions near the face where the unit pressure load was applied. The region near the fixed displacement corners are ignored from the study as they will induced more stress due restrictions of the displacement. Low stress region are formed where near the fixed corners. At corrosion time  $t = 15$  minutes (Fig 4.8(b)), due to deposition of the oxide on the surface an uneven induced stress distribution is observed. The depositions of oxides have created few bumps, groove and few pits on the surface which have increased the surface roughness of the model. The bumpy regions shows less stress induced under tension loading and regions with groove and pits which are lower in height seemed to have induced high stress region within them. The maximum stress of 1.4924 MPa is observed at the maximum pit size.

As the corrosion time is further increased (Fig 4.8(c-e)), there is an increase in deposition of the oxide which have change the size and shape of the bump, groove and pits on the surface. There is a change in stress regions due to this change in size and shape of these irregularities on the surface. So it can be predicted that the stress distribution on the model surface is dependents upon the height and shape of the irregularities on it.

Similar stress distributions are observed for all corrosion time when the sample is further corroded. Low stress regions are observed on the regions which are at higher height compared to their neighboring regions and high stress regions are observed on the regions which are at lower heights. The groove on the surface which is less corroded or un-corroded is also considered similar to pit as these region induces high stress region within them. However, maximum stresses are induced on the pits which are at maximum pit depth.



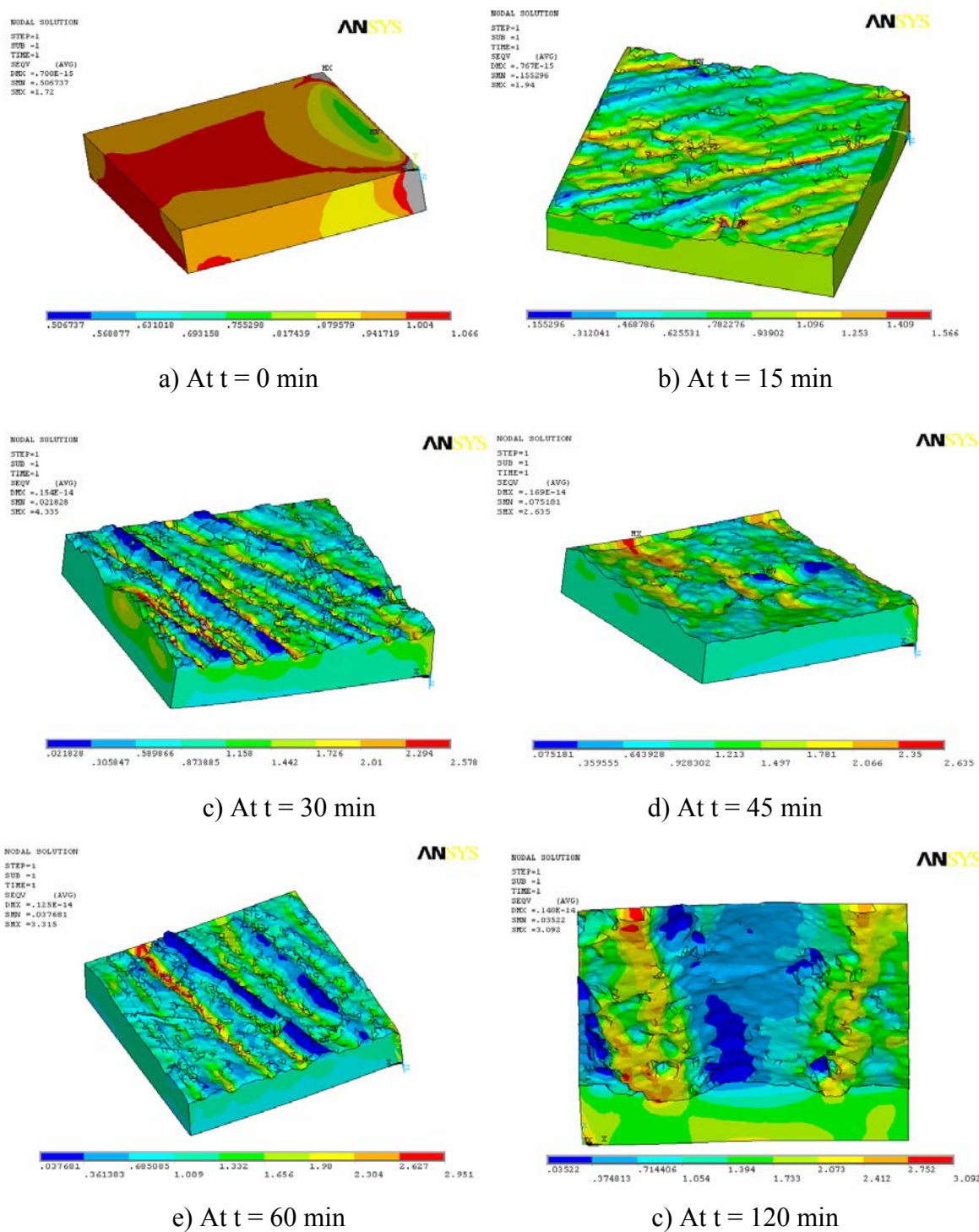


**Figure 4.8: Von-Mises stress distribution on the model surface at different corrosion time for Al2024 under tension loading.**

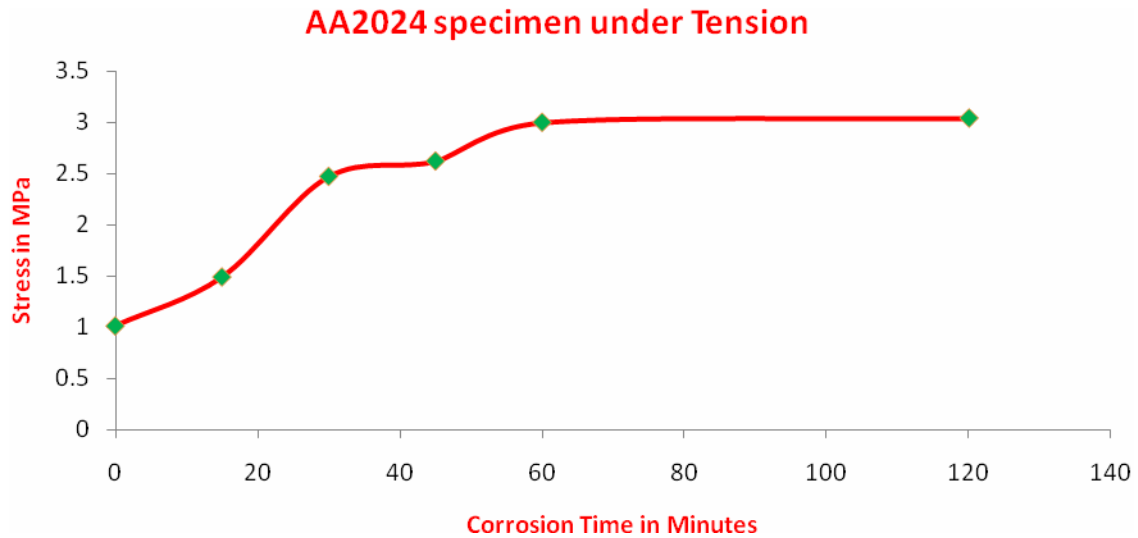


**Figure 4.9: Maximum von-Mises stress predicted from finite element analysis for corroded Al2024 sample at various corrosion time under tensile loading.**

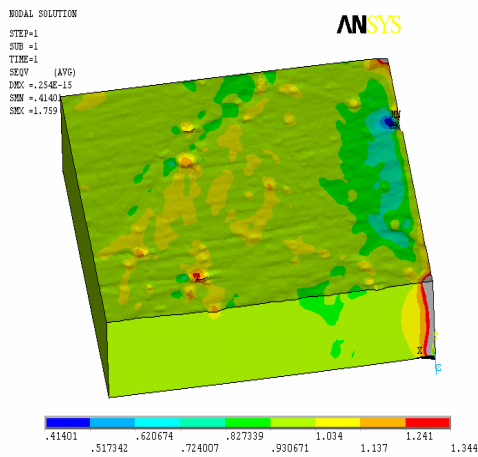
Figure 4.9 show the maximum von-Mises stress predicted for AA2024 at different corrosion time under tensile loading. Initially, when the sample is not corroded the maximum stress induced is closed to 1 MPa same as the stress applied. When the sample is corroded further for 15 minutes there was an increase of 43.5% in maximum stress. This increase was due to increase in surface roughness because the pits and bumps have formed on the surface. During the time interval 15-30 minutes there was further increase in maximum stress by 65.6%. The increase in maximum stress on further corrosion seems to be demising due to saturation on formation of the irregularities on the surface. However, for  $t = 60$  minutes there was a little increase in maximum stress due to increase in deposition of the oxides on it which have increase the relative depth of the pit. The tensile loading can lead to breakdown of the oxide layers on the sample and can even expedite the

process of the pit growth. During the simulation the strength of oxide layers is considered same as that of the AA2024. Overall, the maximum stress increases as the corrosion time is increased and it will reach plateau.

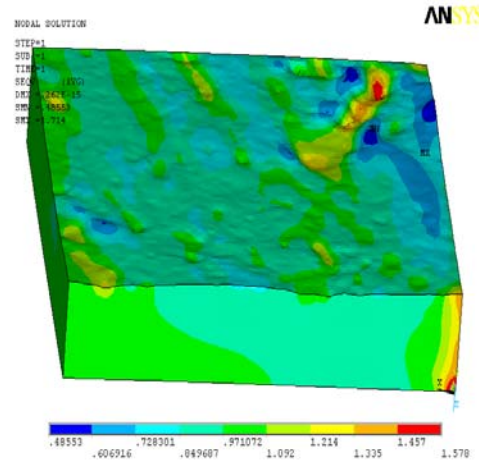
### **SS316 Specimen under Tension Loading**

Figure 4.10 shows the von-Mises stress distributions on the model surface obtained from the finite element analysis of the corroded SS316 specimen at different times under tension loading. Initially when the sample is not corroded the sample does have some irregularities on the surface. Uniform stress distribution is observed on the surface but high stress level is observed on the irregularities on the surface. The induced stress on the surface is 1.3 times higher than that of the input stress due to small irregularities on the surface.

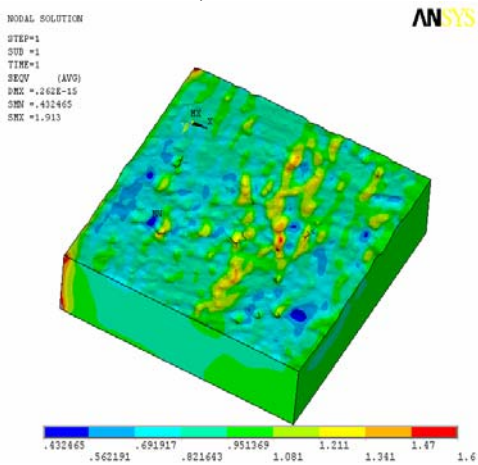
When the SS316 is corroded for first 15 minutes (Fig. 4.10(b)), the high stress regions are observed within the pits on the surface. The stress distribution of the surface other than the pit regions is uniform. A maximum stress is induced on the pit which has maximum pit depth. At time  $t = 30$  minutes (Fig. 4.10(c)), more small pits are observed on the surface. The stress distribution of the surface is non-uniform due to presence of lots of pits on the surface. The pits which have relative low height compare to the regions next to them, have induced high stress within them. There are few regions which have depositions of the oxides layer on the surface due to which low stress regions are induced on those regions. Maximum stress is observed on the pit which has maximum pit depth.



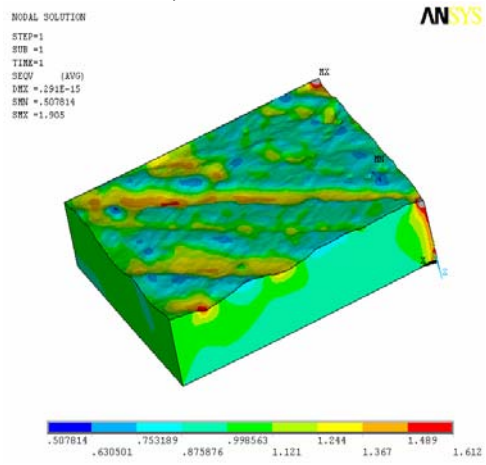
a) at t = 0 min



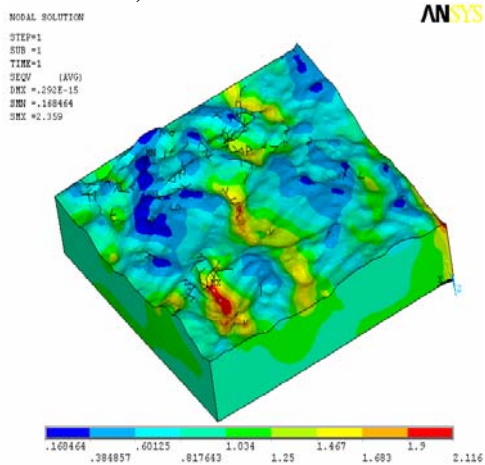
b) at t = 15 min



c) at t = 30 min



d) at t = 60 min



d) at t = 90 min

**Fig 4.10: Von-Mises stress distribution on the model surface at different corrosion time for SS316 under tensile loading**

When the time is further increased by 30 minutes (at  $t = 60$  min, Fig 4.10(d)), the accumulation of the oxide layers have increased and a wavy profile is seen on the surface. The wavy profile is seen due to uneven depositions of the oxide throughout the surface. So the induced stress distribution is also uneven depending upon the irregularity, if the irregularity height is lower than high stress is induced and if the irregularity is higher height than low stress is induced. As seen from the optical result, at time  $t = 90$  minutes the film forming process has begin and the rate deposition of the oxides is increased. Due to these high accumulated oxides the surface roughness is increased and lots of irregularities are observed on the surface. The induced stress distribution is not uniform and is dependent upon the irregularities on the surface. The maximum stress is observed within the pit near to the surface where the load was applied.

The maximum stresses are observed on the pit and low stress is observed on the oxide deposition regions for each corrosion time. The location of the pit and pit depth is very important factor in predicting the occurrence of the maximum stress on the surface. If the difference of pits at different location is low than the location of the pit is dominating and if this difference is high than pit depth is dominating to determine which pit will induce maximum stress on the surface.

Figure 4.11 shows the maximum von-Mises stress predicted for SS316 at different corrosion time under tensile loading. Initially, when the sample is not corroded the maximum stress is at 1.32MPa when 1MPa tension pressure is applied. When the sample is corroded for first 30 minutes there was an increase of 19.64% in maximum stress. This significant increase in maximum stress was due to formation of the pits on the surface

formed during corrosion. But when the sample was corroded further by 30 minutes there was a little or no increase in maximum stress because most of pits have deposited by oxides. During time interval of 60-90 minutes of corrosion time there was an increase of 37.9% in maximum stress because of uneven deposition of oxide during film forming process. The maximum stress increases when the corrosion time increases but amount of increase is dependent on the size and shape of the irregularities on the surface. Overall there is increase in maximum stress during film forming and pitting forms corrosion because they change shape and size of irregularity.

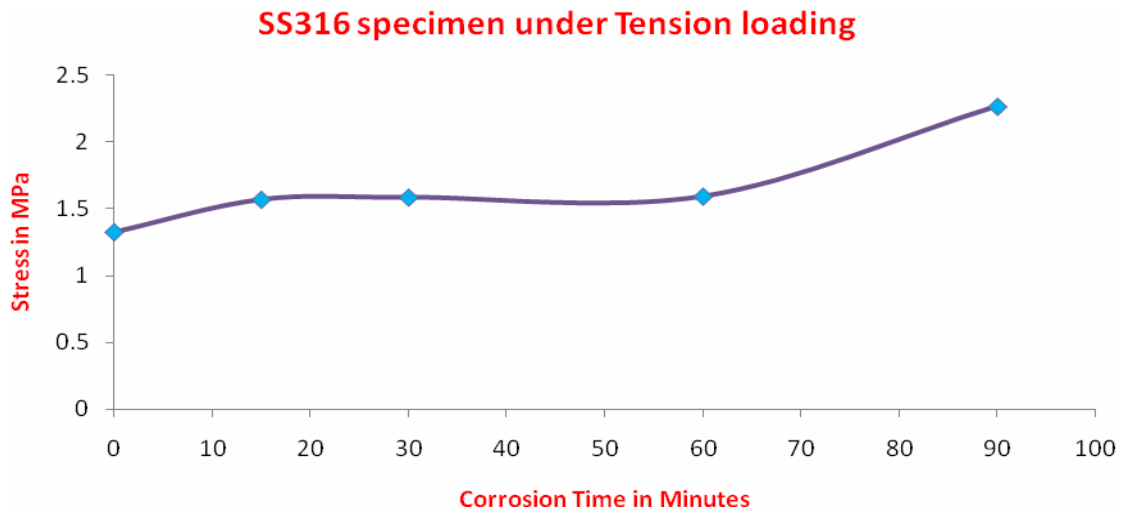


**Fig 4.11: Maximum von-Mises stress predicted from finite element analysis for corroded SS316 sample at various corrosion times under tensile loading**

#### 4.2.3 Corrosion Specimens under Shear

The model of the AA2024 and SS316 specimens for different corrosion time are analyzed under shear for the induced stress distributions.



AA2024 Specimen under Shear Loading

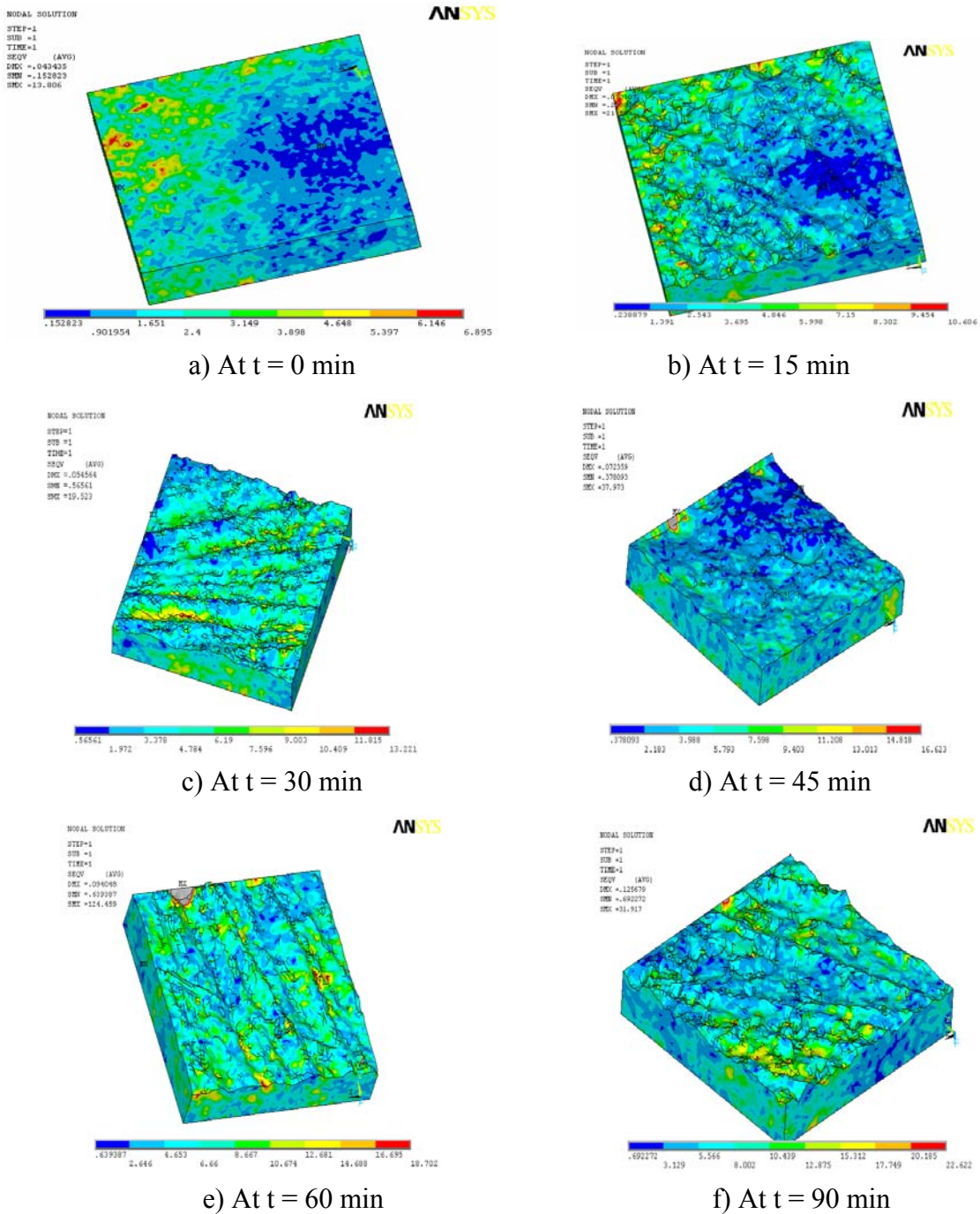
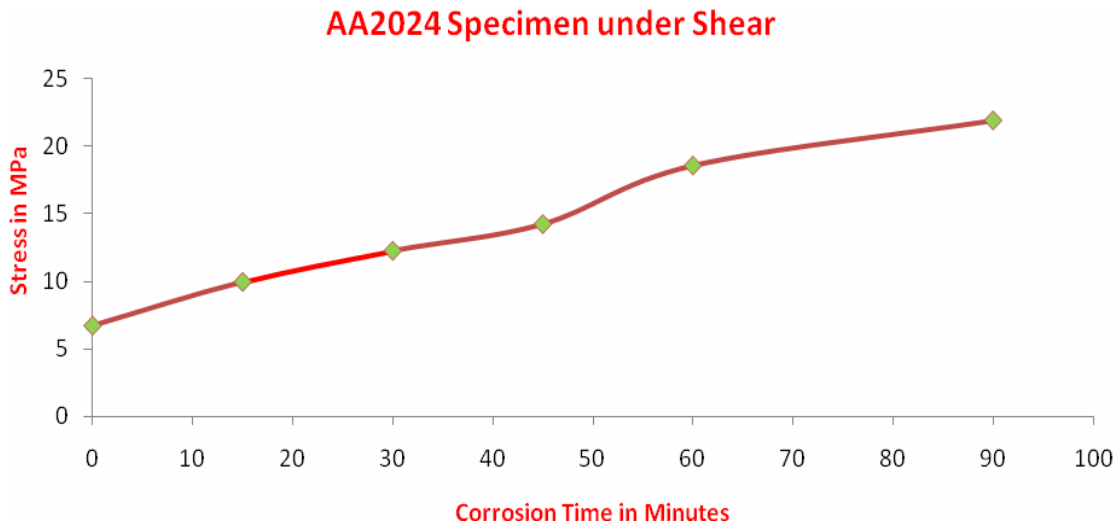


Fig 4.12: Von-Mises stress distribution on the model surface at different corrosion time for AA2024 under shear loading.

Figure 4.12 shows the von-Mises stress distribution on the model surface obtained from the finite element analysis of the corroded AA2024 specimen at different times under shear loading. As seen from Fig 4.12(a), when the sample is not corroded the induced stress distribution on the surface seems to be uniform. The maximum stress regions are observed on the face where the force is applied and low stress regions are observed near the fixed face. Due to little or no irregularities on the surface the stress distribution seemed to be uniform. When the sample is corroded for first 15 minutes, some irregularities like bump and pits have formed on the surface. Due to this the randomness of these irregularities the stress regions on the surface are varied on the basis of these irregularities. The maximum stress is observed on the pit which has maximum pit but location of the pit is also a vital factor.

As the sample is corroded further (Fig 4.12(c-e)), there was an increase in surface roughness. Due to this there was a change in shape and size of irregularities on the sample surface which have changed the induced stress distribution on the surface. The maximum stress regions are observed at pits which have high pit depth. The bumps formed due to accumulation of the oxides have low stress regions and region next to that bump are at high stress region. However, the maximum stress on the surface is dependent on location of the pit and maximum pit depth. The pits located near the face where the shear force is applied are at higher stress level than that of the pits of same height located on the other regions. If the pit depth is higher than the other pits then there are chances that maximum stress can occur on that pit. More study is required to see the effect of location and depth of pits on the maximum induced stress.





**Figure 4.13: Maximum von-Mises stress predicted from finite element analysis for corroded Al2024 sample at various corrosion time under tensile loading.**

Figure 4.13 shows the maximum von-Mises stress predicted for AA2024 at different corrosion time under shear loading. Initially, when the sample is not corroded the maximum stress induced is closed to 6.7 MPa when the applied shear pressure is 1 MPa. When the sample is corroded for 15 minutes there was an increase of 48.3% in maximum stress. This increase in maximum stress seemed to be demising as the corrosion time was increased further. But there was a sudden increase of 30.5% in maximum stress when the corrosion time was increased from 45-60 minutes due to a sudden increase in deposition of the oxides on the surface. This deposition has increased the pit depth relatively to the regions next to them. So it can be suggested the maximum stress increases as the corrosion time is increased and soon it will reach plateau.

SS316 Specimen under shear loading

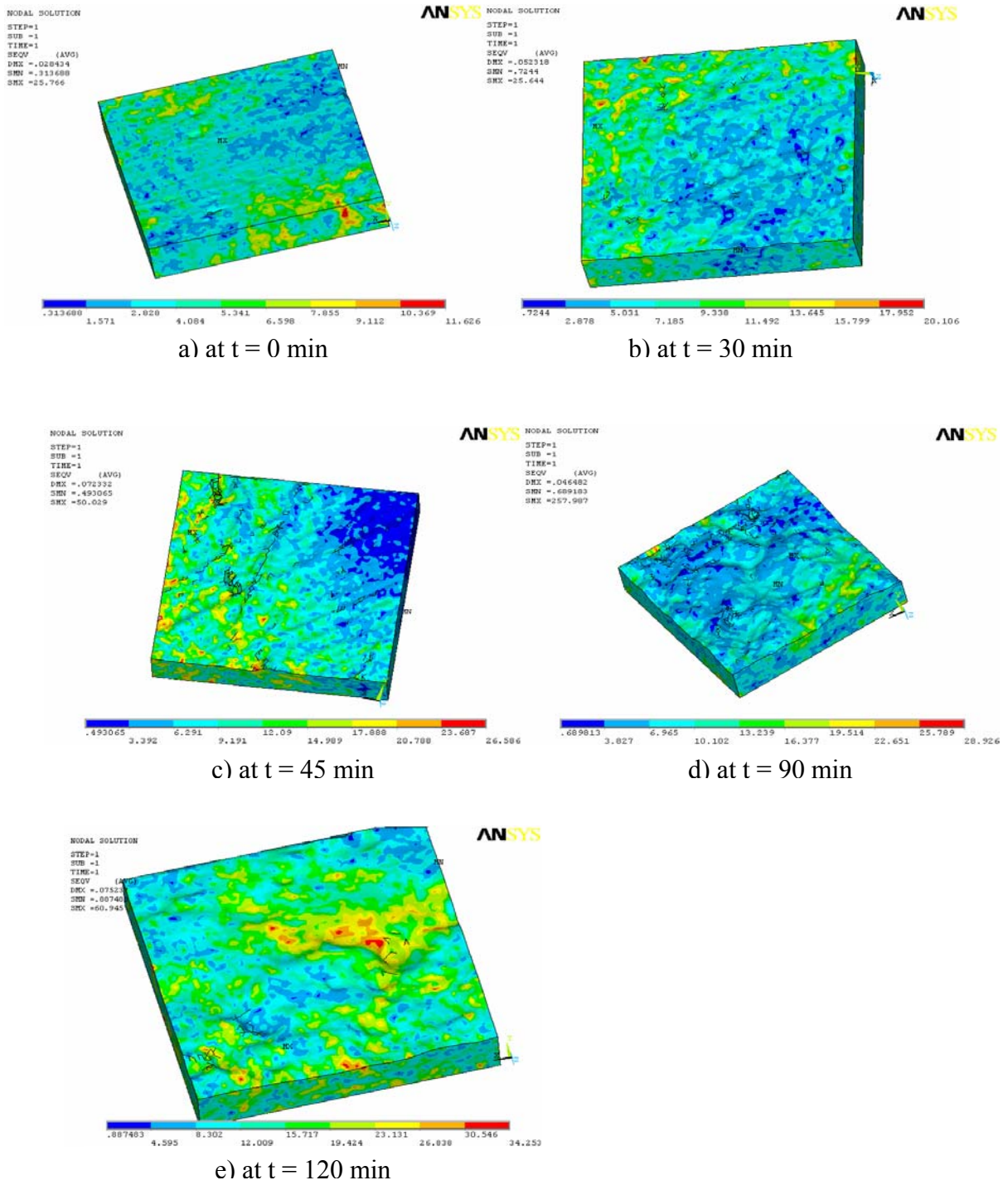


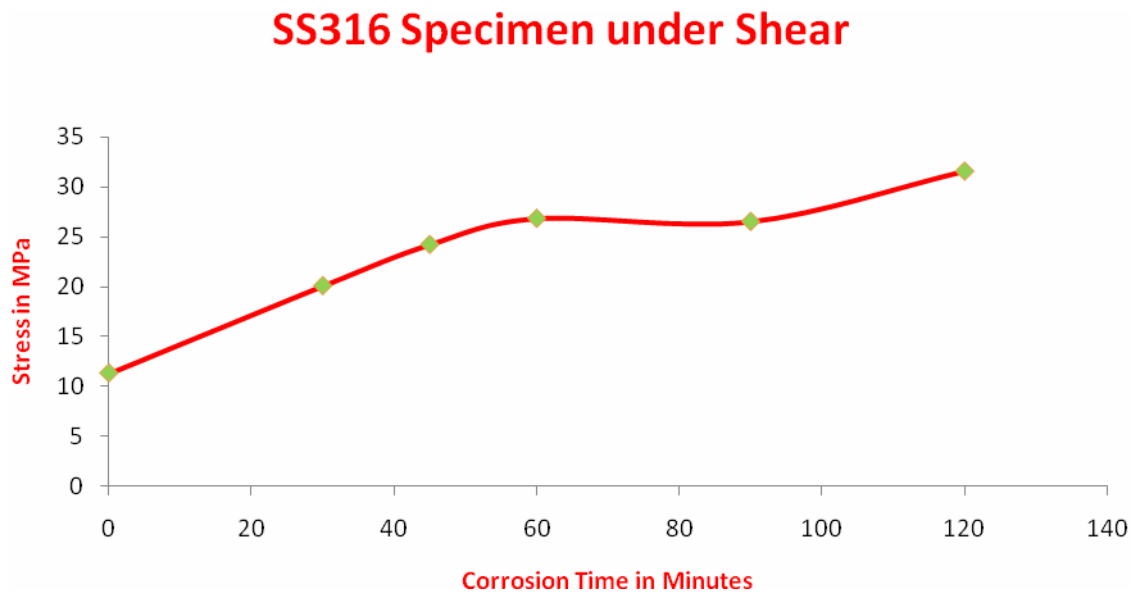
Fig 4.14: Von-Mises stress distribution on the model surface at different corrosion time for SS316 under shear loading.

Figure 4.14 shows the von-Mises stress distribution on the model surface obtained from the finite element analysis of the corroded SS316 specimen at different corrosion times under tension loading. When the sample is not corroded uniform stress distribution is induced on the surface. Regions with irregularity like small pits have induced more stress than other regions on the surface. Maximum stress is induced on the pit which has maximum pit depth on the surface. When the sample is corroded for first 30 minutes, there were few pits and deposited regions are observed on the surface of the sample. A non-uniform stress distribution is observed on the surface due to irregularity on the surface. High stress levels are observed on the pits and low stress regions are observed on the regions where there was a deposition of the oxides. The maximum stress is observed on the pit which was near to the face where the load was applied.

When the sample was corroded for 45 minutes, a wavy profile is observed on the sample surface. A non-uniform stress distribution is observed on the surface and the regions with pit shows high stress level are observed. However, maximum stress is observed on the pits near the face where the load was applied. Location of the pit is important to predict the maximum stress under shear loading when the comparative pits depth is low. During time  $t = 90$  minutes, during film forming process a non-uniform stress distribution is observed depending upon the irregularities on the surface. There are many pits on the surface but the maximum stress is observed on the pit near the face where the load is applied. However, the depth of the pit is little less than that of the other pit but it has a sharp pit shape due to which that region might have induced maximum stress during shear loading. When the corrosion time is further increased by 30 minutes, there was

deposition of the oxides in few regions. The stress distribution was varied from region to region depending upon irregularities formed on the surface. The regions near pits also induced more stress than that of other regions of same height.

Overall the maximum stresses are observed on the pit and low stresses are observed on the deposition regions for each corrosion time. The location of pit and pit depth are very important factors in determining the occurrence of the maximum stress on the surface.



**Fig 4.15: Maximum von-Mises stress predicted from finite element analysis for corroded SS316 sample at various corrosion times under shear loading.**

Figure 4.15 shows the maximum von-Mises stress predicted for SS316 at different corrosion time under shear loading. When the sample is not corroded the maximum stress is at 11.332 MPa when a unit shear pressure is applied. When the stainless steel is corroded

for first 30 minutes there is an increase of 77.26 % in maximum stress. This increase is due to formation new pits or enlargement of the pit before corrosion. When corroded further for 60 minutes, there was an increase of 32.05% in maximum stress. This might be due to huge deposition of oxide which has increased the roughness of the surface by forming bumps and pits. There is a further decrease in the increase in maximum stress when the corrosion time is further increase. If this trend continues then maximum stress soon reach a value and then there will be no further increase in stress. Overall, the maximum stress increases as the corrosion time increase but the amount of increase in maximum stress decreases as the corrosion time is increased.

#### **4.3 Comparison of maximum stresses in AA2024 and SS316 Specimen**

Fig 4.16 shows comparison of predicted von-Mises maximum stresses for AA2024 and SS316 for different type of loadings. It is clearly seen that type of loading is very important in inducing stresses on the surface. A bending and shear load induces more than that of the tensile loads and the stresses induced are in almost in the range of the fracture toughness of the material. However, a tensile load induces the stress three times that of the input stress.

As it is seen from the finite element analysis that stress increases as the corrosion time was increased .When a bending load was applied on the models of AA2024 and SS316 specimens at different corrosion time, the maximum stress induced in AA2024 was higher than that of SS316 at any given time. The maximum induced stresses under bending loading seemed to close to the facture toughness of the materials.

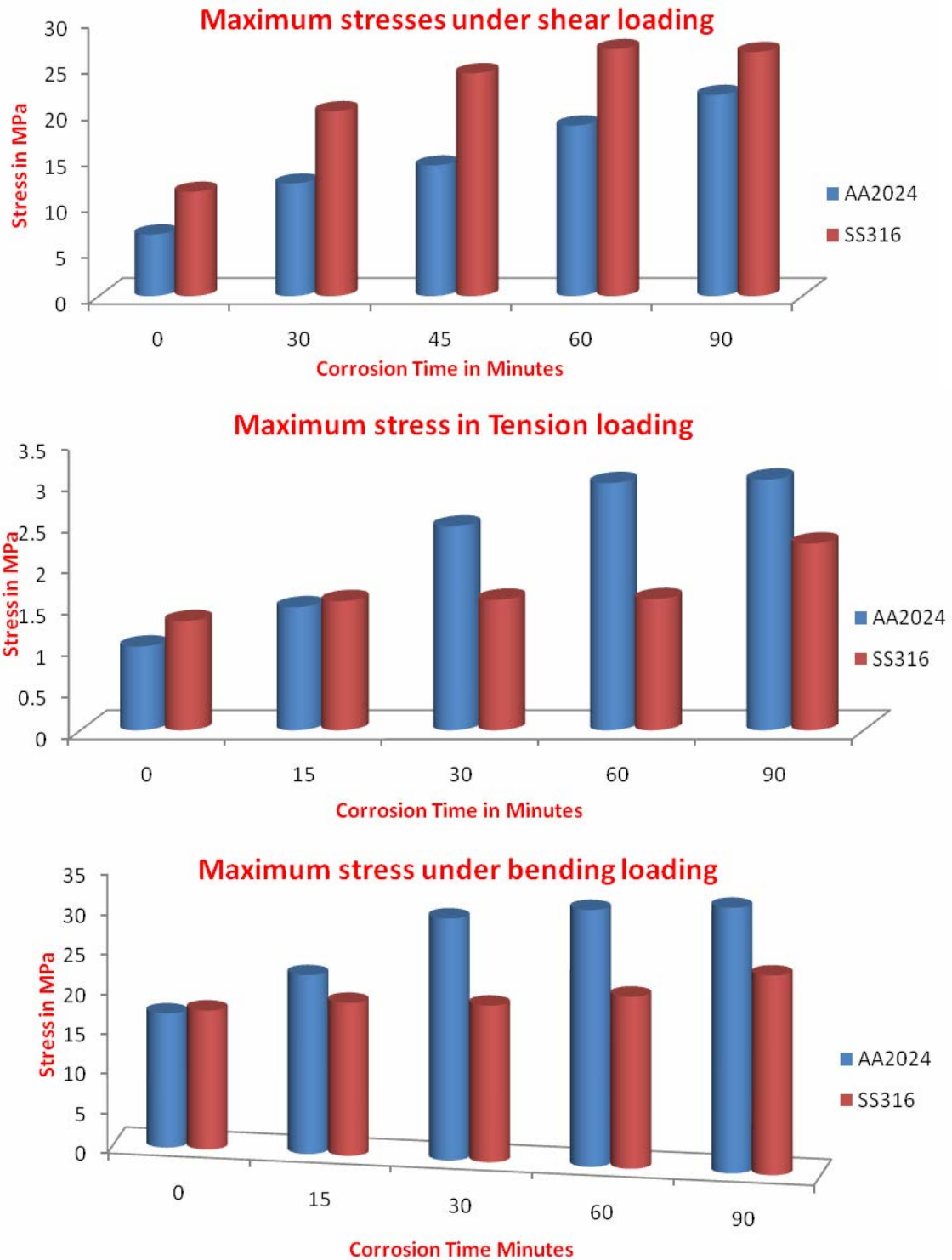


**Figure 4.16: Maximum predicted stresses for AA2024 and SS316 specimens at different corrosion time for different types of loading**

Due to bending the pits will grow in size and depth and can easily form the crack due to high induced stress around them. When the specimens were not corroded the maximum stress induced in both specimens was almost the same. At time  $t = 15$  minutes, the maximum stress induced in AA2024 was 16.9% higher than that of SS316. When the corrosion time was further increased by 15 minutes, the maximum stress induced in AA2024 and SS316 specimen was also increased. At this particular time, the maximum induced stress in AA2024 was 54.4% higher than that of the SS316 specimen. As the time is further increased the difference between the maximum induced stresses in both specimens seemed to be decreasing by small amount. It was clearly seen from the microscopy results that the corrosion damage of AA2024 specimen was much higher than that of the SS316 specimen at any given time. So the stress induced in the AA2024 was higher than that of the SS316 at given time.

When a tensile load is applied on models of AA2024 and SS316 specimens at different corrosion time, the maximum stress is predicted is close to the input stress. Initially, when the specimens are not corroded the maximum induced stress in SS316 is higher than that of the AA2024. The maximum stress in AA2024 was same as the input stress but the maximum stress in SS316 was higher due to some irregularity on the surface. At time  $t = 15$  minutes, the maximum stress induced on both specimens was almost the same. There was formation of some irregularity in both specimen but AA2024 had formed more irregularity than that of the SS316. It was clearly seen from the finite element results that as time increases the induced stress increases in both specimens and soon reaches plateau. At  $t = 30$  minutes, the stress induced in AA2024 is 56.2% higher than that of the

SS316. The localized corrosion for the AA2024 seemed to be increasing as the time was increased but the SS316 had offered high resistance to corrosion due to which AA2024 had more irregularities on the surface compared to SS316 specimen. At time  $t = 60$  minutes, the stress induced in AA2024 is 88.5% higher than that of the SS316. When the specimens was further corroded by 30 minutes ( $t = 90$  minutes), SS316 seemed to have a formed a film on the surface which had increased the surface roughness of the specimens. Due to this the SS316 have lot of irregularity on the surface which induces more stress on this specimen. The maximum stress induced at 90 minutes in AA2024 is 34.2% higher than that of the SS316. The difference between the induced stresses in both materials seemed to be demising as the maximum stress reaches plateau.

When a shear loading is applied on the models of AA2024 and SS316 specimens at different corrosion time, the maximum stress induced is close to the facture toughness of the materials. The maximum induced stress in both specimens increases as the corrosion time increases and soon reaches plateau. The stresses induced in SS316 specimen are higher than that of AA2024 at any given time. Initially, when the specimens were not corroded the stress induced in SS316 is 69.2% higher than that of AA2024 specimen. This was due to some imperfection on SS316 specimen due grinding. This stress difference between these specimens was observed further as the corrosion time was increased to 30 minutes. At time  $t = 45$  minutes, the stress induced in SS316 sample is 70.6% higher than the AA2024. The maximum stress induced in the SS316 seems to reach plateau and the stress induced in the AA2024 specimen is still increasing. The difference in maximum stress between these specimens seems to be demising as the corrosion time was further



increased. The maximum stress induced on the pit but occurrence of the maximum stress on the pit seems to be dominated by the location of the pit on surface compared to maximum pit depth.

## CHAPTER 5 CONCLUSION

### Conclusions

The Aluminum alloys AA2024 and Stainless steel alloy SS316 both offers high resistance to corrosion. Both materials have a complex microstructure due to which they are subjected to localized form of corrosion like; pitting and film forming. AA2024 have S-phase intermetallics microstructure due to which it is subjected to localized corrosion. The copper (Cu) element improve the mechanical strength of the alloy but it precipitate as bigger intermetallics (IM) which are weak electrochemically, so localized form of corrosion occurs in AA2024. The stainless steel alloy SS316 have a duplex microstructure due to elements like Chromium, Carbon, Molybdenum, Nickel and Manganese. SS316 is subjected to form a passive film on the surface which offers high resistance to further corrosion. The corrosion resistance of SS316 is higher than that of the AA2024 due its microstructure which they offer high passivity to corrosion.

The Aluminum alloys AA2024 and Stainless steel alloy SS316 are corroded in the forced corrosion environment of 2 Molar NaCl. The corrosion rate for AA2024 is much higher than that of SS316 at any given time. The corrosion rate for AA2024 increases as the time as the time increases. During initial corrosion period (0-45 minutes) of the AA2024 continues to provide high resistance to corrosion due to which the corrosion rate remains the same. But as the time is increased the corrosion resistance for AA2024

decreases and the rate of corrosion increases sharply and soon reaches plateau (45-90 minutes). After this period of time the corrosion rate seems to be demising due to high corrosion resistance offered by the corroded regions. The corrosion rate for SS316 increases sharply when initially corroded (0-15 minutes) but after that SS316 seemed to offer high corrosion resistance when further corroded (15-60 minutes) due which the corrosion rate decreases by 84.2%. The corrosion resistance decreases as the film forming process (60-120 minutes) due to which the rate of corrosion increases sharply and soon will reach plateau. The corrosion resistance of SS316 specimen is higher than AA2024 for this particular corrosive environment since, the average corrosion rate for AA2024 is six times higher than that of the SS316. The SS316 offers high passivity compared to AA2024 after initial corrosion due to its duplex microstructure.

The optical microscopy of the corroded specimens suggests that both AA2024 and SS316 are subjected to localized form of corrosion. Initially, when AA2024 is corroded under this particular environment some localized regions are randomly corroded. These localized regions seemed to be expanded in size and shape when further corroded. The corroded regions offer less resistance due to change in polarity of intermetallics which provoke the corrosion of the adjacent regions. Soon a uniform form of corrosion was observed due to further growth of these corroded regions and soon these regions get united. Some pitting corrosion was also observed during corrosion. So overall AA2024 is subjected to pitting and oxide accumulation type of corrosion on localized regions during initial corrosion and since these regions expands in size and shape a uniform form of corrosion is expected in this type of corrosive environment. When the SS316 is initially

corroded, few localized regions are corroded randomly and two big pits are observed. The pits formed during initial period of corrosion are seemed to be expanded and new pits are formed due to removal of oxide layers when further corroded. SS316 had formed a film on the surface of the specimen after 60 minutes of total corrosion. These film formed may majorly consist of chromium oxide since chromium element in SS316 is supposed to formed a corrosive resistant film when corroded. So overall SS316 is subjected to localized pitting corrosion and few regions with oxide depositions and these pits are expected to expand in size. Film forming is also expected when further corroded and more pitting is expected if the film breakdown.

The Atomic Force Microscopy of the corroded specimens suggests that surface roughness of AA2024 and SS316 increases as the corrosion is increased. A uniform corrosion is observed on the AA2024 specimen when scanned at micro-level. Initially, when the AA2024 is corroded a wavy pattern is observed and there was a further growth in wavy pattern due to random deposition of the corrosion oxides. The wavy profile is observed at different corrosion time but the profile of the surface becomes random when corrosion regions are saturated. The average surface roughness for AA2024 had increased sharply during initial corrosion and as corrosion progresses the amount of increases in surface roughness demises due to passivity. There was a sharp increase in surface roughness when the specimens recover from passivity. Pits, grooves and bumps are appeared on the surface due to corrosion and these irregularities are expanding with increased corrosion. A localized corrosion is observed in SS316 even at micro-scale, when initially corroded. On further corrosion, a uniform corrosion was observed along with few

pits and bumps on the surface of SS316 specimen. The average surface roughness of the SS316 increases as the corrosion increases but the amount of increase is low during initial period of corrosion due to passivity. Erosion type of corrosion was observed at time  $t = 45$  minutes, when the corrosion oxides are removed from the surface and a new pit was formed due to it. A huge deposition of oxides was observed during the film forming process and the surface roughness have drastically increased by 80%. On further corrosion this accumulation in SS316 seemed to be increasing along with little increase in surface roughness.

An analysis procedure was developed using CAD and ANSYS, finite element software to predict the stresses due to corrosion damage. It was clearly seen from the results of finite element analysis of AA2024 and SS316 that the maximum induced stress increases as the corrosion time was increased and soon reaches plateau under different type of loading. Usually a uniform stress distribution is expected and observed prior to corrosion in the specimens. Even a small irregularity on the surface increases the induced stress for example; SS316 specimen had few irregularities due to the induced stress had increased due to these irregularities on the surface. As the specimens were corroded the irregularities on the surface had also increases depending upon type of material. Usually the pits, groove and bump are observed as the irregularity on the surface. The stress distribution on the specimens seems to be non-uniform as the irregularity on the surface increases. High stresses are induced on those regions on the pits or on those regions which have relatively low height compared to their neighboring regions. Low stress regions are observed on the regions which have oxide accumulation on the surface. As the size of the

pits and groove increases with further corrosion, the intensity of the induced stress also increases. Ideally, maximum stress is induced on the pits which have maximum pit depth under any type of loading. The finite element results indicate that occurrences of maximum stress are within the pit but it depends upon both pit depth and location of the pit on the surface. If the relative depth between two pits is high then the maximum stress will be induced on the pit with maximum pit depth or it will be induced on the pit which is near to the loading surface.

The type of loading on the specimens can also change the intensity of the induced stress on the surface. The maximum stresses induced in AA2024 and SS316 specimens are close to fracture toughness in bending and shear type of loading. In tension loading, the maximum stress induced is three times the input stress. The stress induced in AA2024 is higher than that of SS316 at any given time in case of bending and tension loading. However, the stress induced in SS316 is higher than AA2024 under shear loading. In AA2024, the induced stress increases sharply during first 30 minutes of corrosion under different types of loading and then the induced stress increases but amount of increase diminishes as the corroding time increases. For SS316, the induced stress gradually increases between the corrosion times (0-60 minutes) and after that the amount of increase in induced stress diminishes. However, under shear type of loading in SS316 specimen, the induced stress increases sharply during the initial corrosion (0-60 minutes) and on further corrosion the amount of increase in induced stress seemed to be diminishing.

**Recommendations and Future work**

Corrosion of AA2024 and SS316 specimens is studied under one particular environment. More research work is needed to study these materials under different kind of corroding environment to avoid the errors in predicting the expected form of corrosion. A model is required which can relate the experimental forced corrosion with the natural atmospheric corrosion

An analysis procedure was achieved using AFM images of the corroded specimens to predict the maximum stresses induced under different types of loading. The future research work will be to develop a complete model which can predict the crack initiation life using effect of both corrosion as well as fatigue under different type of corroding environment. This model should be able to predict the remaining crack initiation life with high accuracy at given corrosion time.

## Literature Cited

1. H.H. Uhling and R.W.Revie, “Corrosion and Corrosion Control”, 3<sup>rd</sup> ed., Wiley, New York, p. 3,1985
2. H. Kaesche, “Corrosion of Metals”, 1<sup>st</sup> ed., Springer,2003
3. Mars G. Fontana and Norbert D. Greene, “Corrosion Engineering”, 2<sup>nd</sup> ed., McGraw-Hill,1978
4. N. Narasaiah, K. K. Ray, “Initiation and Growth of Micro-Cracks under Cyclic Loading”, Materials Science and Engineering, 2008. 474: p. 48-59
5. S. Sivaprasad, S. Tarafder, V. R. Ranganath, M. Tarafder, K. K. Ray, “Corrosion Fatigue Crack Growth Behaviors of Naval Steels”, Corrosion Science, 2006. 48:p. 1996-2013
6. De-Guang Shang, Wei-Xing Yao, De-Jun Wang, “A New Approach to the Determination of Fatigue Crack Initiation size”, International journal of Fatigue, 1998. 20:p 683-687
7. M. G. Fontana, “Corrosion Engineering”, 3<sup>rd</sup> ed., McGraw-Hill, New York, p. 1-5 1986
8. Denny A. Jones, “Principle and Prevention of Corrosion”, 2<sup>nd</sup> ed., Prentice Hall, 1996
9. Marcus P, Oudar J, editors, “Corrosion Mechanisms in theory and practice”, New York: Marcel Dekker, Inc;1995



10. Qu Jun-e, Guo Xing-peng, Wang Hai-ren, Huang Jin-ying, "Corrosion Behavior of Pure Aluminum in FeCl<sub>3</sub> Solution", Transaction of Nonferrous Metal Society China, 2006. 16:p. 1460-1466
11. P. Ernst, R. C. Newman, "Explanation of Effect of High Chloride Concentration on the Critical Pitting Temperature of Stainless steel" Corrosion Science, 2007. 49:p. 3705-3715
12. J. Hahm, S. J. Sibener, "Stress-Modified Electrochemical reactivity of Metallic Surfaces: Atomic Force Microscopy Imaging Studies of Nickel and Alloyed Aluminum", Applied Surface Science, 2000. 161:p 375-384
13. Paul S. Prevey, John T. Cammett, "The Influence of Surface Enhancement by Low Plasticity Burnishing on the Corrosion Fatigue Performance of AA7075-T6", International Journal of Fatigue, 2004. 26:p 975-982
14. Vincent Vignal, Nicolas Mary, Roland Oltra, Jermone Peultier, "A Mechanical-Electrochemical Approach for the Determination of Precursor Sites for Pitting Corrosion at the Microscale", Journal of Electrochemical Society, 2006. 153:p B352-B357
15. Oltra R, Vignal V., "Recent Advance in Local Probe Techniques in Corrosion Research-Analysis of the Role of Stress on Pitting Sensitivity", Corrosion Science, 2007. 49:p. 158-165
16. H. S. Isaacs, "Initiation of Stress Corrosion Cracking of Sensitized Type 304 Stainless Steel in Ductile Thiosulfate Solution", Journal of Electrochemical Society, 1988. 135:p. 2180-2183.

17. Suter T, Bohni H., “A New Microelectrochemical Method to Study Pit Initiation on Stainless Steels”, *Electrochemical Acta.*,1997. 42:p. 3275–3280.
18. Paik CH, Alkire RC., “Role of Sulfide Inclusions on Localized Corrosion of Ni200 in NaCl Solutions”, *Journal of Electrochemical Society*, 2001.148:p. B276–B281.
19. www.
20. T. V. Rajan, V. P. Sharma, Ashok Sharma, “Heat Treatment”, Revised Edition 2004
21. NASA [www.nasa.gov](http://www.nasa.gov)
22. [www.google.com](http://www.google.com)
23. D. Gary Harlow, Robert P. Wei, “Probability Modeling and Material Microstructure Applied to Corrosion and Fatigue of Aluminum and Steel”, *Engng Fract. Mechanics*. 2008
24. S. Ishihara, Z.Y. Nan, A. J. McEvily, T. Goshima, S. Sunada, “On the Initiation and Growth Behavior of corrosion Pits During Corrosion Fatigue Process of Industrial Pure Aluminum”, *International Journal of Fatigue*. 2007.
25. Gregory A Henshall, “Modeling Pitting Degradation of Corrosion Resistant Alloys”, Lawrence Livermore National Laboratory, 1996.
26. Xiaodong Liu, G. S. Frankel, “Effects of Compressive Stress on Localized Corrosion in AA2024-T3”, *Corrosion Science*, 2006. 48:p 3309-3329
27. E. V. Abolikhina, A. G. Molyar, “Corrosion of Aircraft Structures Made of Aluminum Alloys” *Material Science*, 2003. 39: p889-894
28. Q. Y. Wang, R. M. Pidaparti, M. J. Palakal, “Comparative Study of Corrosion-Fatigue in Aircraft Materials” *AIAA Journal*, 2001. 39:p 325-330

29. D. W Hoepfner, "Model for Prediction of Fatigue Lives Based Upon a Pitting Corrosion Fatigue Process", American Society for Testing and Materials, 1979. p.841-863
30. R. P. Wei, D. G. Harlow, T. H. Flournoy, "Probability Modeling of Corrosion Fatigue Crack Growth and Pitting Corrosion", ICAF,1997
31. D. G. Harlow, R. P. Wei, "Probability Model for the Growth of Corrosion Pits in Aluminum Alloys Induced by Constituent Particles", Engineering Fracture Mechanics, 1998. 59:p. 305-325
32. D. G. Harlow, and R. P. Wei, "Probability Approach for Prediction of Corrosion and Corrosion Fatigue Life", AIAA Journal, 1994. 32:p. 2073-2079
33. Rokhlin, S. I. Kim, J. Y. Nagh, Zoofan, " Effect of Pitting Corrosion on Fatigue Crack Initiation and Fatigue Life", Engineering Fracture Mechanics,1999. 62:p. 425-444
34. Lietai Yang, "Techniques for Corrosion Monitoring", Woodhead Publishing Limited. 1<sup>st</sup> edition, 2008.
35. Gamry Instrument, Inc [www.gamry.com](http://www.gamry.com)
36. Institute For Biophysics [www.bphys.uni-linz.ac.at/bioph](http://www.bphys.uni-linz.ac.at/bioph)
37. Bruker AXS Inc [www.bruker-axis.de](http://www.bruker-axis.de)
38. P. Schmutz, G. S. Frankel, "Corrosion study of AA2024-T3 by Scanning Kelvin Probe Force Microscope and In situ Atomic Force Microscopy Scratching", J. Electrochemical Soc., 1998. 145:p.295-306
39. R.P. Wei, C. M.Liao, M. Gao, "A Transmission Electron Microscope Study of 7075-T6 and 2024-T3 Aluminum Alloys" Metal Mater Trans. 1999. 29: p 1153-1998

40. F. A. Martin, C. Bataillon, J. Cousty, "In Situ AFM Detection of Pit Onset Location on a 304L Stainless Steel", 2008. 50:p 84-92
41. Lei Tao, Shizhe Song, Xiaoyun Zhang, Zheng Zhang, Feng Lu, "Image Analysis of Atmospheric Corrosion of Field Exposure High Strength Aluminum Alloys", Applied Surface Science, 2008. 254:p 6870-6874
42. Pacific Nanotechnology. [www.pacificnanotech.com](http://www.pacificnanotech.com)
43. M. Jackubowski, "A Model of Corrosion Fatigue Crack Growth in Ship and Offshore Steel", Fatigue Fract. Engng Mater Struct, 2007. 30:p.682-688
44. J. E. Zamber, Hillbery. "Probabilistic Approach to Predicting Fatigue Lives of Corroded 2024-T3", AIAA Journal, 1999. 37:p. 1311-1317
45. D. L. DueQuesnay, P. R. Underhill, H. J. Britt, "Fatigue and Crack Growth from Corrosion Damage in 7075-T6511 Aluminum Alloy under Aircraft Loading", International Journal of Fatigue, 2003. 25:p. 371-377
46. S. Ishihara, S. Saka, T. Goshima, S. Sunada, H. Chiba, A. J. McEvily, S. Nomata, "Effect of Stress Amplitude on the Corrosion-Pit-Growth Behavior of Pure Aluminum in a Sodium Chloride Solution", International Conference on Environment Sensitive Cracking and Corrosion Damage Hiroshima, Japan, 2001. p. 354-361
47. Ramana M. Pidaparti, Ronak R. Patel, "Correlation between Corrosion Pits and Stresses in Al Alloy", Material letters, 2008. 62:p. 4497-4499
48. Ramana M. Pidaparti, Appajoyula S. Rao, "Analysis of Pits Induced Stresses due to Metal Corrosion", Corrosion Science, 2008. 50:p 1932-1938

49. D. Gary Harlow, Robert P. Wei, "Probability Modeling and Material Microstructure Applied to Corrosion and Fatigue of Aluminum and Steel", Engng Fract. Mechanics. 2008
50. S. Ishihara, T. Goshima, A. J. McEvily, S. Sunada, S. Nomata, "Corrosion-Pit-Growth behavior During the Corrosion Fatigue Process in Aluminum", Proceeding of 10<sup>th</sup> International Conference on the Fracture Hawaii, USA. 2001
51. Hui-Ji Shi, C. Ruan, Xide Li, "Study on the Initiation Stage of Stress Corrosion of an Aluminum Alloy Using the Subjective Speckle Technique", Material Science and Engineering, 2006. A419:p. 218-224
52. E. N. Codaro, R. Z. Nakazato, A. L. Horovistiz, L. M. F. Ribeiro, R. B. Ribeiro, L. R. O. Hein, "An Image Processing Method for Morphology Characterization and Pitting Corrosion Evaluation", Material Science Engineering.2002. A334:p 298-306
53. F. M. Queiroz, M. Magnani, I. Costa, H. G. de Melo, "Investigation of the Corrosion Behavior of AA 2024-T3 in Low Concentrated Chloride Media", Corrosion Science,2008. 50:p 2646-2657
54. J. W. J. Silva, A. G. Bustamante, E. N. Codaro, R. Z. Nakazato, L. R. O. Hein., "Morphological Analysis of Pits Formed on AL2024-T3 in Chloride Aqueous Solution", Applied Surface Science, 2004. 236:p356-365
55. S. N. Magonov, M. H. Whangbo, "Surface Analysis with STM and AFM", New York,1996

56. S. N. Magonov, "Surface Characterization of Materials at Ambient Condition by Scanning Tunneling Microscope and Atomic Force Microscope", *Appl. Spect. Rev.*, 1993. 28:p. 1
57. Hiroki Tamura, "The Role of Rusts in Corrosion Protection of Iron and Steel", *Corrosion Science*, 2008. 50:p 1872-1883

## VITA

### **RONAK R. PATEL**

Telephone:(804)-536-1181 \_\_\_\_\_ Email: [ronak545@gmail.com](mailto:ronak545@gmail.com)

#### **Education:**

- Virginia Commonwealth University. VA. USA  
Masters in Mechanical Engineering: GPA 3.57 (expected Dec.2008)  
Thesis: Corrosion Damage Studies through Microscopy and Stress Analysis
  
- S. P. University, V.V. Nagar, Gujarat, India  
B. E. Mechatronics Engineering: First class; Jan 2004  
Senior Project: Design of Automatic Storage and Retrieval System

#### **Peer-Reviewed Journal Article:**

Ramana Pidaparti, Ronak R. Patel(2008), “Correlation Between Corrosion Pits and Stresses in Al Alloy”, Materials Letters (62): 4497-4499

#### **Conference Abstract:**

Ronak R. Patel, Ramana Pidaparti (2008). The Effect of Corrosion on the Stresses in AL2024 using Finite Element Analysis. AIAA Region Student Conference 2008 (Region I) Baltimore Maryland.

Ronak R. Patel , Ramana Pidaparti (2007). Corrosion Damage on Metals at Micro-level using Micro-imaging technique. AIAA Region I Young Professional, Student and Education Conference 2007. Baltimore Maryland.

**Work Experience:**

Research Asst. Computational intelligence and Simulation Lab. Virginia  
Commonwealth University, July '07- Dec '08.

- Conducted corrosion experiments on AA2024 and stainless steel type 316 in artificial corroding environment, predicted the form of corrosion occurring under this environment and developed a method to estimate the maximum stress on the corroded surface.
- Conducted simulations on the molecular dynamics simulation for draft free drug delivery

Intern-Mechanical Engineer, Elecon Gear Co. Anand, India. May '02- July '02

- Assist mechanical engineer in project of automated storage and retrieval system.

Intern-Mechanical Engineer, PVS Engineering Co. Ahemdabad, India. Jan '03-  
Dec '03

- Assist Mechanical and Industrial Engineer with design and documentation of engineering project.
- Assist Manufacturing engineer with equipment reliability and critical assessment.
- Generate design and document for equipments like Automated Stone crusher, Reaction vessels.